12-2004

Fundamental Investigations and Analysis of Chiral Matter Using Simple Spectroscopic Techniques

Rodney Jamel Sullivan
University of Tennessee - Knoxville

To the Graduate Council:

I am submitting herewith a dissertation written by Rodney Jamel Sullivan entitled "Fundamental Investigations and Analysis of Chiral Matter Using Simple Spectroscopic Techniques." I have examined the final electronic copy of this dissertation for form and content and recommend that it be accepted in partial fulfillment of the requirements for the degree of Doctor of Philosophy, with a major in Physics.

Robert N. Compton, Major Professor

We have read this dissertation and recommend its acceptance:

Richard Pagni, James R. Thompson, Marianne Breinig

Accepted for the Council:
Carolyn R. Hodges

Vice Provost and Dean of the Graduate School

(Original signatures are on file with official student records.)

To the Graduate Council:

I am submitting herewith a dissertation written by Rodney Jamel Sullivan entitled "Fundamental Investigations and Analysis of Chiral Matter Using Simple Spectroscopic Techniques." I have examined the final electronic copy of this dissertation for form and content and recommend that it be accepted in partial fulfillment of the requirements for the degree of Doctor of Philosophy, with a major in Physics.

Robert N. Compton
Major Professor

We have read this dissertation
and recommend its acceptance:

Richard Pagni

James R. Thompson

Marianne Breinig

Accepted for the Council:

Anne Mayhew
Vice Chancellor and Dean of
Graduate Studies

(Original signatures are on file with official student records)

Fundamental Investigations and Analysis of Chiral Matter Using Simple Spectroscopic Techniques

A Dissertation

Presented for the

Doctor of Philosophy

Degree

The University of Tennessee, Knoxville

Rodney Jamel Sullivan

December 2004

DEDICATION

This dissertation is dedicated to my parents, Hazel B. Sullivan and the late John H. Sullivan, to my brothers and sisters, to the rest of my family, and to my friends for always believing in me, encouraging me, strengthening me, and supporting me during the course of this endeavor.

ACKNOWLEDGEMENTS

First things first, I would like to thank Jesus Christ my Lord and Savior for dying on the cross, rising on the third day, and carrying me on His shoulders to make this moment possible.

I would like to thank my advisor, Dr. Robert N. Compton, for allowing me to become a member of his group. He was always available for questions and discussions, and his guidance, knowledge, and patience have led me to the truth of elementary discoveries in science. He was a great help in my development as a physicist.

I would like to thank the members of my committee, Dr. Richard Pagni; Dr. Marianne Breinig; Dr. James R. Thompson; and Dr. Solon Georghiou, for their willingness to serve and to offer ideas.

I would like to thank Dr. Richard Pagni and Dr. Fang Gao, for their assistance in the development of the 1,1'-binaphthyl experiment. Appreciation is shown to Dr. Jim Bogard for handling the radiation source.

Finally, a special thanks goes out to all my friends and colleagues in Dr. Compton's group. I would like to thank "Young Hairy" Andy Fischer for aiding in the irradiation and analysis of the laser induced crystallization studies. Another thanks goes to Dr. Runhua Li for participating in the multiphoton ionization study. All the members in Compton's group have made my experience such a blessing, especially the times spent talking and joking with "Young Arrogant" Wesley Robertson. Also, I would like to thank "Word Girl" Catherine Longmire for proofing this dissertation and for the uplifting and encouraging conversations in her office.

ABSTRACT

Fundamental investigations of circular dichroism were performed on (*R*)-(+)-3-methylcyclopentanone, (*R*)-(-)-2-butylamine, and (*S*)-(+)-2-butylamine in the liquid and vapor phase to show that solvents often have a structure-masking effect on the circular dichroism for a given molecule. Also, the solid state circular dichroism of cubic sodium chlorate crystals was successfully measured in the midst of adverse experimental circumstances. With these single photon circular dichroism studies at hand, a new technique for measuring circular dichroism was introduced for an advanced investigation of (*R*)-(+)-3-methylcyclopentanone. The resonance enhanced multiphoton ionization of (*R*)-(+)-3-methylcyclopentanone was performed with left and right circularly polarized laser light at a wavelength of 397.5 nm. This technique gave a dissymmetric factor g of $4.1 \pm 0.23 \times 10^{-2}$ in favor of the left circularly polarized light.

Parity violating energy difference studies were conducted on the enantiomers of alanine and valine. The conversion of one enantiomer to the other at 273 K was found not to occur due to temperature dependent studies of circular dichroism, x-ray diffraction, C-13 solid state NMR, Raman spectroscopy, magnetic susceptibility, differential scanning calorimetry, and theoretical calculations.

Highly intense 1064 nm pulsed laser light was used to induce crystallization in sodium chlorate, sodium bromate, and glycine aqueous solutions. The symmetry of sodium chlorate crystals and the asymmetry of sodium bromate crystals were broken by right circularly polarized and linearly polarized light, respectively. The γ-polymorph of glycine was produced by an acidic pH change induced by the intense laser light. Under a

Sr-90 source, 1,1’-binaphthyl crystallized into crystals showing a slight enantiomeric excess.

TABLE OF CONTENTS

LIST OF TABLES

LIST OF FIGURES

DEFINITIONS AND ABBREVIATIONS

Definitions

Asymmetric	synthesis of crystals that results in highly unequal numbers of (+) and (-) crystals
Carbonyl group	a functional group containing a carbon oxygen double bond (C=O)
Chiral	derived from the Greek word *cheir*, meaning "hand" or "handedness"
Enantiomers	pairs of molecules that exist as nonsuperimposable mirror images of each other enantiomer
Enantiomeric excess	the abundance of one enantiomer over the other enantiomer
Optical activity	the rotation of plane polarized light as it passes through an optical medium
Symmetric	synthesis of crystals that results in nearly equal numbers of (+) and (-) crystals

Abbreviations

CD	circular dichroism
CDAD	circular dichrosim in the angular distribution
CPL	circularly polarized light
D	right-handed configuration of an amino acid
ee	enantiomeric excess
L	left-handed configuration of an amino acid
LCPL	left circularly polarized light
LPL	linearly polarized light
MPICD	multiphoton ionization circular dichrosim
NMR	nuclear magnetic resonance
ORD	optical rotatory dispersion
(*R*)	right-handed configuration of a chiral molecule
RCPL	right circularly polarized light
REMPI	resonance enhanced multiphoton ionization
(2+1) REMPI	two photons to reach resonance and one more photon to ionize a molecule using resonance enhanced multiphoton ionization
(3+2) REMPI	three photons to reach resonance and two more photons to ionize a molecule using resonance enhanced multiphoton ionization
(*S*)	left-handed configuration of a chiral molecule
(+)	positive or clockwise rotation of plane polarized light
(-)	negative of counterclockwise rotation of plane polarized light

CHAPTER I

INTRODUCTION

Introduction

In this dissertation a variety of experiments were conducted under the umbrella of chirality. Fundamental investigations and analysis of chiral matter were performed through spectroscopic methods. The dissertation is divided into three major parts.

The first part, Chapters II and III, involves the probing of asymmetries in chiral molecules by circular dichroism. Circular dichroism, which will be discussed later, is a way of analyzing chiral molecules and matter by their differential absorption of left and right circularly polarized light. While single photon circular dichroism spectra were taken for a few molecules, a new method of analyzing chiral molecules by multiphoton ionization circular dichroism was employed in the study of (*R*)-(+)-3-methylcyclopentanone (Chapter III).

The second division of the dissertation, Chapters IV, V, and VI, involves the crystallization of chiral and achiral molecules into optically activity crystals using external chiral forces. The external chiral forces used are left-handed helical beta particles and circularly polarized light. In Chapter 4, the irradiation 1,1'-binaphthyl with beta particles to make resolved crystals is discussed. In Chapter V, the behavior of sodium chlorate and sodium bromate when irradiated with linearly polarized and circularly polarized light is described. These irradiations were performed in order to observe the preferential selection of crystals with certain handedness or helicity. In Chapter VI, a description of what happened when glycine was irradiated with linearly and circularly polarized light is described.

The third division, Chapter VII, describes the search for the effects of the very small parity violating energy difference on macroscopic crystals of amino acids. Many experimental techniques were employed on alanine and valine crystals. This chapter was a temperature dependent test for the Salam hypothesis.

The purpose for all the experiments is to gain insight and understanding about the world of chirality. The experiments to be presented in the coming chapters provide clean and effective methods of influencing chiral matter into a certain handedness. These experimental methods could be used for enantiomeric enrichment and chiral selection, which is helpful to pharmacology, biology, and many other fields of study.

CHAPTER II

INTRODUCTION TO CIRCULAR DICHROISM

Introduction

The purpose of this chapter is to give a brief description of circular dichorism. This description will involve samples of data that I have taken in order to illustrate certain aspects of circular dichroism. Circular dichroism is a phenomenon of optical activity. Optical activity is the rotation of the plane of polarized light as it passes through a chiral medium. The medium that displays optical activity is said to be optical active.

Optical activity was discovered by Arago in 1811. Later, Cotton showed that optically active materials absorb left-handed and right-handed circularly polarized light to different extents.[1] Optical rotation, an effect of optical activity, is the rotation of plane polarized light as it passes through an optically active medium. This physical property occurs for enantiomers, which are molecules with nonsuperimposable mirror images. The mathematical description of Optical Rotatory Dispersion (ORD) is expressed by the angle of rotation of the plane of linearly polarized light

$$\alpha = \frac{\pi}{\lambda}\left(n_L - n_R\right), \tag{2.1}$$

where n_L and n_R represent the indices of the refraction index for left and right circularly polarized light and α is the rotation. The magnitude of the difference in n_L and n_R is on order of 10^{-6} to 10^{-9} percent. The unit dimensions of α are radians per unit length. Typical ORD α rotations are on the order of 0.001° to 1° when measured in a 1 dm cell at room temperature.[2] The ORD spectra of enantiomers are equal in magnitude and opposite in sign. Thus, an enantiomer is labeled positive, (+), if the polarized light is rotated

clockwise (dextrorotatory) as viewed in the direction of the light source. Consequently, the other enantiomer will exhibit a counterclockwise rotation (levorotataory) and is labeled negative, (-).

The specific rotation of a sample is given by

$$[\alpha] = \frac{\alpha}{c} \cdot \frac{1800}{p} \qquad (2.2)$$

where α is the angle of rotation, c is the concentration in gram per milliliter of solution, and $1800/\pi$ is a simple conversion factor.[3] Specific rotation is measured at a given wavelength and temperature. The most commonly used wavelength and temperature are the sodium D line, 589 nm, and room temperature, ~ 23°C. The molecular rotation is

$$[\phi] = \frac{[\alpha] \cdot M}{100} \qquad (2.3)$$

where M is the molecular weight. Another form of optical activity that is very closely related to ORD is circular dichroism.

Circular Dichroism (CD) is the differential absorption between left and right circularly polarized light, $\Delta A = A_L - A_R$ (2.4) and is characteristic of enantiomers. CD is commomly employed to study chiral molecules including most biological molecules. A common application of CD is to probe the structure of biological macromolecules and to prove if chiral molecules were synthesized or resolved during a chemical reaction or process.[4] A CD signal contains all the information about the asymmetries of a molecule and offers a 50 percent chance of assigning which enantiomer is in solution. The CD spectra of enantiomers yield signals, which are equal in magnitude and opposite in sign.

Besides chiral organic substances, other materials that display optical activity are crystalline compounds, semi-crystalline materials, and thin films of ferromagnetic metals.

Early theories for optical activity[1] expressed CD through an equation for the difference in extinction coefficients:

$$\varepsilon_l - \varepsilon_R = \frac{64\pi^2 N_1}{3hc} \log e \sum_a Pa \sum_b \frac{\nu^3 \Gamma_{oba} R_{ba}}{\left(\nu_{ba}^2 - \nu^2\right)^2 + \nu^2 \Gamma_{oba}^2} \qquad (2.5)$$

where N_1 is the number of active moles per liter, ν is the frequency of light, Pa is the probability of the molecule being in the ground state a, ν_{ba} is the characteristic frequency of the transition a→b, R_{ba} is the rotational strength of the molecule for the transition a→b, and Γ_{oba} is the half-width of the band corresponding to the transition a→b.[1] Nowadays, CD spectropolarimeters produce CD signal in units of ellipticity, θ, which is easily measured in millidegree per wavelength rather than the differential absorption, ΔA, versus wavelength.[4] The CD signal becomes

$$CD = \Delta A = A_L - A_R = \frac{4\pi\theta(\text{deg rees})}{180 \ln 10} = \frac{\theta(\text{milli deg rees})}{32{,}982}. \qquad (2.6)$$

CD differential absorption, ΔA, is very small with a magnitude around 0.1 to 0.001.[2] As one example, Figure 1 displays the CD spectra for (*R*)-(-)- and (*S*)-(+)-1,1'-binaphthyl, $C_{20}H_{14}$, dissolved in benzene at a concentration of 0.04915M with a one centimeter pathlength (see Figure A-1). As mentioned earlier, ORD and CD are manifestations of one and the same phenomenon dealing with the interaction between polarized light and an asymmetric molecular structure.[1]

Both ORD and CD are related by Kronig-Kramer's[2] theorem where

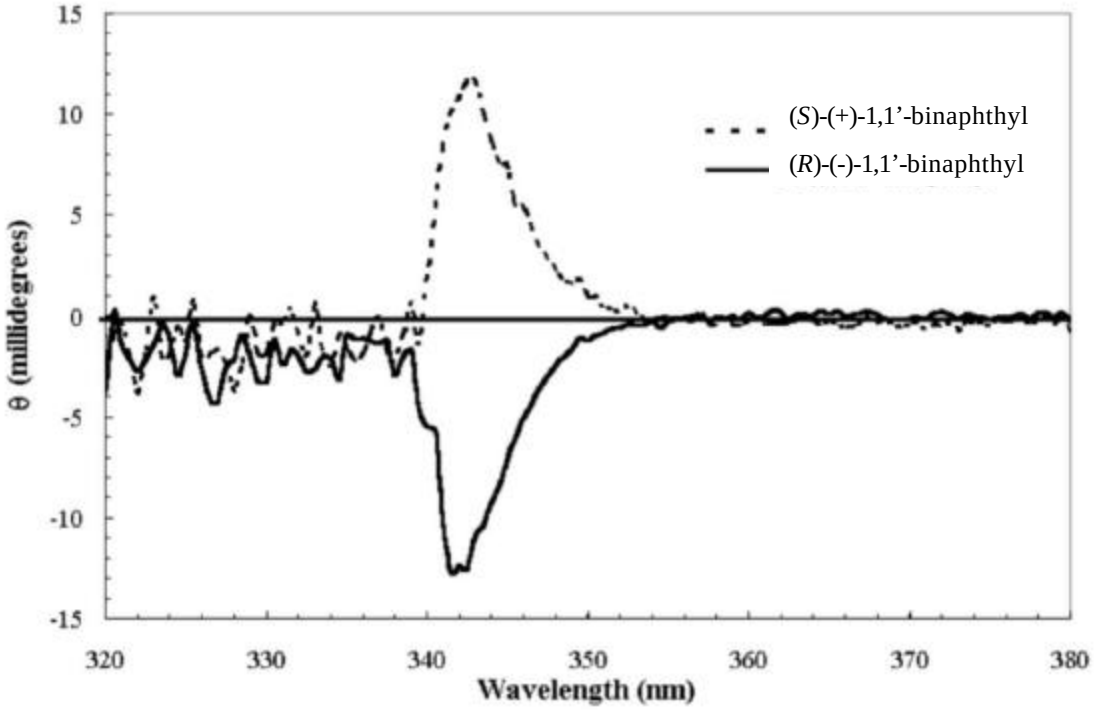

Figure 1. Circular Dichroism of (*S*)-(+) and (*R*)-(-)-1,1'-binaphthyl dissolved in benzene.

$$\left[\theta_k(\lambda_o)\right] = -2(\pi\lambda_o)^{-1}\int_0^{\infty}\left[f_k(\lambda)\right]\frac{\lambda^2}{\left(\lambda_o^2 - \lambda^2\right)}\,d\lambda \qquad (2.7)$$

and

$$\left[f_k(\lambda_o)\right] = 2\pi^{-1}\int_0^{\infty}\left[\theta_k(\lambda)\right]\frac{\lambda}{\left(\lambda_0^2 - \lambda^2\right)}\,d\lambda\,. \qquad (2.8)$$

ORD and CD are seen to be complementary. An important factor that arises when measuring CD is the absorption coefficient. The absorption coefficient, ε, is equal to

$$\varepsilon = \frac{4\pi\kappa}{\lambda}\log e\,, \qquad (2.9)$$

where κ is the index of extinction and λ is the wavelength. The differential dichroic absorption is $\Delta\varepsilon = \varepsilon_L - \varepsilon_R$ (2.10) where ε_L and ε_R are absorption coefficients for left and right circular polarized light, respectively.[1] The differential absorption coefficient, Δε, for CD is related to the molecular ellipticity, [θ], by the relationship:

$$\Delta\varepsilon = \frac{[\theta]}{3300} \qquad (2.11)$$

where [θ] is equal to

$$[\theta] = \frac{\phi}{100\cdot c\cdot d} \text{ and } \phi \approx \frac{180}{4\pi\cdot\log e}\Delta\varepsilon\cdot c\cdot d \text{ (measured in degrees).} \qquad (2.12)$$

Here, c is the concentration in gram-moles per milliliter, ϕ is the difference in angle measured in millidegrees, and d is the pathlength in decimeters.[1] The molecular amplitude of ORD can be related to the dichroic absorption by the equations

a = 0.0122·[θ] or a = 40.28·Δε in terms of molecular ellipticity for the $n\rightarrow\pi^*$ transition of carbonyl groups.[3]

As with ORD, CD is very closely related to UV-visible spectroscopy. An important ratio that relates CD to UV-visible spectroscopy is the g-factor. The g-factor for CD is:

$$g = \frac{2\left(I_L - I_R\right)}{\left(I_L + I_R\right)} = \frac{\Delta e}{e}. \qquad (2.13)$$

This g-factor is known as the dissymmetric factor or optical anisotropy[9]. The I_L and I_R are the relative intensities of left and right circularly polarized light as they pass through a medium. This factor is typically on order of magnitude of 10^{-2} to 10^{-5}, which is very important to Multiphoton Ionization Circular Dichroism (MPICD) to be described in detail later.[5]

Circular dichroism results from the quantum interference between the electric and the much weaker magnetic dipole terms in the total cross-section, which is difficult to interpret[6]; however, circular dichroism in the photoelectron angular distribution (CDAD) arises from the stronger interference between the pure electric dipole terms in the differential cross-section.[6-8] Circular dichroism and UV-visible spectroscopy have the same photophysical process because both arise from the movement of an electron in the electronic ground state to an electronically excited state.[2]

The typical energy range for UV-visible spectroscopy is 2 $\rightarrow$12 x 10^{-19} J/molecule and ranges from 170 – 800 nm. This amount of energy is required for the rearrangement of electron's distribution in a molecule.[4] Energy is absorbed and changes the electron density by exciting the electron to a higher final energy level. The Beer-Lambert law for absorption states that $A=\varepsilon CL$ (2.14), where L is the pathlength of light through the sample, ε is the extinction coefficient, and C is the concentration. The units for the

concentration and the extinction coefficient are C=M= [mol]/[dm]^3 and ε = dm^3/(mol·cm).[4] The optimal concentrations and cell lengths for a sample should give a transmission of 5-20% in the spectra region.[1] The absorption spectrum is plotted as absorbance versus wavelength; whereas a CD spectrum is plotted as millidegrees versus wavelength. Most solutions and materials can be analyzed using UV-visible spectroscopy. On the other hand, CD can only be performed on chiral molecules or helical structures because they posses no plane of symmetry; therefore, the rearrangement of electrons will not have a plane of symmetry either. This fact leads the electron motion to be helical.[4] This helical motion reacts differently to helical left and right circularly polarized light.[4] Thus, the CD signal gives the asymmetric part of the change probed by the magnetic field and electric field of radiation. This change between the absorption of left and right circularly polarized light (LCPL and RCPL, respectively) is a small difference between two large absorptions. Since the magnetic field interaction strength is about 1000 times weaker than the electric field interaction energies, this weakness in field strength is responsible for the smallness in the difference of absorption.[4] The electric field causes a linear rearrangement of the electron displacements, resulting in an electric dipole transition moment while the magnetic field induces a circular rearrangement of the electrons' density. This net electron charge circulation produces a magnetic dipole transition moment.[4] A chiral molecule's electron rearrangement is always helical, but planar for an achiral molecule. This explains why achiral molecules do not produce a CD signal - because chirality does not exist in two dimensions. These moving helical electrons react differently to circularly polarized light. Working inversely to their helicity, left helical electrons are easily induced by RCPL rather than LCPL, thus

resulting in a negative CD and vice versa.[4] Now, the Beer-Lambert Law has a new version for the CD, $\Delta A = (\Delta\varepsilon)CL$.[4] (2.15)

CD absorption spectrum with LCPL differs by at most two percent from the unpolarized and RCPL CD. The difference in absorption between RCPL and LCPL rarely exceeds ±0.001 percent.[4]

Circular Dichroism Transitions and Spectra

There are three major catergories for CD spectra: empirical, ab initio, and chromophoric. Empirical is based on experience with related systems while ab initio employs calculations with complete molecular wavefunctions. Chromophoric analysis divides the molecule into separate chromophores and some simple calculations are performed.[4] A chromophore is a subunit of a system whose wavefunctions have no overlap with the rest of the system. Since many biological molecules contain the carbonyl group, the CD of the $n\rightarrow\pi^*$ transition of carbonyl has received more attention than any other type of transition.[4]

To describe chromophores, the Octant ORD rule was formulated by Djerassi about 40 years ago. The rule is used to determine the absolute configuration of a saturated ketone when its conformation is known; or conversely to determine its conformation when the absolute configuration is known. The Octant rule is the first sector rule in organic stereochemistry.[2] The most successful correlation between the Cotton effect, which is a curve that ascends or descends rapidly, and the Octant rule happens to involve the $n\rightarrow\pi^*$ transition of saturated alkyl ketones.[2] In particular, the Octant rule is used for carbonyl functional groups. These functional groups guarantee a weak transition around 280 – 300 nm.[3] This rule is deduced from symmetric principles

that relate the sign and amplitude of the Cotton effect exhibited by an optically active saturated ketone to the spatial orientation of atoms about the carbonyl group.[3] Most methyl groups fall into positive octants.

The carbonyl chromphore has C_{2v} symmetry.[9] For the $n \rightarrow \pi^*$ transition, the carbonyl CO double bond has a symmetric electric dipole moment; thus, the transition is forbidden by symmetry, $\langle A_1 | m_c | A_2 \rangle = 0$. The magnetic dipole moment operator is antisymmetric and transforms the A_1 symmetric ground state to the A_2 symmetric excited state, such that $\langle A_1 | m_m | A_2 \rangle \neq 0$.[2] The $n \rightarrow \pi^*$ transition involves a circular movement of charge around the oxygen, which leads to a large induced magnetic dipole moment. This $n \rightarrow \pi^*$ transition specifies the promotion of an electron from a free pair on a hetero-atom to a π-antibonding molecular orbital, while $n \rightarrow \sigma^*$ transition represents the promotion to the antibonding σ-orbital.[1]

Even though the transition is electric dipole forbidden and magnetic dipole allowed, the absorption is weak (ε~ 10-100) around 300 nm.[2] Electric dipole intensity is "borrowed" by vibronic coupling from electronic dipole-allowed transitions of higher energy, like $\pi \rightarrow \pi^*$, which is magnetically forbidden, or the $\sigma \rightarrow \sigma^*$.[2] The singlet-singlet $n \rightarrow \pi^*$ transition has a very weak UV-visible absorption of about $\varepsilon \approx$10-200, and the singlet-triplet is even weaker, $\varepsilon \approx 0.1$.[1]

An example of a molecule with a carbonyl chromophore is 3-methylcyclopentanone, which has the chemical formula of $C_6H_{10}O$ (see Figure A-1). 3-Methylcyclopentanone has two conformations, axial and equilateral. The CD of (*R*)-(+)-3-methylcyclopentanone has Rydberg transitions around 195 nm, 177 nm, and 165 nm,

each corresponding to the n→3s, n→3p, and n→3d transitions, respectively.[2,9] The absorption due to the n→π^* transition at 300 nm and the n→3d transition has a positive sign in both cases.[9] The CD for a few of these transitions for (*R*)-(+)-3-methylcyclopentanone are displayed in Figure 2 for both the solution and gaseous phases. One will note vibrationally resolved features in the gaseous phase data.

Solvents, temperature, and sample concentration can affect CD signal. Polar solvents arrange around the carbonyl group in such a way that the ground state is stabilized.[1] The effects of the solvents can easily be seen in Figures 2 and 3. In Figure 2, the (*R*)-(+)-3-methylcyclopentanone is 2.599 mM in aqueous solution. The fine structure of the spectrum is completely masked when in solution, as opposed to the unmasked vapor phase spectrum. For the vapor phase spectrum[22], 5 μL of (*R*)-(+)-3-methylcyclopentanone was allowed to vaporize in a cuvette without condensing on the cell walls. The spectra for both enantiomers of sec-butylamine, $C_4H_{11}N$ (see Figure A-1), are presented in Figure 3. Both enantiomers with a concentration of 0.32554M were dissolved in ethanol. There appear to be no major differences in the spectra except what is common to both the sec-butylamine and (*R*)-(+)-3-methylcyclopentanone. A noticeable difference is the magnitude of the differential absorption coefficient, Δε, but still one cannot compare the two since the concentration units are different. The Δε for (*R*)-(+)-3-methylcyclopenatone in the vapor is about –0.00485 and about –1.5 for the aqueous solution at about 190 nm. As for the (*R*)-(-) and (*S*)-(+)-2-butylamine, Δε is about ±0.0013 for the vapor and ±0.003 when dissolved in ethanol at about 226 nm. The differential absorption is smaller in the vapor phase than in solution. An Aviv Model 202 Series Circular Dichroism Spectrometer was used to record all the CD spectra. A

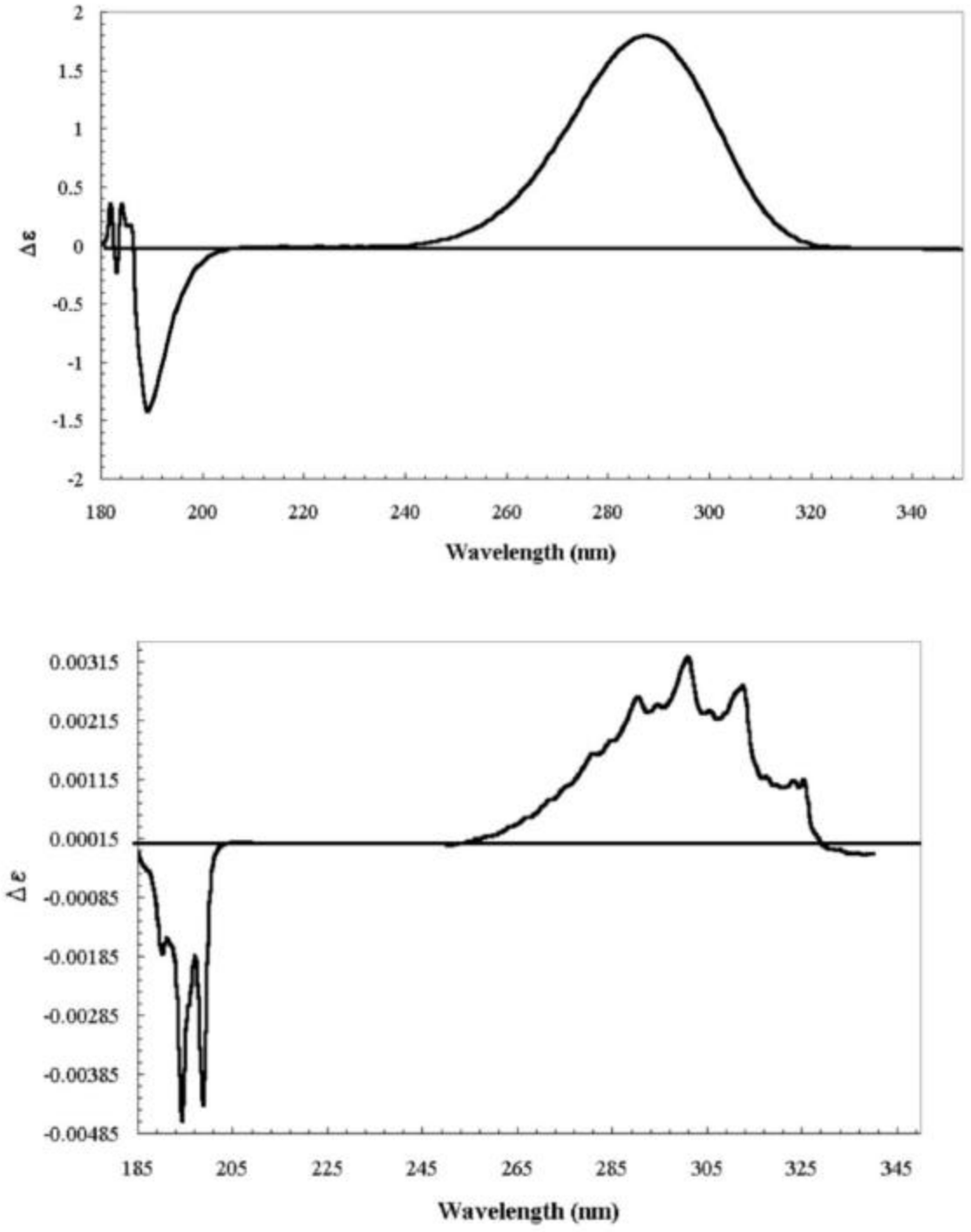

Figure 2. Circular dichroism of (*R*)-(+)-3-methylcyclopentanone. The top graph shows the circular dichroism when dissolved in water while the bottom graph contains the vapor phase circular dichroism.

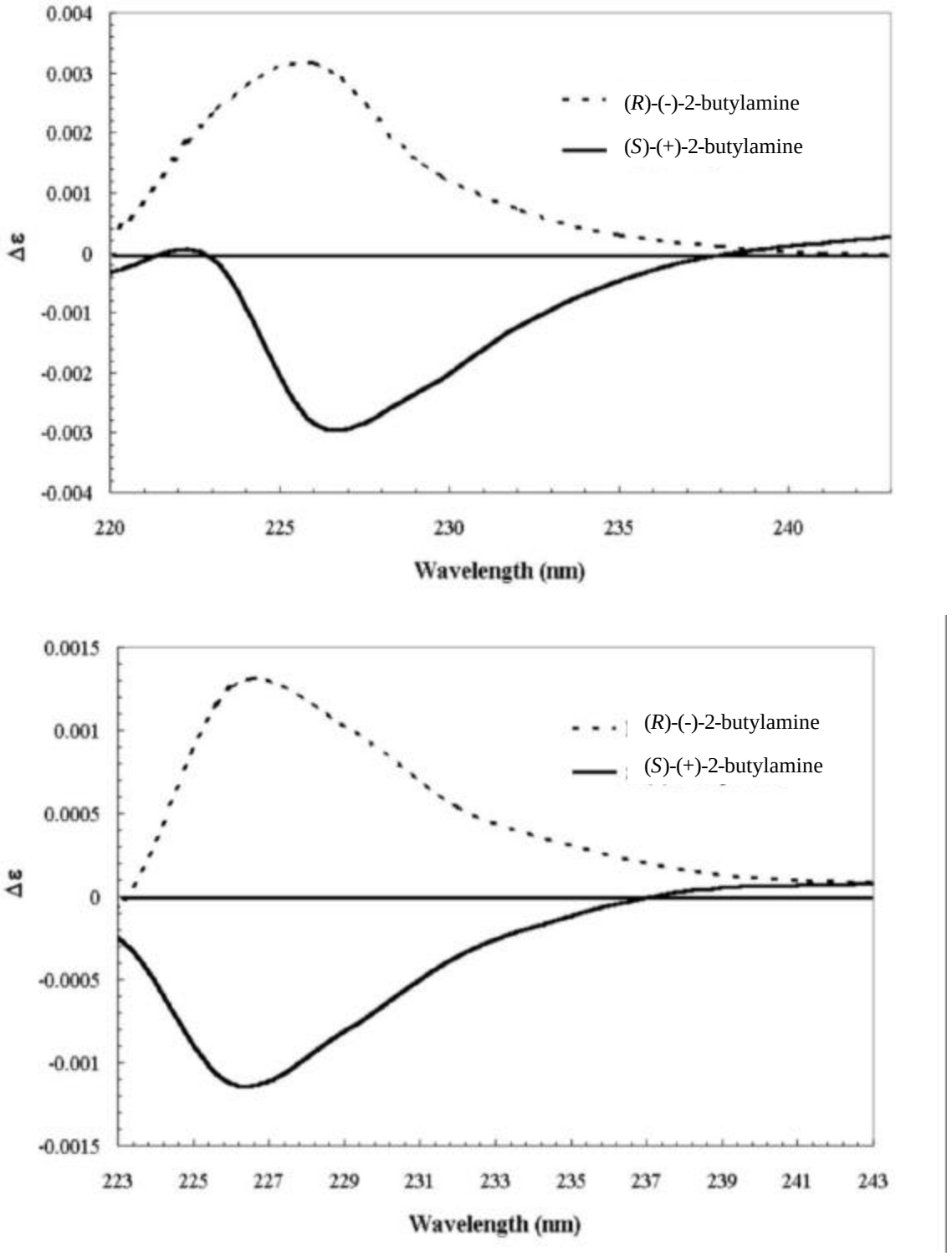

Figure 3. Circular dichroism of (*R*)-(-) and (*S*)-(+)-2-butylamine. The top graph shows the circular dichroism in ethanol while the bottom graph contains the vapor phase circular dichroism.

one centimeter pathlength was used for all spectra except for the vapor phase spectrum of (*R*)-(+)-3-methylcyclopentanone, where a 0.5 cm pathlength was employed.

Solid State Circular Dichroism

A rarely-used and difficult technique is solid state CD. Solid state CD gives information on solute solvent interactions because in solution the nature of the solvent may effect the rotatory power of optically active molecules by forming a coordination compound around the molecule, causing a conformation alteration.[10] Now, solid state CD offers a densely packed crystal with nearest neighbor influences. Due to the packing of the crystal, an achiral molecule can form optically active crystals. An achiral molecule can display optical activity by severely restricting a degree of freedom, whether rotation or orientation, about chemical bonds in a crystalline lattice. Also, optical activity can be caused by helical interactions between neighboring molecules.[10]

Even though solid state CD is difficult to obtain, a wealth of important information can be obtained from such spectra. One can find out the bonding nature of atoms or intermolecular interactions in crystals[10], as well as information about band assignments. Rotatory strengths can be gained from the optical activity of single crystals. The functions of molecules in solid state CD can be revealed in x-ray diffraction analysis.

As mentioned earlier, solid state CD is difficult to obtain and theoretical complexities arise from the fact that there are many crystal categories and subgroups as well as large birefringence due to the off axes of the crystal.[10] Of the 230 space groups that arise from Bravais translations, only 65 are chiral. When taking spectra, one has to be careful of artifactual signals, grain boundaries, and inhomogeneities in the crystalline lattice. With cubic, uniaxial, and biaxial crystals, the correction of birefringence is

unnecessary.[10] Since most crystals are monoclinic or orthorhombic, solid state CD technique cannot be applied in a straightforward manner.

The origin of optical activity in the crystalline state is not well understood since optical activity can arise if there are strong intermolecular interactions between chirally arranged achiral molecules in a noncentrosymmetric crystal.[10] Crystal thicknesses are typically 0.01 to 0.08 mm. Faces perpendicular to the optical axis were polished and analyzed with polarizers to ensure the direction of the optical axis and the clarity of the crystal. The solid state CD spectra of (+)- and (-)- sodium chlorate which crystallizes in the $P2_13$ are displayed in Figure 4. After both crystals were grown from an aqueous solution, they were shaved and polished to a thickness of 0.508 mm. The CD of sodium chlorate, $NaClO_3$, matched that in the literature.[11] A transition occurred are 220 nm. Futher studies on sodium chlorate are described in Chapter V.

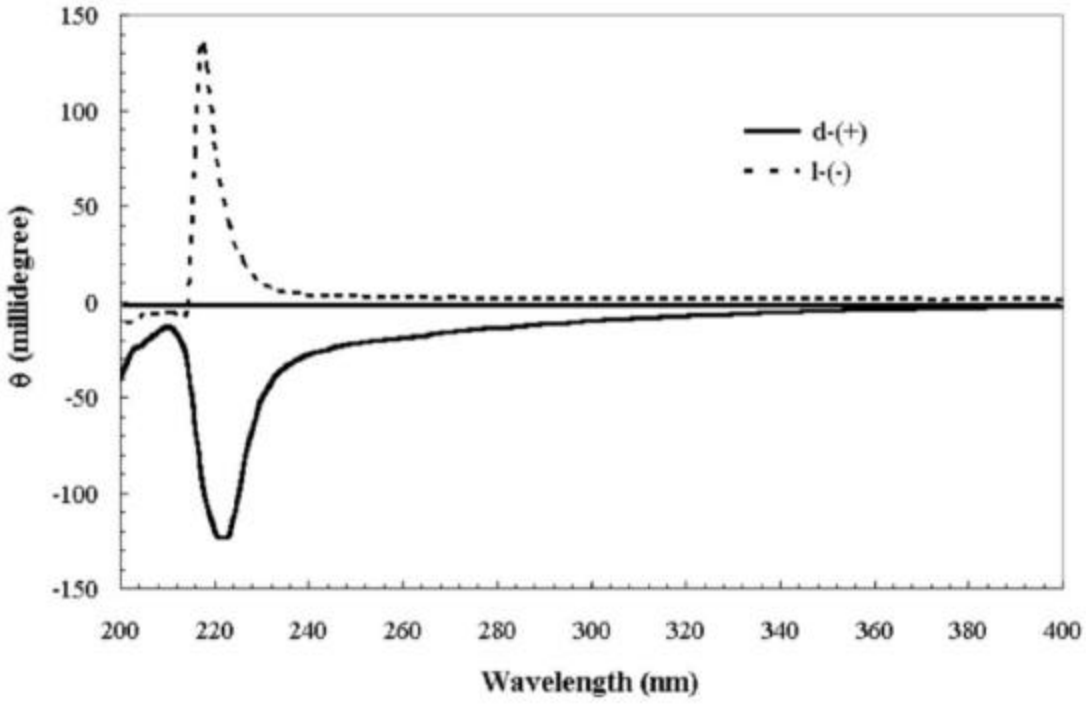

Figure 4. Solid state circular dichroism of sodium chlorate crystals.

CHAPTER III

MULTIPHOTON IONIZATION CIRCULAR DICHROISM OF 3-METHYLCYCLOPENTANONE

Introduction

As mentioned in the previous chapter, circular dichroism is the differential absorption of left- and right-handed circularly polarized light by chiral molecules. This difference results from the interaction of electric and magnetic dipole transitions. Circular dichroism is sometimes expressed in term of the dissymmetric g factor, $\Delta\varepsilon/\varepsilon$, which is a ratio that happens to be on the order of 10^{-3} to 10^{-4} and can only be observed for optically active or chiral molecules. Since circular dichroism contains information on asymmetric conformation, it can be used to probe the microstructures of molecules. For example, measurements of circular dichroism in the ultraviolet and vacuum ultarviolet regions have already been developed as a sensitive structure probe for macromolecules such as proteins, peptides, and nucleic acids which are higher order effects.[12]

Circular dichroism can also be observed for achiral molecules when their environment is chiral. For example, circular dichorism of angular distribution (CDAD) of electrons ejected from aligned or oriented molecules was observed experimentally for gaseous nitric oxide[13] and carbon monoxide on a surface.[14] In these experiments, the chiral geometry was produced by the different-handed coordination systems given by the directions of light propagation whether by photoelectron ejection or by the alignment of the molecules. Since CDAD is derived from pure electric dipole interaction, one is able to observe molecular asymmetries on order of 10 percent to 80 percent, which is very large when considering the naturally small asymmetries of circular dichroism. A large circular

dichroism effect in the second harmonic generation for anistropic achiral surfaces was reported and explained by the electric dipole-allowed surface nonlinearity.[15,16] Also, nanoparticles made with chiral compounds have shown a large circular dichroism effect up to 10 percent in single-photon photoionization.[17,18]

In this chapter, the first experimental investigation of multiphoton ionization circular dichroism (MPICD) is reported for an optically active molecule employing the resonance-enhanced multiphoton ionization (REMPI) technique. The REMPI technique has already been used to discriminate different enantiomers in the gas phase[19-21], but there are no reports about an observation of circular dichroism for chiral molecule using this technique. The purpose for my investigation is to observe asymmetries of CD in the multiphoton realm as well as to probe the CD effect of electron transitions not arising from the ground state.

Racemic and (*R*)-(+)-3-methylcyclopentanone were studied in this experiment. (*R*)-(+)-3-Methylcyclopentanone was chosen to study as a result of its large asymmetric g factor, $\Delta\varepsilon/\varepsilon$, of ~ 2 x 10^{-3} at 199 nm, which corresponds to n$\rightarrow$3s transition.[22] The large optical rotation specific angle of $[\alpha]_D = 148^\circ$ provides another good reason why (*R*)-(+)-3-methylcyclopentanone is a very good candidate for this study. Futhermore, this compound has been examined by vibrational Raman optical activity[23] and by modulated-polarization spectroscopy.[24] Since racemic and (*R*)-(+)-3-methylcyclopentanone have been studied thoroughly by many methods, their electronic energy levels are well known.[25, 26]

Experiment

In this experiment, a Continuum Powerlite 9000 Nd:YAG pulsed laser operating at 10 Hz was used. The laser was set to use its third harmonic light output of 355 nm in a seeded Q-switch mode to avoid any optical damage arising from sudden increases in peak power. Also, the seeder allowed the beam to possess more stability in its shot-to-shot variations. In seeded mode, the variability for the 355 nm or third harmonic pulsed laser light was less than 3 percent while having a pulse width of 6 ns. The pulsed 355 nm laser light was used to pump a Quanta-Ray PDL-2 dye laser. Exalite 398 laser dye was used to observe the multiphoton ionization of racemic and (*R*)-(+)-3-methylcyclopentanone. Dissolved in *p*-dioxane, the Exalite 398 laser dye provided a wavelength range from 403 nm to 393 nm. This wavelength range was chosen because the n→3s transition that occurs at 199 nm in the vapor phase single photon CD in Figure 2 could not be achieved with the laser due to the small wavelength; thus, the wavelength was doubled to 398 nm in order to give a two photon excitation to the n→3s transition. Since MPICD spectra was to be observed, circularly polarized light had to be produced. Left and right circularly polarized light were achieved by the use of a Glan-Taylor polarizer, a double Fresnel rhomb, and a single Fresnel rhomb (Figure 5). The selected laser light from the dye laser was directed to pass through a Glan-Taylor polarizer, where it became highly pure linearly polarized light. Then, the linearly polarized light passed through a double Fresnel rhomb and a single Fresnel rhomb where it became circularly polarized. The double Fresnel rhomb was used to continuously rotate the direction of the polarization plane for the linearly polarized laser light. Right and left circularly polarized light were obtained with linearly polarized light incident at $+45^{\circ}$ and -45° respectively on a single

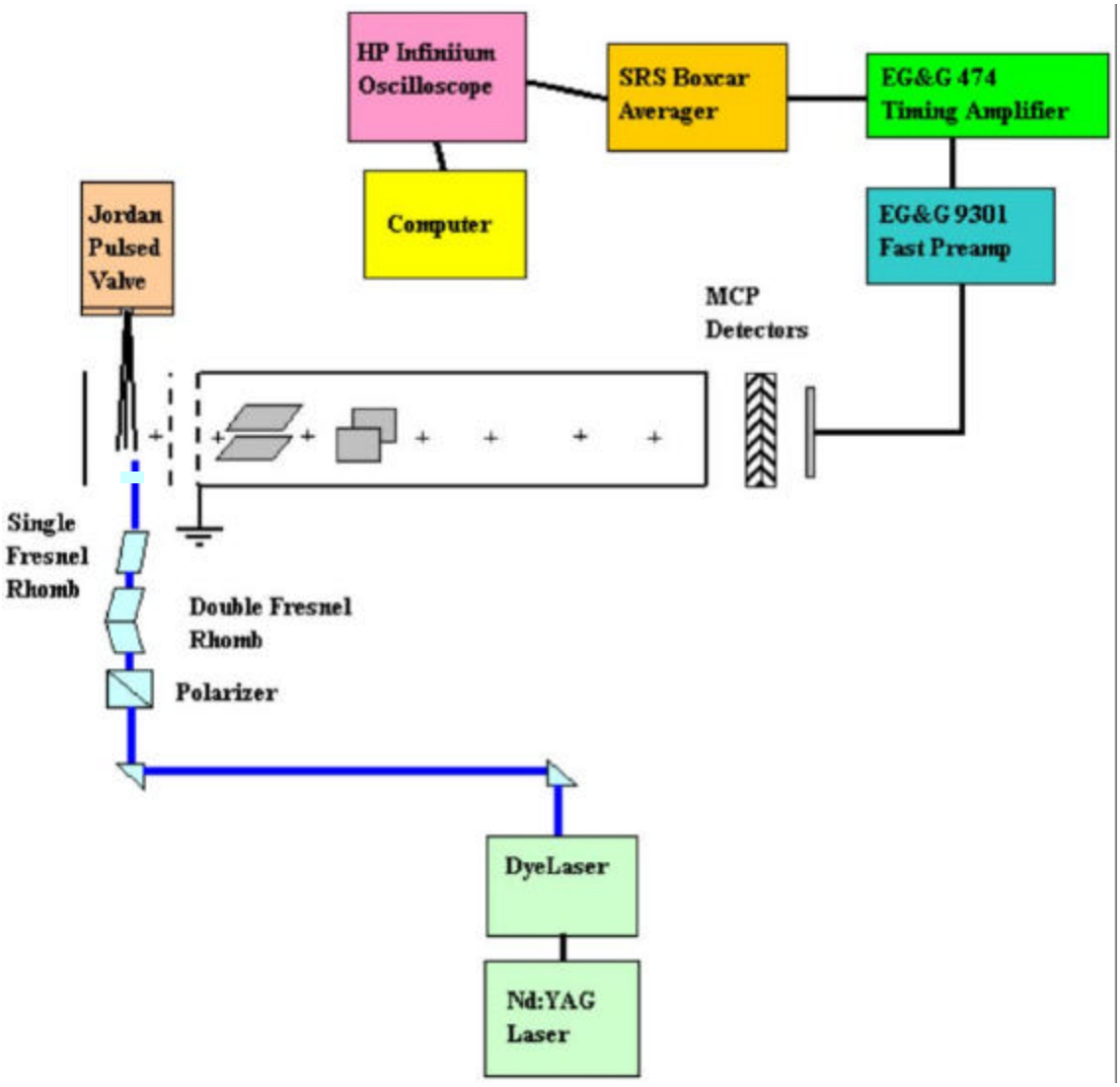

Figure 5. Diagram of the complete setup to acquire time-of-flight mass spectra and multiphoton ionization as a function of laser light polarization.

Fresnel rhomb. The purity of the circularly polarized light was assured by using the (3+2) REMPI of xenon. When the light was circularly polarized, the mass spectrum of xenon would decrease to minimum very close to zero. This effect in xenon arises from the fact that a three-photon excitation from the ground state to the 6s state is a forbidden transition when using circularly polarized light. Once the angles for the circularly polarized light were known, a circularly polarized light identification card was used to identify the helicity of the light as right or left circularly polarized for a given angle. The observations of the angle between the plane polarized light and the axis of the single Fresnel rhomb helped to confirm the helicity also. Thus, al1 the polarization components were carefully aligned to ensure satisfactory circularly polarized light. After becoming circularly polarized, the laser light entered a linear time of flight mass spectrometer previously used by Shannon Mahurin (Dissertation 2000). The mass spectrum and multiphoton ionization spectra were performed on this apparatus.

Racemic and (*R*)-(+)-3-methylcyclopentanone were purchased from Sigma-Aldrich with both having a purity of 99 percent and employed without any further purification. About 1 mL of sample was placed into a valve-controlled glass bulb attached to a pulsed valve on the time-of-flight mass spectrometer. The 3 Torr vapor pressure of the sample was seeded in about 450 Torr of helium, and the mixture gas was injected into a vacuum chamber by way of a pulsed valve purchased from RM Jordan Company, Inc. The mixture gas underwent nozzle-jet expansion as it was injected into the chamber of the time-of-flight mass spectrometer. The chamber pressure was held to 3.0×10^{-6} Torr during the experiments. The dye laser beam had an average power 11.5 mW. Positive ions produced a (2+1) REMPI through 3s Rydberg state of racemic and

(*R*)-(+)-3-methylcyclopentanone, and they were extracted from the ion source using a high voltage pulse and detected by a dual microchannel plate detector at the end of the 1.5 m long flight tube in the time-of-flight mass spectrometer. After being detected by the micro-channel plates, the signal was amplified by a preamplifier, which fed into an Ortec 474 Timing Filter Amplifier, and processed with a Stanford Research System 250 Gated Integrator and Boxcar Averager. The signal was monitored with a digital Agilent Infiniium 500 MHz oscilloscope. For recording spectra, data acquisition was achieved with a Stanford Research System 245 Computer Interface attached to a computer using a Labview program.

Before recording the MPICD data using the REMPI technique, a mass-selected positive ion signal was chosen to be recorded and averaged for 1000 shots using Agilent Infiniium 500 MHz oscilloscope. By averaging over 1000 shots on the oscilloscope, the signal-to-noise ratio was enhanced while smoothing any very small signal difference between the left and right circularly polarized light excitations. The mean value was used as final signal intensity. The same measurement was repeated 20 times with racemic 3-methylcyclopentanone and then the sample was immediately changed to (*R*)-(+)-3-methylpentanone without altering any other experimental conditions. The averaged parameter, g factor, was used to evaluate MPICD effect. The dissymmetric g factor takes on the form as seen in the previous chapter on circular dichorism. The g factor is represented in Equation 2.13 as

$$g = \frac{2\left(I_L - I_R\right)}{\left(I_L + I_R\right)} = \frac{\Delta\varepsilon}{\varepsilon}.$$

Results and Discussion

The first data to be recorded for racemic and (*R*)-(+)-3-methylpentanone were the mass spectrum. The dye laser output wavelength of 397.5 nm was used to view the REMPI through the 3s Rydberg state while achieving the mass spectrum (see Figure 6). The wavelength of 397.5 nm corresponded to the two-photon resonance for the n→3s 0-0 Rydberg transition. The parent ion signal is absent in the time-of-flight mass spectrum because of its rapid photodissociation into various fragment ions. The mass spectrum matches the previously published mass spectrum.[26]

From the mass spectrum, the mass 39 signal that corresponds to the $C_3H_3^+$ positive ion was gated with the boxcar and set to be used for the (2+1) REMPI spectrum of racemic and (*R*)-(+)-3-methylpentanone. The REMPI spectrum was observed over the wavelength range of 393 nm to 400 nm using the dye laser (Figure 7). Both racemic and (*R*)-(+)-3-methylpentanone displayed similar multiphoton ionization spectra. The largest signal intensity for the multiphoton ionization spectrum occurred at 397.5 nm. In Figure 7 the (2+1) REMPI spectrum of 3-methylcyclopentanone shows n→3s transition by monitoring mass 39 signal.

Keeping the dye laser wavelength at 397.5 nm and still gating the mass 39 cation, the MPICD data were recorded by measuring the signal intensities for left and right circularly polarized light. Each data point was averaged for 1000 shots when using the left and right circularly polarized light. The left and right circularly polarized light signal intensities, I_L and I_R, respectively, were normalized by a factor of $(I_L+I_R)/2$ for each data point of racemic and (*R*)-(+)-3-methylpentanone. The normalized signal intensities for racemic and (*R*)-(+)-3-methylpentanone are shown in Figures 8 and 9.

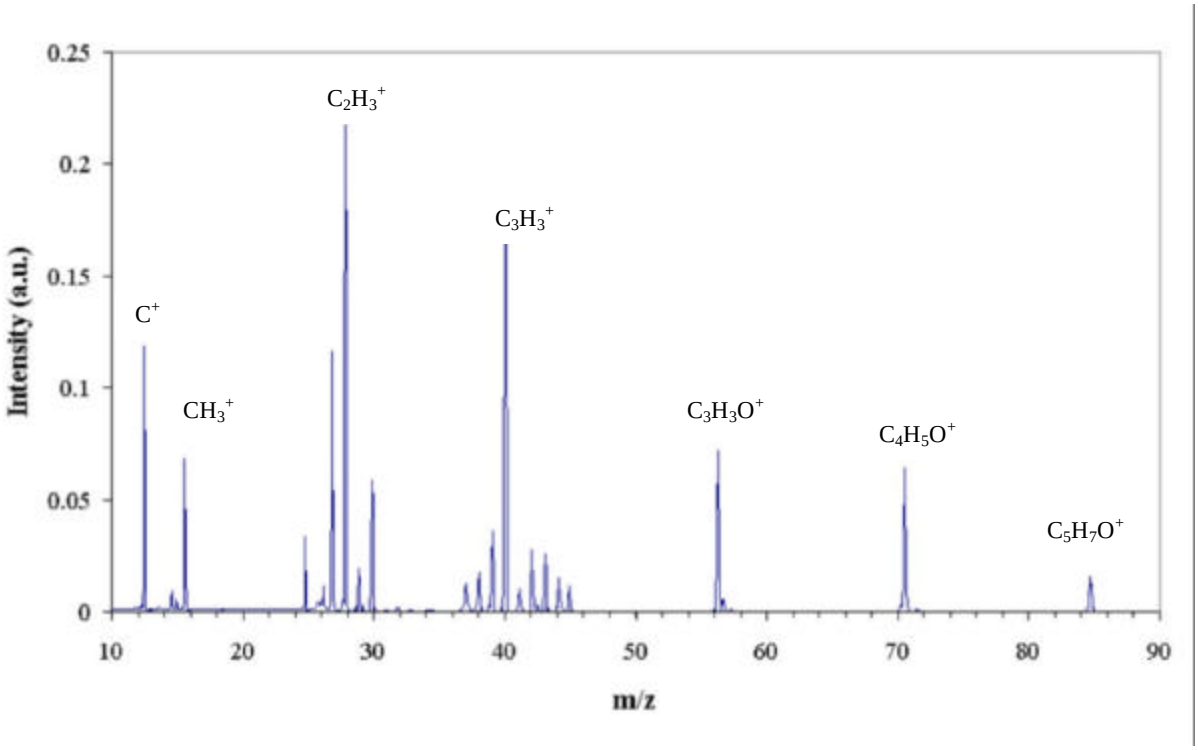

Figure 6. The (2+1) REMPI time-of-flight mass spectrum of 3-methylcyclopentanone with two-photon excitation of 3s Rydberg state at 397.5 nm. No parent ion is seen in this spectrum.

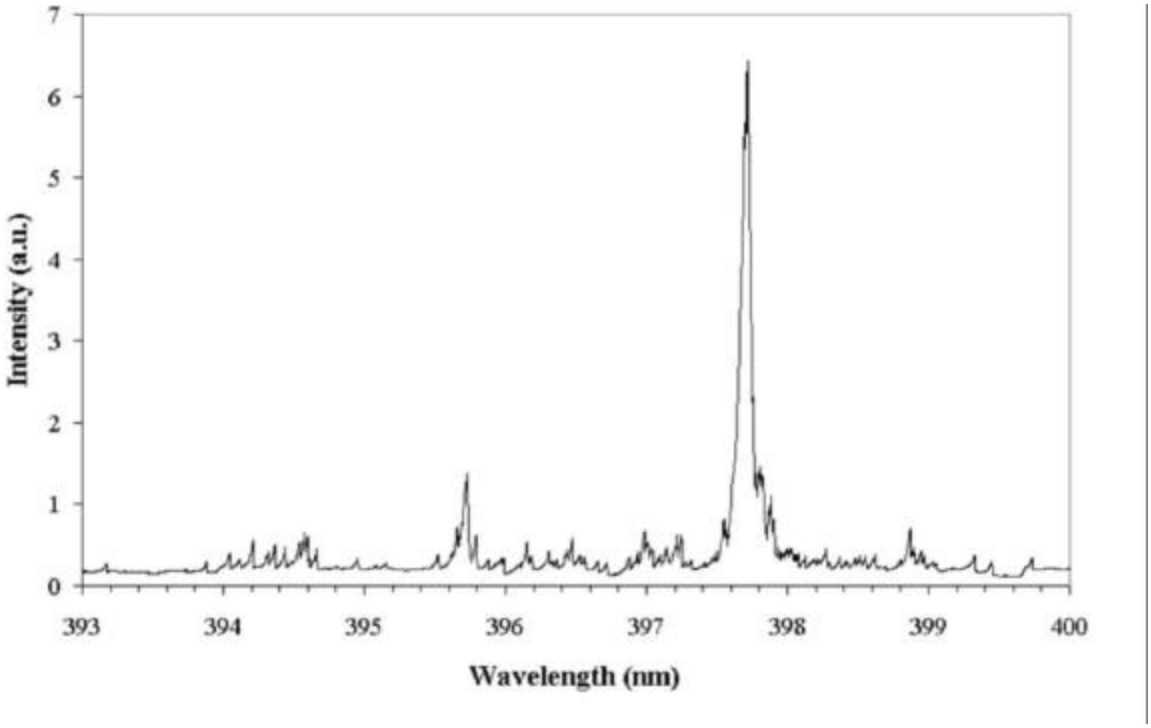

Figure 7. The (2+1) REMPI spectrum of 3-methylcyclopentanone for n→3s transition, which shows a strong 0-0 band origin and some vibronic bands. The largest ionization intensity is around 397.7 nm.

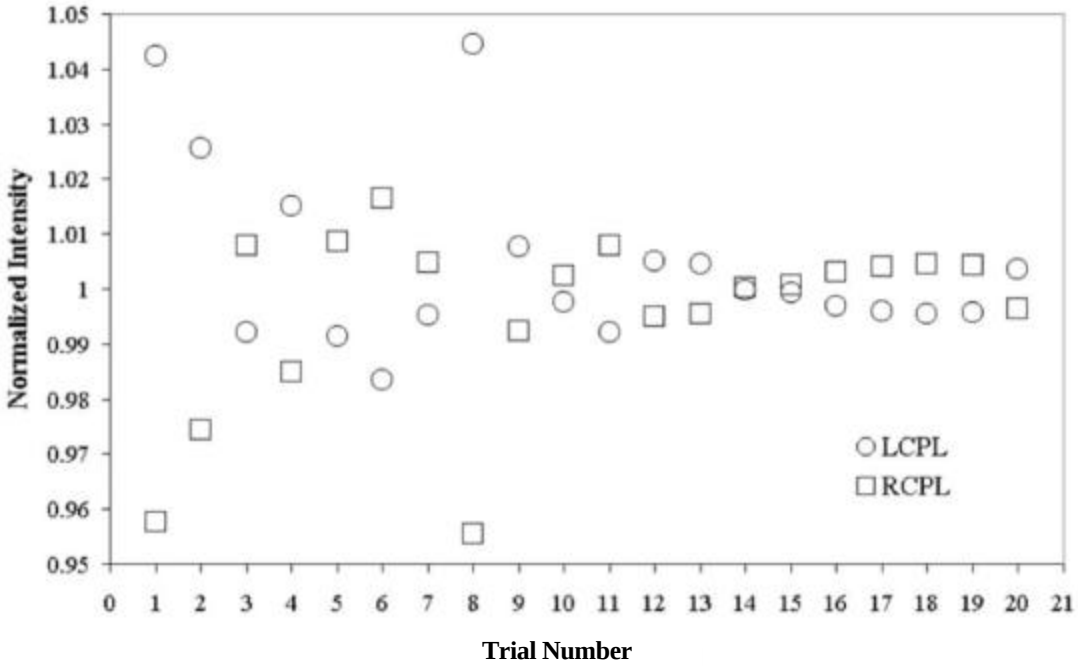

Figure 8. The normalized signal intensities for (2+1) REMPI of racemic 3-methylcyclopentanone using left and right circularly polarized light with a wavelength of 397.5 nm. The LCPL and RCPL refer to left and right circularly polarized light respectively.

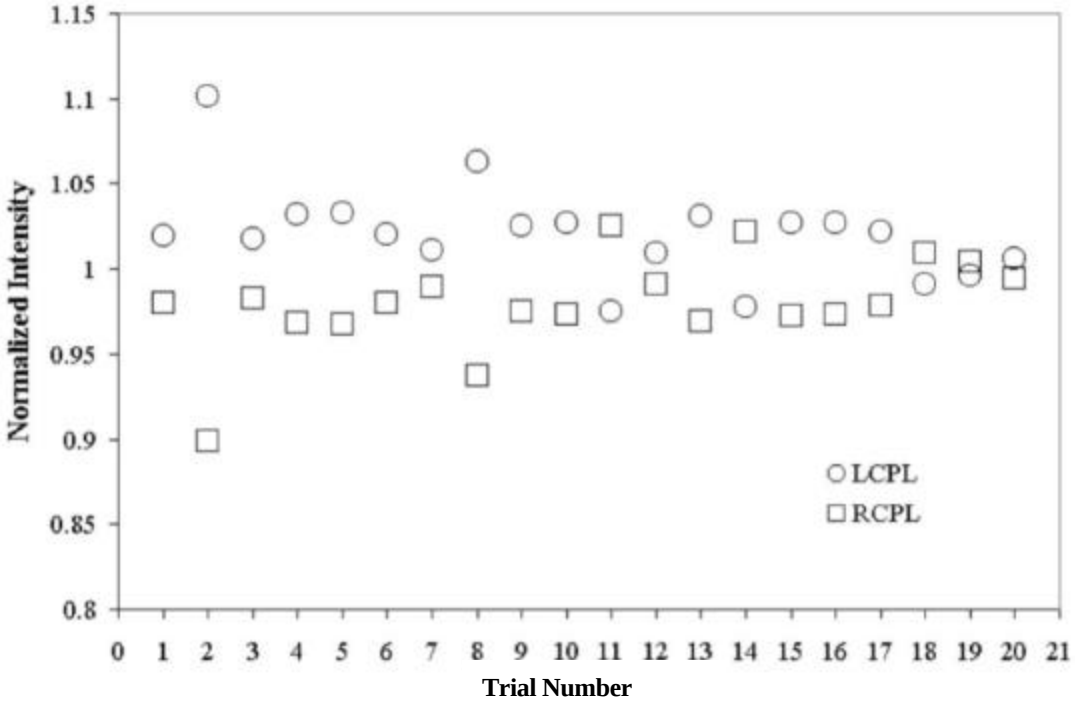

Figure 9. The normalized signal intensities for the (2+1) REMPI of (*R*)-(+)-3-methylcyclopentanone using left and right circularly polarized light with a wavelength of 397.5nm. The LCPL and RCPL refer to left and right circularly polarized light respectively.

From Figure 8, one can see that the MPICD for racemic 3-methylcyclopentanone fluctuates between the intensities for left and right circularly polarized light. This effect comes as no surprise since both enantiomers of 3-methylcyclopentanone are present and possess intensities that tend to cancel one another. When it comes to the MPICD of (*R*)-(+)-3-methylycyclopentanone in Figure 9, one notices that left circularly polarized signal intensities are larger than those signal intensities arising from the use of right circularly polarized light. Due to laser power fluctuations, the signal intensities are different for each run no matter if left or right circularly polarized is being used. The dissymmetric g factor was measured for each of the 20 trials. The average g factor for 20 runs of racemic 3-methylclyopentanone was $0.83 \pm 0.13 \times 10^{-2}$, and the average g factor for the 20 runs (*R*)-(+)-3-methylcyclopentanone was $4.1 \pm 0.23 \times 10^{-2}$. A larger g factor was expected for the (*R*)-(+)-3-methylcyclopentanone because (*R*)-(+) enantiomer reacts differently to each circular polarization of laser light. The MPICD of (*R*)-(+)-3-methylcyclopentanone is positive, just like the single photon circular dichorism around 165 nm, corresponding to the n→3d transition.[9] With the g factor of racemic 3-methylcyclopentanone being small (close to zero), the possibility of system error introducing a false circular dichroism effect was eliminated because the single photon circular dichroism is zero, which gives a g factor of zero. The MPICD measurement of racemic 3-methylcyclopentanone helped exclude the signal intensity variations arising from the laser power fluctuations, the electronic noise, and the beam position shifts when manually rotating the double Fresnel rhomb. The MPICD gives a larger effect than the single photon circular dichroism.

Once again, it is hard to give an exact measurement of error while using the averaged g factor as final result for MPICD process. As mentioned earlier, many

parameters affect the ionization signal stability, including laser power fluctuation, nozzle jet stability, laser beam position shift and power variation while setting the double Fresnel rhomb at different position, signal detection system stability, and much more.

Although 3-methylcyclopentanone was a very good candidate to study the multiphoton ionization circular dichorism, there exists one drawback. As seen and mentioned throughout this chapter, only the racemic and (*R*)-(+) enantiomers were used to acquire data because they were commercially available. The other enantiomer, (*S*)-(-)-3-methylcyclopentanone was not used due to the fact that it is not commercially available and very hard to make. Thus, arrangement was made for Steven Buchwald's group at Massachusetts Institute of Technology (MIT) to make a sample of (*S*)-(-)-3-methylcyclopentanone for the project. Unfortunately, there was not enough (*S*)-(-)-3-methylcyclopentanone to use in the experiment. If the (*S*)-(-)-3-methylcyclopentanone had been enough, the MPICD of this enantiomer would have had the signal intensity of right circularly polarized light larger than the signal intensity of left circularly polarized light because the effect is equal in intensity but opposite in sign to (*R*)-(+)-3-methylcyclopentanone; thus, the effect of MPICD could be verified through the comparison of spectra from each enantiomer. Having this enantiomer with expected spectra would eliminate the causes of system error.

Conclusion

In summary, REMPI with the use of left and right circularly polarized light was used to record the first MPICD effect of (*R*)-(+)-3-methylcyclopentanone. A time-of-flight mass spectrometer was employed to give a mass spectrum as well as the multiphoton ionization spectrum. After measuring the MPICD of racemic 3-

methylcyclopentanone, its dissymmetric g factor was $0.83 \pm 0.13 \times 10^{-2}$ while the g factor for the (*R*)-(+)-3-methylcyclopentanone was $4.10 \pm 0.23 \times 10^{-2}$. The signal intensity for the left circularly polarized light was larger than the signal intensities for right circularly polarized light in R-(+)-3-methylcyclopentanone. For the racemic 3-methylcyclopentanone, the signal intensities for the left and right circularly polarized light toggled back and forth with each other as to which was the larger intensity. The dissymmetric g factor for the MPICD was larger than the g factor for single photon circular dichroism of (*R*)-(+)-3-methylcyclopentanone. System errors existed but were somewhat overcome by the testing of racemic 3-methylcyclopentanone. The MPICD effect could have been verified further had the (*S*)-(-)-3-methylcyclopentanone enantiomer been available. Even though the (*S*)-(-) enantiomer was not available, 3-methylcyclopentanone made a good candidate for MPICD.

CHAPTER IV

CRYSTALLIZATION OF 1,1'-BINAPHTHYL

Introduction

1,1'-Binaphthyl (Figure A-1) is a chiral molecule made of two naphthalene molecules attached to each other at their respective 1 positions; it has a molecular weight of 254.33 amu. 1,1'-Binaphthyl does not possess a stereocenter, but it is chiral because of the staggered orientation of the two naphthalene molecules. When dissolved in acetone, 1,1'-binaphthyl forms chiral crystals on evaporation. Often it is a racemic mixture of enantiomeric crystals called a conglomerate. The enantiomeric excess, ee, of the conglomerate of 1,1'-binaphthyl can be increased by heating it to a melt and letting it slowly cool until crystallization. Thus, the purpose of this chapter is to produce an increased enantiomeric excess of 1,1'-binaphthyl crystals while using beta irradiation.

A little over 30 years ago, Pincock et al. studied the optical activity of 200, 0.20 g samples of 1,1'-binaphthyl crystallizing at 150°C from their melts.[27] This experiment yielded crystals having a guassian-like distribution of optical rotations centered around zero degree while a high optical purity of 90 percent was rare and exceptional. They found that the optical activity of 1,1'-binaphthyl from a melt was truly spontaneous.[28] Pincock discovered that heating and then cooling the substance at certain temperatures, converts racemic optically inactive 1,1'-binaphthyl into an optically active form. The (+)/(-) optical activity refers to the optical rotation where the (+) denotes a positive or clockwise rotation and the (–) denotes a negative or counterclockwise rotation as linearly polarized light passes through the medium. Thus, the crystallization of 1,1'-binaphthyl is like flipping a coin to see if heads come up or tails, but it comes up randomly as (*R*)-(-) or

(*S*)-(+). Pincock later found the handiness could be influenced by other chiral molecules, and the (*R*)-(-) or the (*S*)-(+) enantiomer could be selectively produced.[29]

1,1'-Binaphthyl is a racemic mixture in the liquid or molten phase but can become more resolved in the solid phase.[30] The liquid phase has a low barrier for racemization with a half-life of ~0.5 seconds at 158°C, its melting point (Figure 10). Thus, the melt becomes totally racemic within a few seconds.[30] Above 145°C and especially at 150°C, the chiral form is more stable than the racemic form; but an unstirred melt at 158°C cooling to crystallization will result in a conglomerate crystallization consisting of statistically equal numbers of the (*R*)-(-) and the (*S*)-(+) crystals. When in the crystalline solid state, the racemization rate becomes really small at room temperature, and (*R*)-(-) or (*S*)-(+) enantiomers do not interconvert.[30] Then, the racemization half-life changes to ~ 15 minutes at 50°C.[30] The maximum optical rotation is ± 245° for enantiomerically pure 1,1'-binaphthyl dissolved in benzene.[31] Kondepudi et al. have shown that stirring molten 1,1'-binaphthyl until crystallization will cause an increase in optical purity close to 80 percent while not stirring gives an optical purity close to zero.[31] In the solid state, van der Waals forces dominate 1,1'-binaphthyl and give the naphthalene rings a solid state angle of ~68°.[32] The angle between the naphthalene rings produces the chirality.

Experiments were conducted to see the origin of molecular chirality by parity non-conservation during beta decay.[33] Recently, Mahurin et al. found that by irradiating evaporating aqueous solutions of sodium chlorate with β-particles from a ^{90}Sr source produced more (+) than (-) crystals and vice versa when crystallization took place under

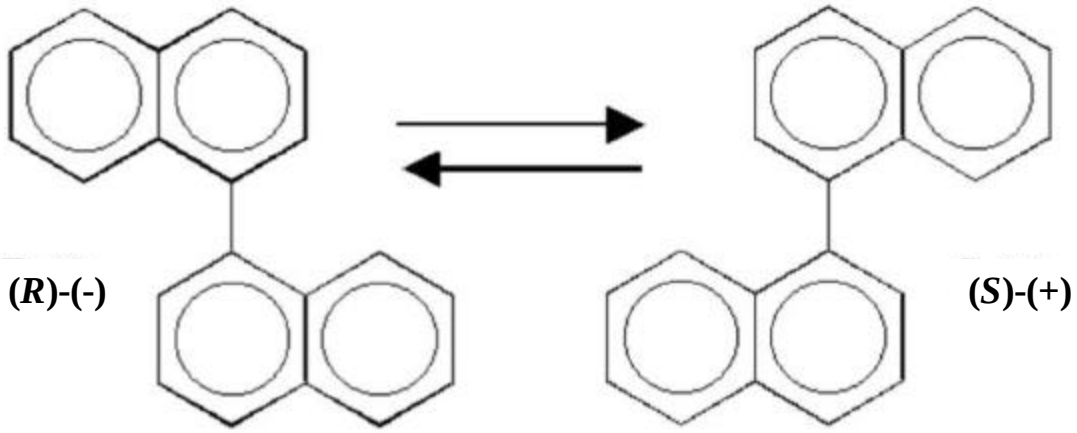

Figure 10. The racemization of 1,1'-binaphthyl enantiomers.

a Na-22 source with β^+-particles.[34] The overall crystal count is about 50/50 even though each Petri dish may have been mainly (+) or (-).[34]

With the findings of Pincock et al.[28], Kondepudi et al.[31], and Mahurin et al.[34] at hand, an attempt was made to mix the best of all the selected experiments. A decision was made to see if irradiating 1,1'-binaphthyl with β-particles would produce an enantiomeric excess of one enantiomer while employing the methods of crystallization used by Pincock et al.[28] The β-particles possess a left-handed helicity that may make the 1,1'-binaphthyl more resolved upon crystallization.

Experiment

In this experiment, a ^{90}Sr source with a radiation dosage of 26.970 mrad/h at a distance of 0.35 meters was used to produce the β-particles. The source's half-life is 28.1 years and each particle emitted has an average energy equal to 0.546 MeV. These β-particles are energetic polarized electrons with an 80 percent left-handed helicity.[34] The ^{90}Sr decays to a Y-90 with a half-life of 2.67 hours, and it emits an electron with an energy of 2.28 MeV. The radioactive source was kept at the Radiation Calibration Laboratory at Oak Ridge National Laboratory (ORNL) and handled by Dr. James Board.

For this experiment, four 0.50 gram samples of 1,1'-binaphthyl, purchased from Acros and immediately vacuum sublimed, were simultaneously heated to 180°C in a silicon oil bath for 20 minutes while being exposed to β-particles. The oil bath was used to eliminate any sudden fluctuations in temperature as well as to ensure a homogenous temperature for the samples. The samples were placed in Pyrex glass holders (Figure 11).

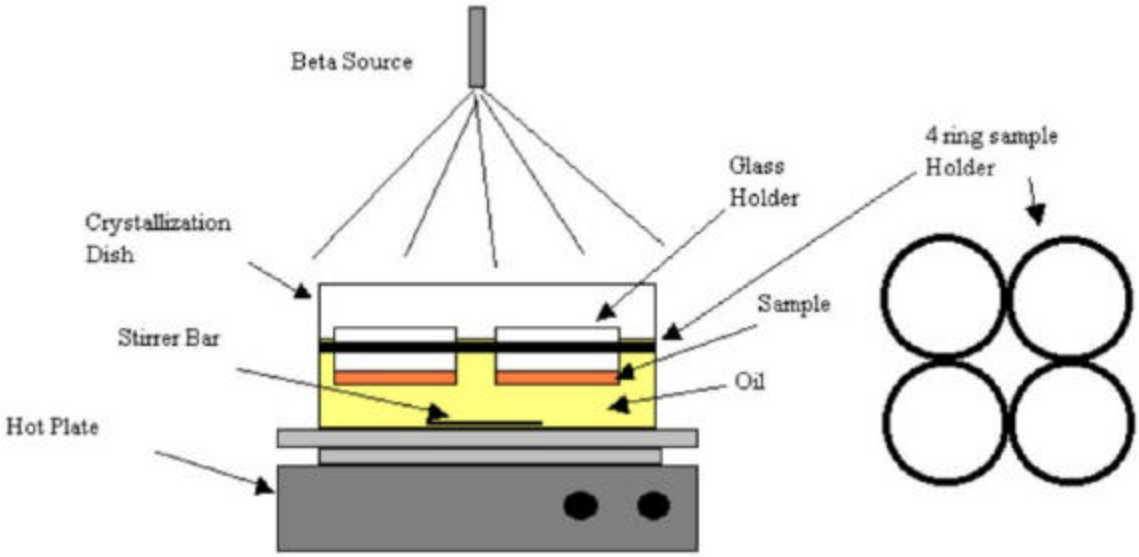

Figure 11. The experimental setup for the beta irradiation of 1,1'-binaphthyl.

The holders were made in such a way as to expose as much surface area to the β-particles as possible. The actual samples were placed about 15 cm from the source and heated until they were completely in the molten state. The melt was then cooled to 150°C while remaining under the β-source until crystallization was complete. Crystallization took anywhere from four to six hours to occur. Any enantiomeric excess obtained during the crystallization process was retained in the crystals since interconversion of enantiomers does not occur in the solid state. The crystals were quickly dissolved in ~ 40 mL of benzene where the racemization of the enantiomers has a half-life of about 10 hours (Figure A-3). Thus, each sample had a concentration of 0.04915M before the enantiomeric excess was observed by an optical rotation measurement using a Perkin-Elmer 241 Polarimator. The sodium D line, 589 nm, and a sample cell with a 10 cm pathlength were used to collect the data. Controlled sample sets without β-irradiation were carried out in the same manner. After the optical rotation measurement, the 1,1'-binaphthyl was recovered from the benzene by evaporation using a rotating evaporator so that it could be used for future trials. Unlike Kondepudi et al.[31], the variable and the control trials were all performed without physically stirring the sample. Both variables and control samples were left unstirred.

Results and Discussion

For 12 crystallizations under the β-source, the average excess was $-2.7 \pm 10.3\%$ and $-5.1 \pm 5.3\%$ for the 13 samples not under the β-source. Both cases are close to zero as expected since both enantiomers were randomly produced. The greater spread of the enantiomeric excess under the β-source versus not being under the source is similar but not as great as that for stirring 1,1'-binaphthyl until crystallization with a stirrer bar. The

frequency of enantiomeric excess can be seen in Figure 12 for the samples not under the beta source and in Figure 13 for samples under the beta source (see Tables A-1 and A-2). It is easily seen that the rotations are small for both case, but in the case of the beta irradiated, the deviation from zero becomes greater and more frequent. Both the beta irradiated and controlled samples are presented in Figure 14, which gives a scatter of enantiomeric excess. The reason for this small similarity with Kondepudi et al. is quite simple, but first let us consider the primary and secondary nucleation rate presented by Randolph and Larson.[35] The primary nucleation rates for levorotatory, l, and dextrorotatory, d, crystals are given by the equation

$$P_l = P_d = B \exp\left[\frac{-16\pi N_A \sigma_B \nu^2}{3(RT)^3\left[\ln\left(C / C_s\right)\right]^2}\right] \qquad (4.1)$$

where the P_l and P_d are the primary nucleation rates of l and d crystals, B is a constant that depends on the number of nucleation sites, N_A is Avogadro's number, ν is the molar volume of the solid, R is the gas constant, T is the temperature, σ_B is the surface energy constant, C is the concentration, and C_s is the concentration at saturation. Randolph and Larson went on to give the secondary nucleation rates. The secondary nucleation rates for l and d crystals are

$$S_i = S\sigma_i K_S\left(C - C_S\right)^a \qquad (4.2)$$

where S_i is the rate of nucleation for either l or d crystals, S is the rate of stirring, σ_I is the surface area of either l or d crystals, K_S is a temperature dependent constant, and α is a constant that depends on the compound. Now that rates of nucleation are presented, one can go on further with the explanation.

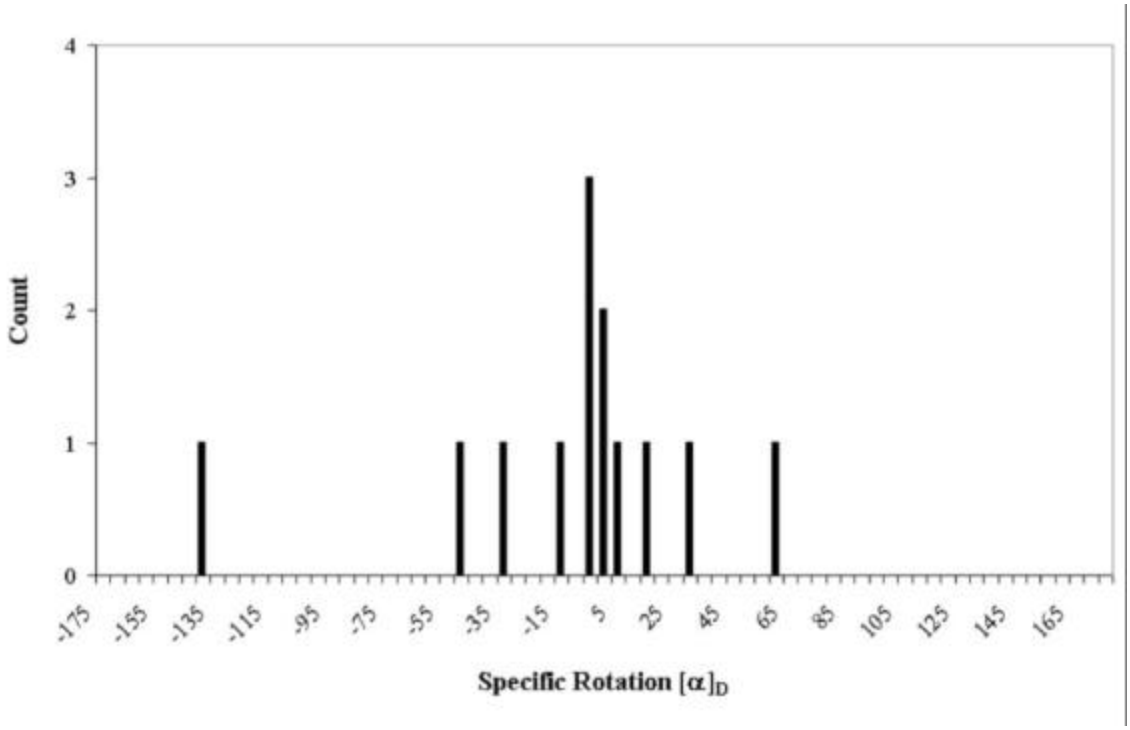

Figure 12. The frequency of specific rotations for the thirteen 1,1'-binaphthyl samples not placed under the Sr^{90} beta source.

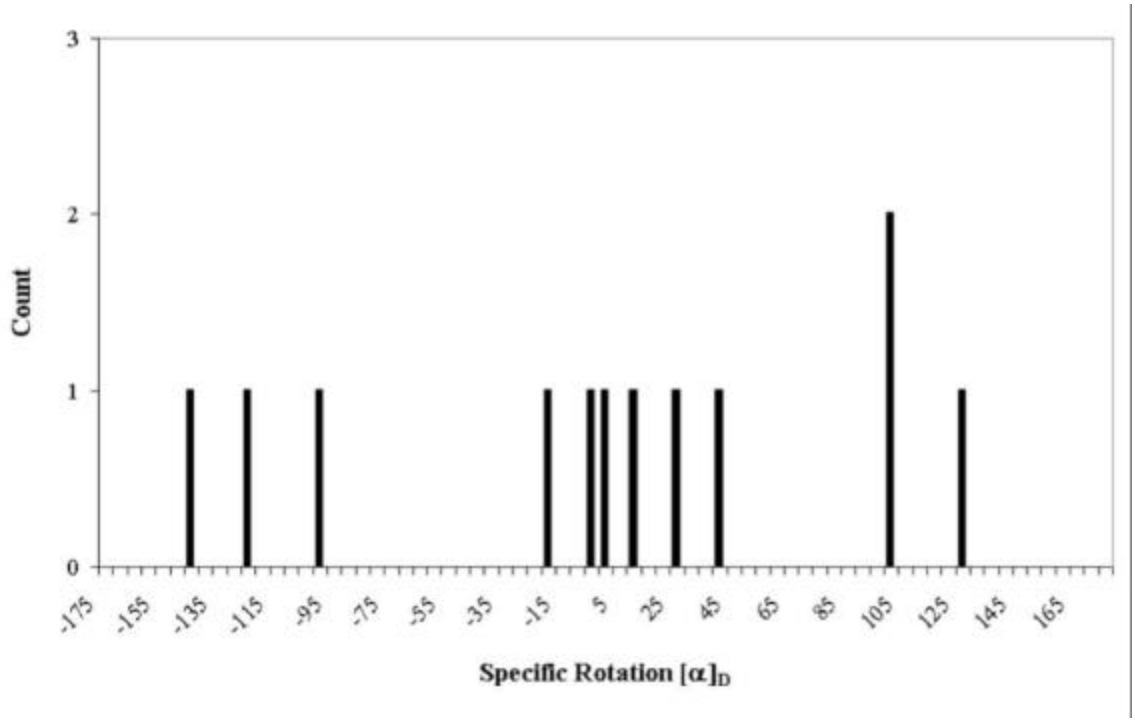

Figure 13. The frequency of specific rotations for the twelve 1,1'-binaphthyl samples placed under the Sr^{90} beta source.

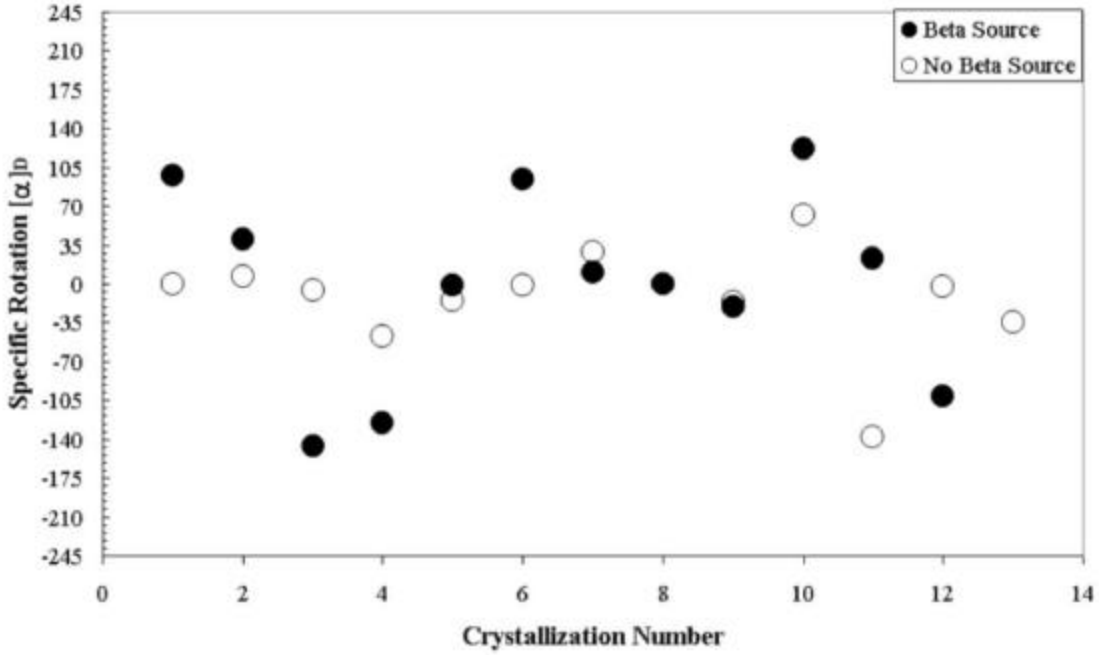

Figure 14. A scatter plot of the enantiomeric excess for 1,1'-binaphthyl irradiated and not irradiated by the Sr^{90} beta source.

Since the β-particles are very energetic, a lot of heat was dumped into the medium as the particles were slowed down; thus creating convection currents in the melt that facilitated secondary nucleation similar to that in stirring, which resulted in anenantiomeric excess.[31, 36-38] Thermal stirring occurs as β-particles slow down. For a simple calculation, consider the assumption that all the energy of a 0.54 MeV electron goes into heating the sample. For now, let the sample be water with a surface radius of 0.015 m and a depth of 0.003 m. The electron has a penetration depth of 0.1 mm and a path radius of 0.529 x 10^{-10} m. Using the equation, $Q = mc\Delta T$ (4.3), and taking the specific heat and density of water to be c = 4186 J/kg·°C and 1000 kg/m^3, respectively, one can find the temperature difference along the electrons path. One finds that the slowing down of these β-particles can result in localized temperature increase of about 24,000°C. Since most of the heat will quickly dissipate into the rest of the solution, a more realistic value for the change in temperature comes from observing the entire volume of the sample while noting the activity of the beta source used in the experiment to be 1.6 x 10^9 electrons/sec. Taking the volume of the whole sample to be 2.12 x 10^{-6} m^3, the rate for the temperature change becomes 1.56 x 10^{-5} °C/sec, but the total temperature increase after five hours is 0.28°C, which is less than 1°C. This simple calculation was performed under the assumption that water is used instead of 1,1'-binaphthyl, but the point of a temperature rise is made clearer. The temperature increase for 1,1'-binaphthyl may be considerably higher if its specific heat is close to specific heat of graphite, c = 711 J/kg·°C.

Thus, secondary nucleation is amplified by the small initial asymmetries in the number of (*R*)-(-) and (*S*)-(+) crystals, whereas in this process the crystals generate independently of each other as in primary nucleation.[31] Parent crystals make secondary crystals in large numbers by collisions while the primary nucleation rate is slowed down due to the heating of the solution; thus the chance for secondary nucleation increases and dominates.[31] For smaller samples, large ee's can be generated if the primary nucleation is low enough because all crystal growth can come from one crystal. The lower the temperature, the higher the primary nucleation rate is to produce roughly equal numbers of both (*R*)-(-) and (*S*)-(+) enantiomers.[31] Many have made ORD and CD measurements of 1,1'-binaphthyl.[39] Primary nucleation can occur in two ways: heterogeneous, when a foreign body is involved, and homogenous, when a foreign body is not involved. Secondary nucleation produces crystals of the same chirality and inhibits the growth of other crystals due to the fact that the materials are being removed from solution.[34] The slowing down of the beta rays and secondary electrons produces partially circularly polarized Bremsstrahlung.[34] The asymmetric growth of the crystals could be affected by circular dichroism absorption of this light. Fortunately, it has been shown that circularly polarized Bremsstrahlung is not the source of great optical purity.[33, 40]

Calculations were performed to prove that no Cerenkov radiation took place. Cerenkov radiation happens when charged particles travel faster than electromagnetic waves in the same medium. Beta particles lose their helicity after several collisions.[41]

Conclusion

In conclusion, β-particles do not effect the primary nucleation of the organic compounds when the enantiomeric excess is averaged over all the crystallizations. The

chance for more secondary nucleation occurs more readily with the β-particles. The spontaneity of the (*R*)-(-) and (*S*)-(+) enantiomers remains the same as for previous experiments of Pincock et al.[28] Thus, the left-handed helical β-particles do not influence the 1,1'-binaphthyl to crystallize in one particular handedness. The localized heating and convection stirring of the sample due to the bombardment of beta particles are the factors for the secondary nucleation to overcome the primary nucleation rate. If the time of crystallization were longer, the secondary nucleation could produce more chiral crystals, resulting in a higher enantiomeric excess. Another possible reason for the low enantiomeric excess arises from the fact that one of the effects of beta radiation is racemization, which counteracts the eventual selective radiolysis process (Bonner and Lemmon, 1978). This statement is contrasted by the experiments of Mahurin et al.[34] during their crystallization of beta irradiated sodium chlorate.

CHAPTER V

LASER-INDUCED CRYSTALLIZATION OF SODIUM BROMATE AND SODIUM CHLORATE

Introduction

Sodium chlorate and sodium bromate crystals (Figure A-1) have been grown by evaporation in experiments over the years. The sodium chlorate crystal synthesis has been found to be symmetric, and the crystal synthesis for the sodium bromate crystals has been found to be asymmetric. The purpose of this chapter is to use intense laser light to break the symmetric and asymmetric synthesis of sodium chlorate and sodium bromate crystals while making correlations with the polarization of the laser. For many years people have been aligning and orienting gaseous molecules with strong laser fields. Recently, ideas to align and orient molecules in solution have come into question. In this chapter an attempt was made to align or orient molecules in solution by a strong laser field prior to crystallization. These experiments were conducted to see if the polarization of the laser could influence the chirality of the crystal. The molecules studied were sodium bromate and sodium chlorate. More information about these molecules will be mentioned later, but for now, a description of how aligning or orienting molecules with a strong laser field will be discussed.

Nanosecond laser pulses have been shown theoretically and experimentally to align of molecules during the pulse duration. This is called adiabatic alignment.[48] The laser field has to be turned on slowly compared to the rotational periods in order to induce an adiabatic transport along the addressed state. This process is often interpreted as the Stark Shift to align the molecules.[48] In order for alignment to occur, laser fields

must range between 10^{10}- 10^{13} W/cm^2.[49] In diatomic molecules this corresponds to an angular amplitude of the axis of about ± 30° for the lowest molecular state.[49] An electrostatic field (DC) of 0.1 to 10 kV/cm is comparable to the pulsed field and can be enough to convert alignment and orientation. The laser pulse duration, τ, is such that $\tau \geq 5h/2\pi B$ where B is the rotational constant of the molecule. This pulse duration gives the molecule an appearance of a static field at that instant.[49] If there is no interaction between the laser field and a possible permanent dipole moment, the molecules are aligned rather than oriented.[46] Laser-induced alignment should be applicable to most molecules that posses a polarizability anisotropy, although the magnitude of the polarizability may vary greatly from molecule to molecule.[46] Friedrich and Herschbach recently suggested that exploiting the anisotropic polarizability interaction of an intense nonresonant laser field with the induced dipole moment of molecules would produce pendular states.[50] This interaction creates a potential minimum for the molecules along the polarization axis of the electric field, forcing them to liberate over a limited angular range instead of rotating freely with random spatial orientations.[46] Thus, the molecules aligned in a particular direction.

One must keep in mind that it is very important to have nonresonant laser light for the alignment with respect to both the electric and vibrational structure of the molecule, as excitation of any of these internal degrees of freedom can lead to dissociation or ionization before alignment.[46] Neutral molecules can be aligned by intense nonresonant nanosecond laser pulses. The studies of ICl, CS_2, CH_3I, and C_6H_5I demonstrate the applicability of laser alignment with YAG laser light. The maximum degree of alignment was 26.6°($\langle\cos^2\theta\rangle$ = 0.8), which is the same for I_2.[46] Alignment along the polarization

direction for a molecule will give the strongest enhanced ionization. Intense laser fields offer a rich variety of control processes allowing one to manipulate the internal degrees of freedom of a molecule.[48] Circularly polarized light can lead to nearly optically pure compounds that might function as chiral catalysts and hence be the starting point for the propagation of optical purity.[51]

While trying to increase optical purity with an intense laser, one may be able to break chiral asymmetries and symmetries using the same techniques. Intense laser fields of linear and circular polarizations were used in an attempt to break the asymmetric synthesis of sodium bromate and to promote an enantiomeric excess in highly symmetric sodium chlorate. Sodium chlorate is an achiral molecule that crystallizes into the chiral $P2_13$ space group. The crystallization of sodium chlorate produces a crystal count enantiomeric excess centered around zero when the symmetry is not broken. The enantiomeric excess for crystals is defined as the percentage excess of levorotatory or dextrotatory crystals,

$$\frac{N_d - N_l}{N_d + N_l} \times 100\% = ee \text{ (enantiomeric excess)} \qquad (5.1)$$

where N_d and N_l refer to the number of dextrotatory and levorotatory crystals, respectively. Like sodium chlorate, sodium bromate is an achiral molecule that crystallizes in the chiral cubic $P2_13$ space group. Despite the similarities with sodium chlorate, the undisturbed crystallization of sodium bromate is highly asymmetric with a larger number of dextrotatory crystals than levorotatory crystals being observed. The spontaneous crystallization of sodium bromate into predominantly (+) crystals is not understood. These asymmetries and symmetries for sodium bromate and sodium chlorate

are studied and exploited with the use of highly-intense laser light inducing their crystallization.

Experiment

Sodium chlorate, $NaClO_3$, and sodium bromate, $NaBrO_3$, were purchased from Sigma-Aldrich and used directly out of the bottle. Supersaturated solutions were prepared by dissolving sodium chlorate and sodium bromate in high-purity research-grade water (HPLC). Supersaturation was achieved by adding 100 g of sodium chlorate into 100 mL of water and adding 40 g of sodium bromate into 100 mL of water. The solutions had to be heated to about 60°C while being stirred on a hot plate to ensure complete dissolution of the solid. The solutions were removed from the hot plate, and the stirrer bar was removed from the solutions. The solutions were then placed in a Fisher Scientific FS30 sonicator for about two to three hours at a temperature of around 60°C. After sonication, the solutions were allowed to slowly cool back to room temperature. The solutions remained untouched and unperturbed for two to three days. This waiting process insured that the sodium bromate and sodium chlorate would not spontaneously crystallize out of solution but remain a supersaturated solution.

After waiting two to three days and having no spontaneous crystallization, the samples were irradiated with pulsed laser light. The samples were irradiated with a Quanta-Ray DCR Nd:YAG laser with a fundamental wavelength of 1064 nm. This fundamental beam's wavelength had a pulse width ranging from 8 nsec to 9 nsec. The beam, exiting the laser, passed through a polarizer, a quarter-wave plate, and a 5 cm focal length convex lens, respectively (Figure 15). The polarizer was used to ensure the linear

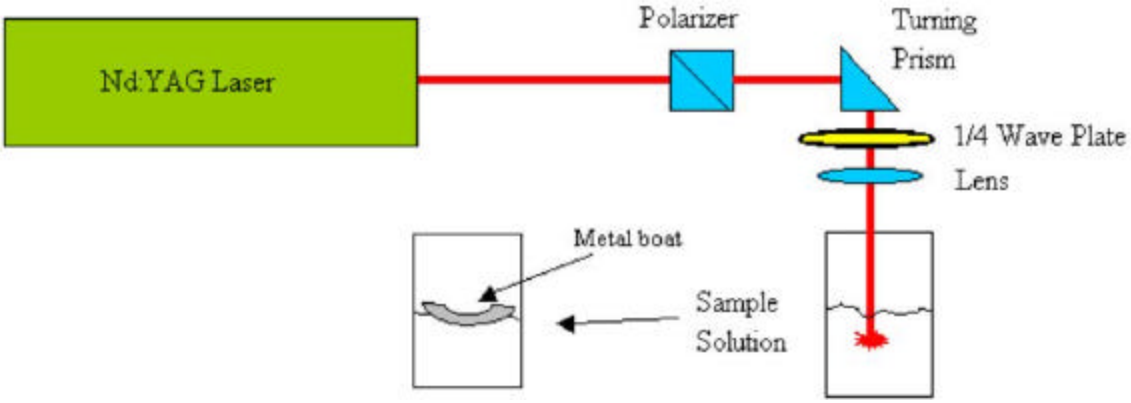

Figure 15. The experimental setup for the laser induced crystallization of sodium bromate and sodium chlorate.

polarization of the laser light before passing through the quarter-wave plate oriented at a particular angle to produce circularly polarized light. The circularly polarized light was focused by a 5 cm focal length lens to increase the power density before entering into the sample solution. The 1064 nm beam at a repetition rate of 10 Hertz had an average laser power of one watt, which results as 0.1 joules per pulse. The peak power of the beam became ~ 1.24 x 10^3 GW/cm^2 after focusing. The samples were exposed to the laser light for one minute. The focusing of the beam into the solution produced an emission of light at the focal point accompanied by an audible snapping sound. The focal point of the laser into the solution was less than a half centimeter below the surface.

The laser light entered the vials or Petri dishes from the openings on top. The Petri dishes were used only for sodium chlorate because the crystals grew large enough to be counted by hand. The concentration was dropped to 85 g of sodium chlorate in 100 mL of water. The concentration was changed to avoid spontaneous crystallization by evaporation due to the large surface area exposed in the Petri dishes. The samples were irradiated with linearly polarized and left and right circularly polarized light. The laser light passed through a given dish at five points within the one minute of irradiation. The Petri dishes were filled with 25 mL of sodium chlorate solution. Seed crystals formed immediately after irradiation. The dishes were set aside to allow the sodium chlorate to crystallize by evaporation. The crystals were allowed to grow into larger crystals for one day. Blank samples that had not been irradiated with 1064 nm light were allowed to crystallize also. When the crystals were removed from solution, the average crystal size was two to three millimeters in length and width and about one millimeter thick. The crystals were analyzed between polariod films with an incandescent light source. The top

polarized film was rotated to determine if the crystal being inspected was rotating the linearly polarized light in a positive, (+), clockwise direction or in a negative, (-), counterclockwise direction. Due to the morphology of the crystals, this method of analysis did not work for the sodium bromate crystals; thus, a new method was employed. The counting method did not work for the sodium bromate crystals because they were too small and, most importantly, too translucent to observe any credible rotation whether clockwise or counterclockwise.

Since the sodium bromate crystals were difficult to analyze, the setup was changed by eliminating the Petri dishes and adding 4 dram vials with screw-on tops to hold the sample solutions. The samples were still to be irradiated with linearly polarized and circularly polarized light for one minute. The light would be focused at one spot in the solution for the entire minute of irradiation. The light would still enter in from the top, but immediately after irradiation, the vial's cap would be screwed into place. This technique would allow the samples to crystallize without being exposed to unnecessary contaminates. The use of the capped vials proved to be superior to the use of the Petri dishes. Both sodium bromate and sodium chlorate were prepared as mentioned earlier. The samples containing 12 mL of solution were irradiated, and once again, crystals began to form immediately after irradiation. The crystals were given one day to grow. Since the vials have a small diameter of about 2 cm, an extremely large number of small crystals were formed along the bottom of the vials. There were too many crystals to be counted, thus the crystals were harvested by removing the excess solution from the vials while allowing the crystals to dry out by evaporation with the cap being removed from the vial. The cap for the blank samples, not irradiated by the laser light, had to be removed in

order to achieve crystallization. Each vial of sodium chlorate and sodium bromate crystals was placed in a mortar and pestle and ground into a coarse granular powder. Then, the index of refraction of the powdered samples were matched to that of a mixture of carbon disulfide, CS_2, and carbon tetrachloride, CCl_4, using known indices of refraction and by observation. Matching the indices of refractions for sodium chlorate and sodium bromate suspensions was first used by Bartus and Vogl.[52] The indices of refraction for carbon disulfide and carbon tetrachloride are 1.63 and 1.460, respectively. The refractive index for the sodium chlorate is 1.513. The index of refraction matching suspension for the sodium chlorate powdered crystals required 450 μL of CS_2 mixture with 1 mL of CCl_4. The index of refraction matching suspension was achieved in sodium bromate by mixing 1 mL of CS_2 with 200 μL of CCl_4. The suspensions index of refraction matched fairly well with the sodium bromate crystal, which has a refractive index around 1.6. Once the index of refraction was matched, the samples were ready to be analyzed in a Perkin-Elmer 241 polarimator. Both the sodium bromate and the sodium chlorate suspensions had all optical rotation measurements recorded at 589 nm in a cell with a one-centimeter pathlength. This method of analysis gives a enantiomeric mass difference as opposed to the enantiomeric crystal count difference.

Results and Discussion

An intense nonresonant laser with linear polarization will align a molecule in the direction of the polarization as measured by $\langle\cos^2\theta\rangle$, which depends on the J, M_J initial conditions.[53] Thus, the alignment depends on the initial rotational states, the difference between the parallel and perpendicular polarizability, the rotational constant of the molecule, and the average laser intensity.[53] Whether a molecule is oriented or aligned, the

extent of its pendular motion is revealed by the hybridization effects seen in the spectra.[54] The above information applies to a free molecule but may not apply to the laser-induced alignment or orientation of molecules in solution.

The laser field definitely initiated crystal growth. However, the aspects of alignment or orientation through strong laser fields seemed not to have a great effect on the crystallization of sodium chlorate because the production of the crystals resulted in a crystal count enantiomeric excess close to zero. Over 20,000 crystals were counted and recorded as either dextrotatory, d, or levorotatory, l, using the polariod films and the incandescent light source. The individual crystal counts for each trial can be seen in the Table A-3. Even though an individual Petri dish for a given trial may have contained more dextrotatory than levorotatory crystals or vice versa, the final count still had a crystal count excess close to zero.

For the sodium chlorate samples irradiated with linearly polarized light, there were 14 trials total with 2761 crystals counted-producing 1203 (43.6%) levorotatory crystals and 1558 (56.4%) dextrotatory crystals with a crystal count excess of 12.8 percent. Likewise for the samples irradiated with left circularly polarized light, there were 18 trials with 7764 crystals counted-producing 3971 (51.1%) levorotatory crystals and 3793 (48.9%) dextrotatory crystals with an enantiomeric excess of –2.3 percent. In the case for samples irradiated with right circularly polarized light, there were 16 trials with 3912 crystals counted-producing 2005 (51.3%) levorotatory crystals and 1907 (48.7%) dextrotatory crystals with a crystal count excess of –2.5 percent. The irradiated samples all displayed an enantiomeric excess close to zero and very similar to the non-irradiated samples. For the non-irradiated samples, the blanks, there were 16 trials total

with 5619 crystals counted-producing 2804 (49.9%) levorotatory crystals and 2815 (50.1%) dextrotatory crystals with a crystal count excess of 0.2 percent. The symmetry of sodium chlorate crystallization was not broken due to the strong laser field irradiation in a Petri dish (Figures 16 and 17) using either linearly polarized or circularly polarized light.

As for the sodium bromate and sodium chlorate using the index of refraction method, the results were slightly different. Left circularly polarized light was not used in this experiment due to the fact that there was not a noticeable difference achieved with laser polarization in the previous examples. For the sodium chlorate suspended in the carbon disulfide and carbon tetrachloride and irradiated with linearly polarized light, the average weight of the sample to be analyzed was 0.54 g. Twenty trials were analyzed with 9 (45%) being levorotatory and 11 (55%) dextrotatory. As for the solutions irradiated with right circularly polarized light, there were 20 trials having an average weight of 0.53 g with 5 (25%) being levorotatory and 15 (75%) dextrotatory. The non-irradiated samples had only 14 trials with an average weight of 0.41 g resulting in 6 (42.9%) levorotatory and 8 (57.1%) dextrotatory. The non-irradiated and the linearly polarized light samples have similar results, but the right circularly polarized light trials show an excess of dextrotatory suspensions, which is unusual for the symmetric sodium chlorate (Figure 18). The mixture of carbon disulfide and carbon tetrachloride was analyzed in the polarimator without any sodium chlorate suspended to give an optical rotation of zero; thus, the mixture had no part in the optical rotation.

For the sodium bromate irradiated with linearly polarized light and suspended in the carbon disulfide and carbon disulfide for analysis, the average weight of the sample to

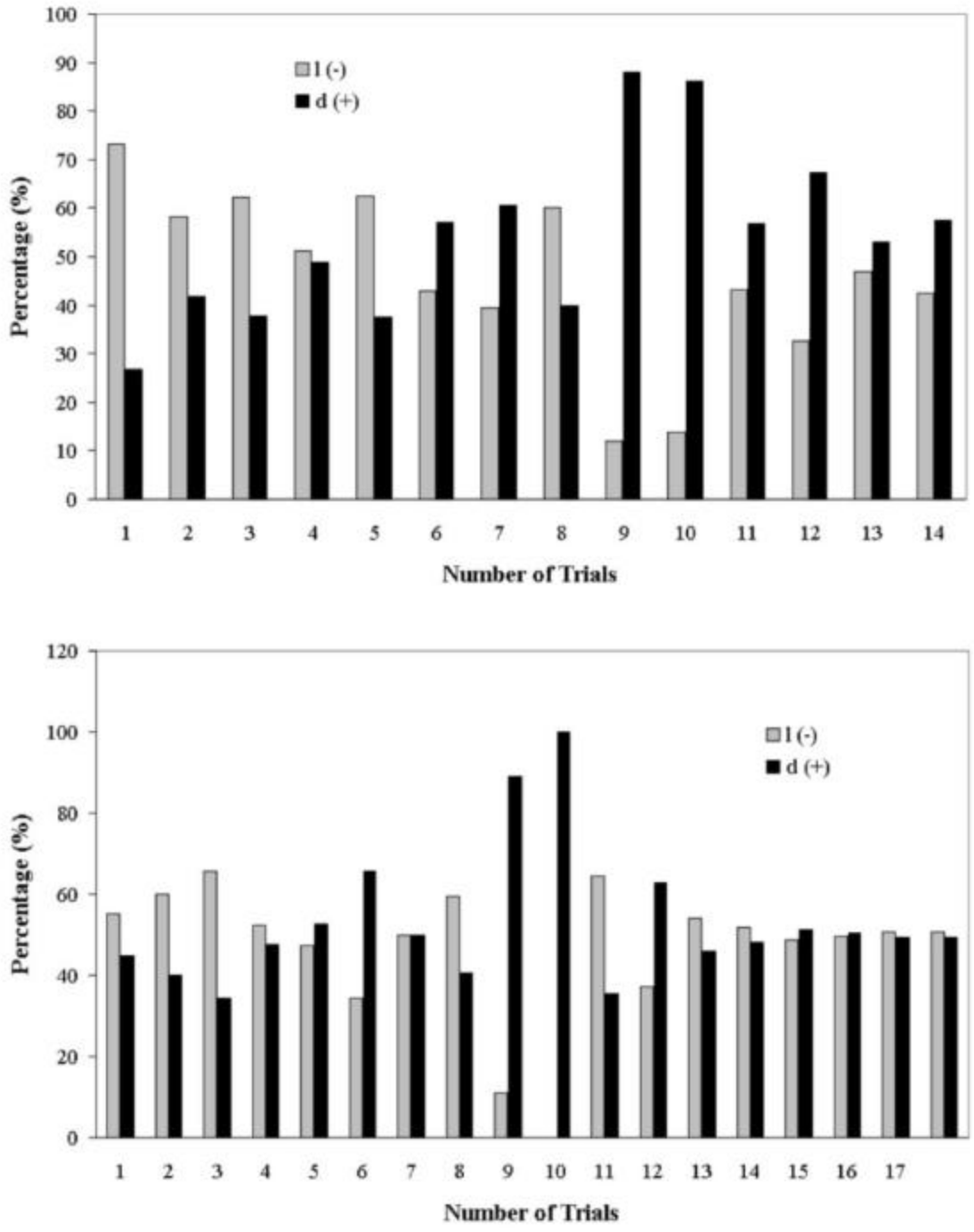

Figure 16. Histograms for the laser induced crystallization of sodium chlorate crystals grown in Petri dishes from the irradiation of linearly polarized (top) and left circularly polarized light (bottom).

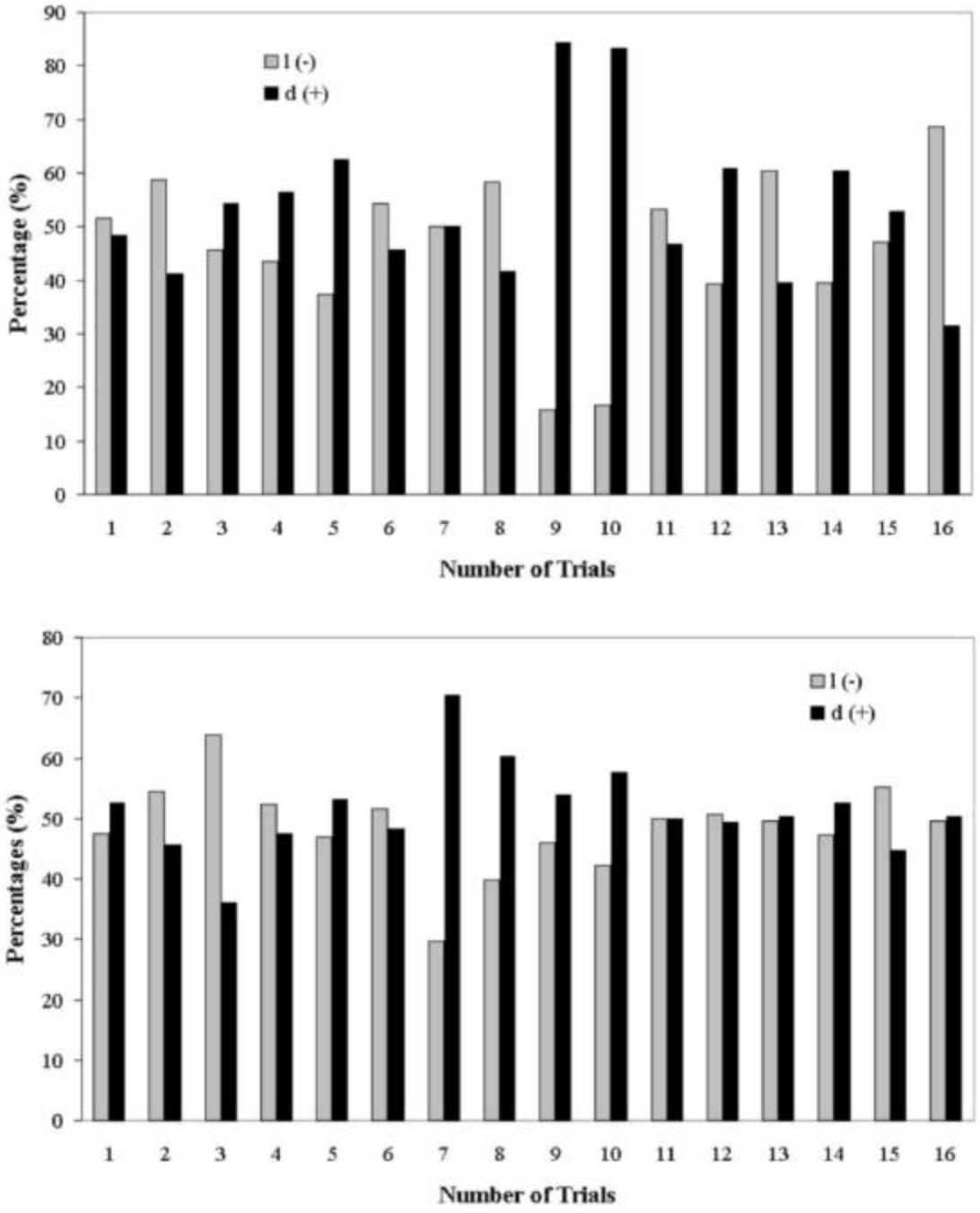

Figure 17. Histograms for the laser induced crystallization of sodium chlorate crystals grown in Petri dishes from the irradiation of right circularly polarized light (top) and from the crystallization of controlled sodium chlorate crystals (bottom).

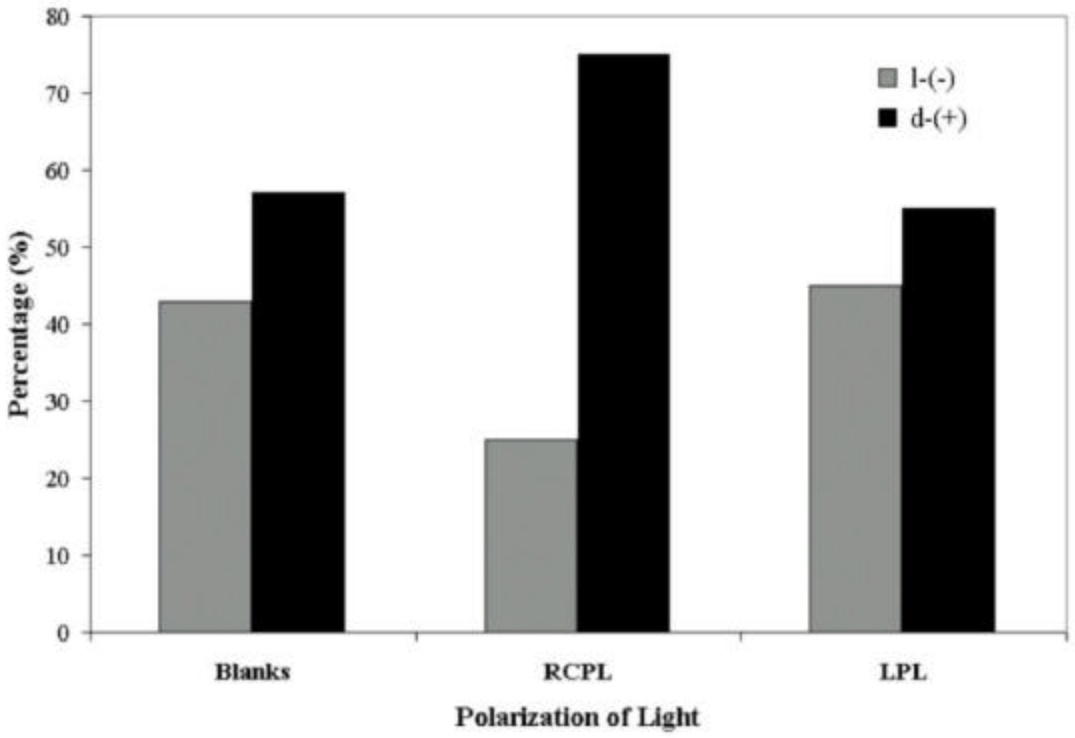

Figure 18. A histrogram for the laser-induced crystallization of sodium chlorate crystals irradiated by linearly polarized and right circularly polarized light. The crystals were suspended in a mixture of carbon tetrachloride and carbon disulfide for their analysis.

be analyzed was 0.469 g (Figure 19). Forty-one trials were analyzed with 21 (51.2%) being levorotatory and 20 (48.8%) dextrotatory. As for the solution irradiated with right circularly polarized light, there were 40 trials having an average weight of 0.51 g with 25 (62.5%) being levorotatory and 15 (37.5%) dextrotatory. The non-irradiated samples had 37 trials with an average weight of 0.79 g and resulted in 27 (73%) being levorotatory and 10 (27%) dextrotatory. The non-irradiated and the right circularly polarized light samples have similar results with an excess of levorotatory suspensions, but the linearly polarized light trials show an almost even number of levorotatory and dextrotatory suspensions, which is unusual for the asymmetric sodium bromate (Figure 19). The mixture of carbon disulfide and carbon tetrachloride was analyzed in the polarimator without any sodium bromate suspended to give an optical rotation of zero; thus, the mixture had no part optical rotation. The asymmetry to the sodium bromate was broken with linearly polarized light, and the symmetry for the sodium chlorate was broken with right circularly polarized light. Therefore, one can conclude that the polarization of the light seems to have little effect on the crystallization mechanisms.

Other eliminating processes were used to rule out any possible theories as to what was happening. The first thought was that sound waves might cause the molecules to break symmetry due to the fact that the longitudinal compression sound waves would push the molecules closer together for crystallization. A small metal boat was constructed to float on top of the aqueous solution of sodium bromate while being irradiated with the 1064 nm laser light. The laser interacting with the metal boat produced sound waves that propagated through the solution. With the assistance of Andy Fischer, 20 trials were examined under the same conditions as before, except for the

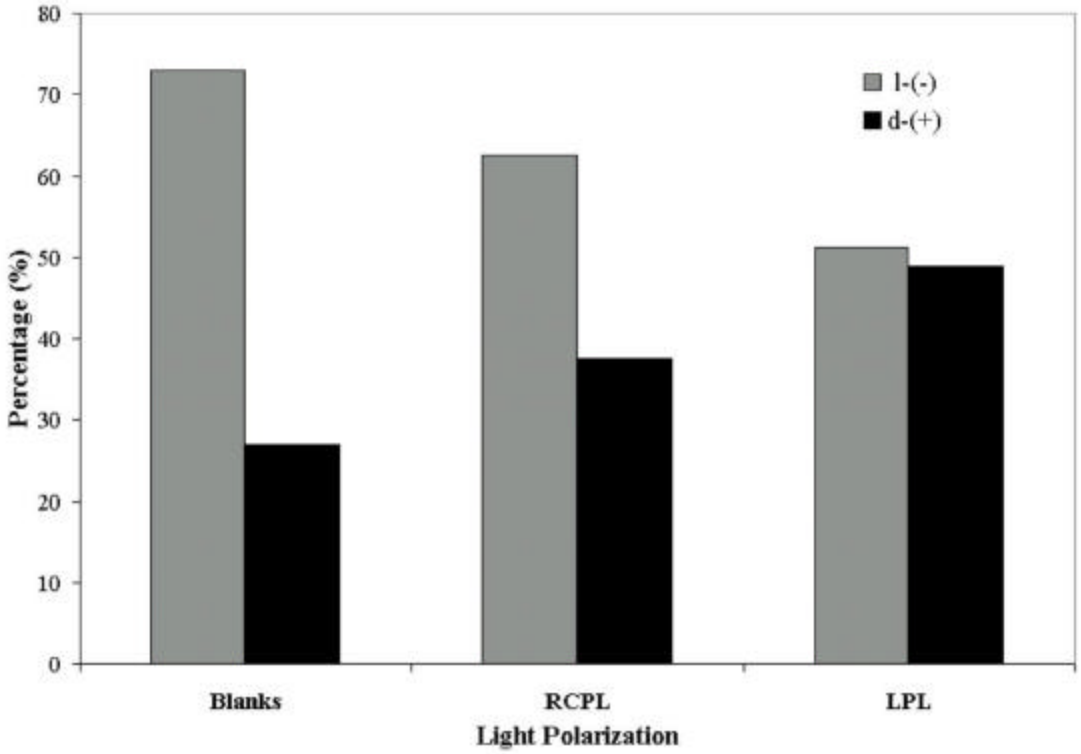

Figure 19. A histrogram for the laser-induced crystallization of sodium bromate crystals irradiated by linearly polarized and right circularly polarized light. The crystals were suspended in a mixture of carbon tetrachloride and carbon disulfide for their analysis.

metal boat, resulting in 100 percent of 20 solutions being levarotatory. Thus, this sound experiment offered evidence that the laser light was inducing the nucleation of the (+) crystal and sound waves. Another attempt was to turn up the laser power. The laser power was adjusted to an average power of 2.4 W, which more than doubled the previous power. This observation took place using the linearly polarized light that broke the asymmetry of sodium bromate. A solution of sodium bromate was irradiated again under the same conditions except for a higher laser power and no metal boat. The result was not the same as before but close to the results of the boat experiment. Mainly, the levorotatory crystal suspensions were produced. Out of the 20 suspensions, 18 (90 %) were levorotatory and 2 (10%) were dextrotatory. The laser power was decreased back to the normal operation power of one watt, and then put in single shot mode. The same conditions as above was applied. The sodium bromate solution was irradiated with a single shot of linearly polarized or right circularly polarized light. When using both linearly polarized or right circularly polarized light, the results were about the same. Levorotatory sodium bromate crystals dominated in both cases. For the solutions irradiated with a single shot of linearly polarized light, 18 trials were conducted with 17 (94.4 %) being levoratotory and 1 (5.6%) dextrotatory. As for the samples irradiated with right circularly polarized light, 14 trials were conducted with 10 (71.4%) being levorotatory and 4 (28.6%) dextrotatory. These extra observations of sound, high power, and single shot did not break the asymmetry of the sodium bromate. These experiments produced grossly larger numbers of levorotatory than dextrotatory sodium bromate (Figure 20). Although this is not understood, these results are inconsistent with the previous studies in Compton’s and Pagni's laboratories, but this inconsistency may arise

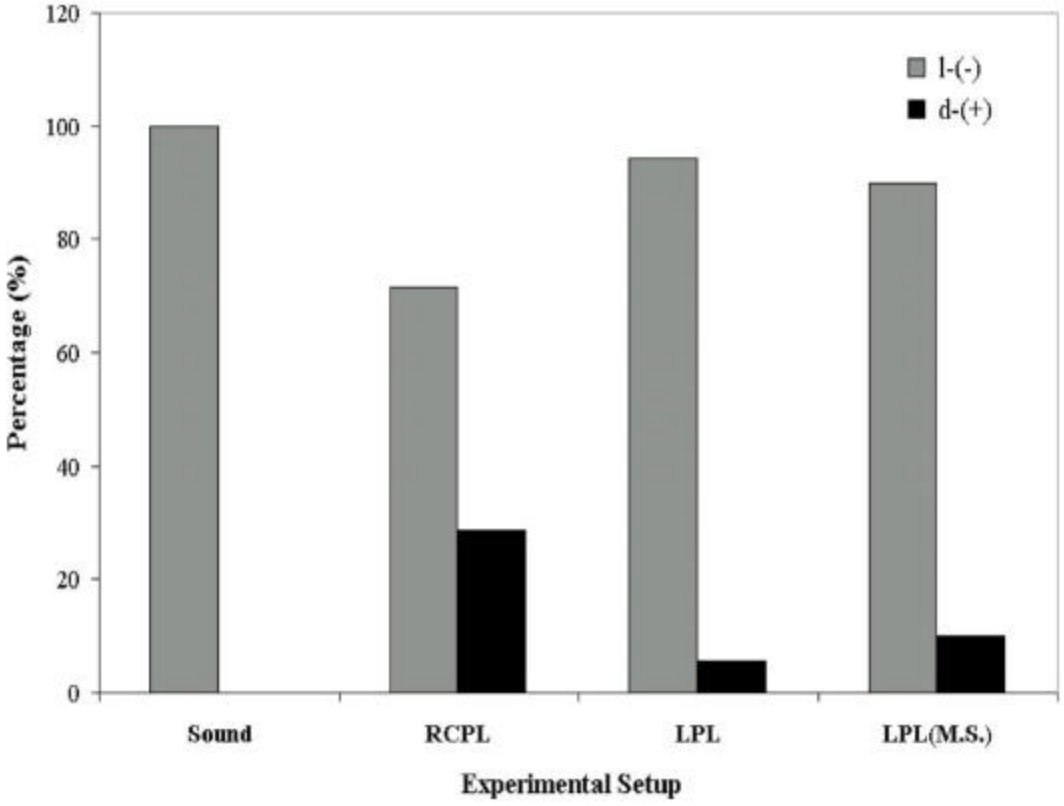

Figure 20. A histogram for the crystallization of sodium bromate crystals by laser irradiation and by sound waves. The linearly polarized and right circularly polarized light were used for the single shot experiment while only linearly polarized light was used for the high power experiment (label M.S. meaning multi-shot). The crystals were suspended and analyzed in a mixture of carbon disulfide and carbon tetrachloride.

from the fact that earlier studies of sodium bromate crystals involved crystallization by evaporation in Petri dishes, which were subject to dust and other debris. As for thjs chapter, the crystals were grown in sealed vials to avoid any unwanted debris and dust. This slight difference in experimental methods may be the cause for the strange inconsistency.

The symmetry breaking of sodium chlorate through the use of right circularly polarized light and the asymmetric breaking of sodium bromate cannot be explained at the moment, but may be due to secondary nucleation. The energy from the laser light is turned into heat and sound energy once inside the solution. The heat that is dissipated creates localized warm spots in the water producing convection currents. The nanoscale sodium chlorate and sodium bromate crystals began to swirl around and collide with one another making other seed crystals. The right circularly polarized laser light may have helped by orienting the molecules in a preferential arrangement for the sodium chlorate solutions while the linearly polarized light may have arranged the sodium bromate to a favorable alignment. Primary nucleation, which produces crystals independent of one another, has its nucleation rate slowed by the localized heating of the solution. Now, the opportunity for more crystals of one handedness is possible. As for the sodium chlorate in the Petri dishes, the laser light never remained in an area long enough during the one minute of irradiation to cause a significant temperature change in the localized region. Therefore, secondary nucleation was not dominant because the temperature change due to heating is not adequate enough to sustain a good nucleation rate; therefore, the primary nucleation rate is dominant, resulting in a crystal count excess close to zero with about an even number of dextrotatory and levorotatory crystals being produced. The intense laser

light had enough energy to heat water, but the increase in temperature does not effect the temperature of the solution for the first minute or so. A few seconds after the first minute, the temperature began to rise considerablely (see Figure A-4). One can make a crude estimate for the change in water temperature during irradiation by taking note that the laser's average power was one watt and lasted for a minute. Using equation 4.3, the specific heat and the density of water from Chapter IV, the temperature increase for a 12 mL solution is about 1.195 $^{\circ}$C. This case holds if all the energy goes into heating the solution.

Conclusion

In summary, the use of intense polarized laser light induced crystallization in supersaturated solutions of sodium bromate and sodium chlorate. The crystals formed within seconds of irradiation. The laser irradiated sodium chlorate crystals grown from the Petri dishes displayed an enantiomeric excess close to zero. As for the irradiated sodium bromate and sodium chlorate in the vials, the laser-induced crystallization broke the asymmetric and symmetric synthesis, respectively, for the crystallization of each molecule. The symmetric synthesis was slightly broken by the use of right circularly polarized light for the sodium chlorate while the linearly polarized light broke the asymmetric synthesis of sodium bromate. The exact mechanisms for laser induced crystallization for the two compounds are not known, but may be explained through primary and secondary nucleation. The primary nucleation rate was the dominant factor for the sodium chlorate crystals grown in the Petri dishes. Secondary nucleation theory helps explain what is taking place with laser irradiated sodium chlorate and sodium

bromate grown in a vial. I would like to acknowledge Andy Fischer for lending a hand in the presented projects.

CHAPTER VI

LASER-INDUCED CRYSTALLIZATION OF GLYCINE

Introduction

Glycine is an achiral amino acid. It happens to be the simplest and the only achiral molecules of the 20 natural amino acids. Its chemical formaula is $C_2H_5NO_2$ with a molecular weight of 75.07 amu (Figure A-1). When glycine is crystallized from aqueous solution, three different crystalline polymorphs, α; β; and γ, may be obtained. Of the three polymorphs, only γ-glycine forms chiral helical chains that are the focus for this chapter. In this chapter experiments were performed by way of laser-induced crystallization trying to encourage the selectivity of the chiral γ-polymorph over the two achiral polymorphs.

Glycine is the most commonly used excipient of freeze dried injectable formulations.[55] Though it is the simplest of all amino acids, glycine crystallizes in three polymorphs. These polymorphs are: γ-glycine, which is in the hexagonal space group P31 or P32, α-glycine which is in the monoclinic space group C2h5, and β-glycine which is in the space group of C2h2-P21/m or C22-P21.[56-58] The γ-glycine is the most stable at room temperature, but α-glycine crystallizes from an aqueous non-acidic or alkaline solution. Beta glycine, which is the least stable, transforms into α- or γ- glycine when in water, and γ-glycine, which is thermodynamically more stable than α-glycine, is converted irreversibly to α-glycine upon heating above 165°C. Since γ-glycine is the most stable at room temperature, this effect indicates that the spontaneous nucleation of glycine is kinetically rather than thermodynamically controlled.[59]

Glycine can take on three forms while in solution during crystallization. The three main forms are: for an aqueous neutral glycine zwitterions, $^{+}H_3NCH_2CO_2^{-}$; for low pH or protonated carbonyl group, $^{+}H_3NCH_2CO_2H$; or for high pH or deprotonation of the amino group, $H_2NCH_2CO_2^{-}$.[60] Glycine has two pK_as with values of 2.35 and 9.78; thus at pH of 3, glycine is predominately a zwitterion as expected. It has been shown that a solution of neutral glycine with no additives undergoes a rapid secondary crystallization during freezing, forming the β-polymorph.[61] The rates of formation for the secondary crystals are influenced by the pH relative to the pK_a's of glycine.[83] An increased change in the ionic strength in glycine caused by the pH adjustment significantly slows the crystallization of the neutral glycine and promotes formation of the γ-polymorph.[61] Neutral glycine adjusted to pH 3 and pH 10 crystallized much more slowly than a solution with no pH adjustment at pH 6.5. At pH 3, neutral glycine freeze dried produced predominantly γ-glycine while at pH 10 it produced a mixture of sodium glycinate and β-glycine.[61] Low rates of crystallization tend to favor the γ-polymorph while rapid crystallization favored the β-polymorph. Neutral glycine crystallizes rapidly whereas glycine hydrochloride crystallizes slowly.[61]

Adjusting the pH of glycine between 1.7 and 10.0 with HCl or NaOH caused glycine solutions to crystallize into two polymorphs during spray drying. The α- and the γ-polymorph of neutral glycine, $^{+}H_3NCH_2CO_2^{-}$, were produced along with three salts.[60] At a pH of 6.2, α-glycine would normally crystallize from aqueous solutions, but changing the pH to 4.0 or 8.0 caused γ-glycine to be the preferred polymorph.[60] Crystallization of γ-glycine by pH adjustments provides a way to improve the physical

stability of glycine-containing formulations. Spray drying glycine solutions between a pH of 9.0 and 10.0 gave predominately γ-glycine and an additional crystalline product, possibly sodium glycinate.[60] For pH's above or below 6.2, the γ-glycine polymorph became the main crystalline component. The pH adjustments prohibited the growth of α-glycine while promoting the growth of γ-glycine.

Recently Garetz et al.[59] irradiated glycine with linearly polarized and circularly polarized light. The linearly polarized light produced 22 nucleated γ-glycines out of 46 trials while the circularly polarized light produced 8 nucleated α-glycines out of 18 trials.[59] The laser induced crystallization has led Garetz et al.[59] to state that linear polarization tends to align the most polarizable axis along Z while circular polarization tends to align the least polarizable axis along Z.[59] If true, the morphology of crystallization can be controlled by laser polarization.

On the other hand, the crystallization may be laser induced, but the aspect of aligning the molecules with the polarization of laser light may not be the major contributor to the production of gamma crystals. The changing of the solution's pH by use of polarized laser light may be the main contributor that results in the solution crystallizing into γ-glycine. In order to examine this question, The laser-induced crystallization and pH change were investigated during following experiments.

Experiment

Glycine was purchased from Sigma-Aldrich and was used directly from the bottle without any modifications. Glycine was dissolved into highly purified water (HPLC) to make supersaturated solutions. The concentration of the glycine in the water was about

3.7 to 3.9 M. The glycine was heated to about 60°C and sonicated for several hours until all the sample was completely dissolved into solution. The solution was allowed to slowly cool back to room temperature. The solution was placed on a shelf for two to three days where it remained unperturbed, although it was checked for spontaneous crystallization. After no signs of spontaneous crystallization, the solution was ready to be placed into 4 drams vials with caps similar to those used in the laser-induced crystallization of sodium bromate and sodium chlorate. Each vial contained 10 to 12 mL of glycine solution. The same setup used for laser-induced crystallization of sodium bromate and sodium chlorate was used in these glycine experiments (see Figure 15). A Quanta Ray DCR Nd:YAG laser was again employed using a doughnut-shaped laser beam with a spatial intensity of

$$I = I_o \exp\left(-\left(r - r_o\right)^2 / d_o^2\right) \qquad (6.1)$$

where r_o is the distance from the beam axis to the peak intensity and d_o is the half-width for electron drop intensity of the doughnut-shaped beam.[62] The laser power used was 0.08 Joules per pulse or an average power of 800 mW, and the average peak power density of 1064 nm light was about 1 x 10^3 GW/cm^2. The samples were irradiated for one minute with linearly polarized and circularly polarized laser light from the top.[59] The solution was quickly capped off and placed on a shelf to allow time for the crystals to grow. The crystals were given a day to grow to a comparable size. The crystals were harvested by the removal of the cap and excess solution from the vials, permitting the crystals to dry by evaporation. Once the crystals were dried, they were analyzed by C-13 solid state NMR performed on a 400 MHz Solid-State NMR Varian Spectrometer. The

crystals were also analyzed by powder x-ray diffraction performed on a Philips X'Pert Difffractometer. The analysis of the crystals by the methods chosen revealed the polymorphic structure of the glycine.

A few experiments were run where the 5 cm focal length lens was removed and a 3 mm aperture was set in place (Figure 21). With the sample concentration still about 3.7 to 3.9 M, the sample solution size was reduced to about 2 mL in a 1 dram vial made of Pyrex glass with a diameter of 1.3 cm. The laser was redirected to go through the side of the vial with the cap in place at all times. The cylindrical curvature of the vial added to the amplification of the laser beam as it passed through the glass into the solution. The average laser power was changed to 0.700 W, which gives a peak power density of slightly < 1 GW/cm^2. This setup comes close to reproducing the experimental setup and conditions of Garetz et al.[63]

A few experiments were also performed using the same floating boat used in the laser-induced crystallization of sodium bromate and sodium chlorate. The boat was placed on top of the solution and irradiated with 1064 nm laser light. The interaction of the laser with the metal boat produces sound waves that propagated throughout the solution causing crystals to nucleate. The conditions remained the same as those trials taken before the solution reduction and the use of unfocused laser light. Another set of experiments involved irradiating with a different wavelength of laser light, such as a pulsed 532 nm beam from the Quanta Ray and a continuous wave 514.5 nm beam from an argon-ion laser. In later experiments, the power of the pulsed 1064 nm laser light was increased to 1.5 W for an experimental set. To check the effects of laser-induced pH of the glycine solution during irradiation, a Fisher Scientific Accumet Basic pH meter was

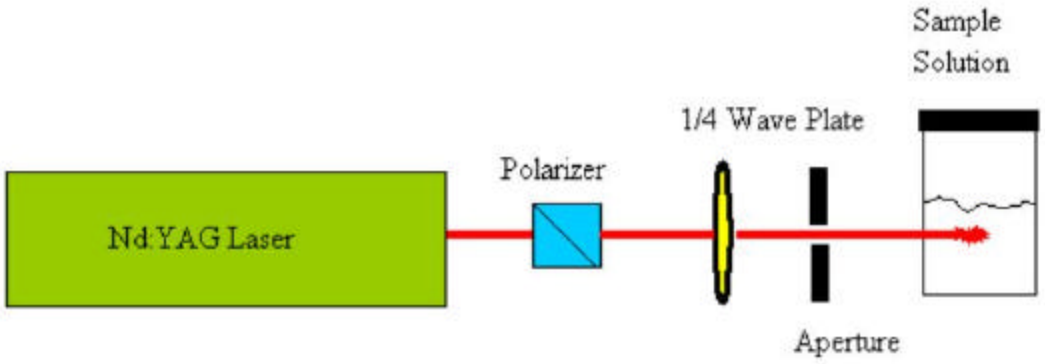

Figure 21. The experimental setup for the laser-induced crystallization of glycine using unfocused laser light.

used to measure the pH of pure water and a solution of glycine with a concentration around 3.7 to 3.9 M. Several aqueous solutions with a pH of 4 of glycine and hydrochloric acid were allowed to crystallize to help in the pH experiments. All supplementary experiments were analyzed by either solid state NMR or powder x-ray diffraction. Since the NMR and x-ray diffraction gave the polymorphs of glycine, the solid state NMR became the most used tool for the analysis due to the higher cost of operating the powder x-ray diffractometer. For all the experiments, non-irradiated glycine solutions were allowed to crystallize as the control for the experiments.

Results and Discussion

Thirty minutes after exposure, small crystals began to form along the bottom of the vials. Analysis of the crystals with solid state NMR and powder x-ray diffraction revealed traces of the α- glycine polymorph in samples containing mostly the γ- glycine polymorph, but there were a few samples of γ-glycine that contained no trace of α-glycine. In samples containing the α-glycine, no γ-glycine was detected. Therefore, if γ-glycine were present in a spectrum, the spectrum was classified as γ- glycine as long as the γ-polymorph was more abundant by peak area than the α-polymorph, and a sample was classified as α- glycine if the γ-polymorph was not present at all (Figure 22).

For the C-13 NMR analysis, the chemical shifts for the carboxyl carbon atoms of α- and γ-glycine were found to be at 176.50 ppm and 174.60 ppm, respectively (Figure 23).[64] These chemical shifts were used to determine the polymorphic structure as alpha or gamma. As for the powder x-ray diffraction (Figure 24), the determination of α- and γ-

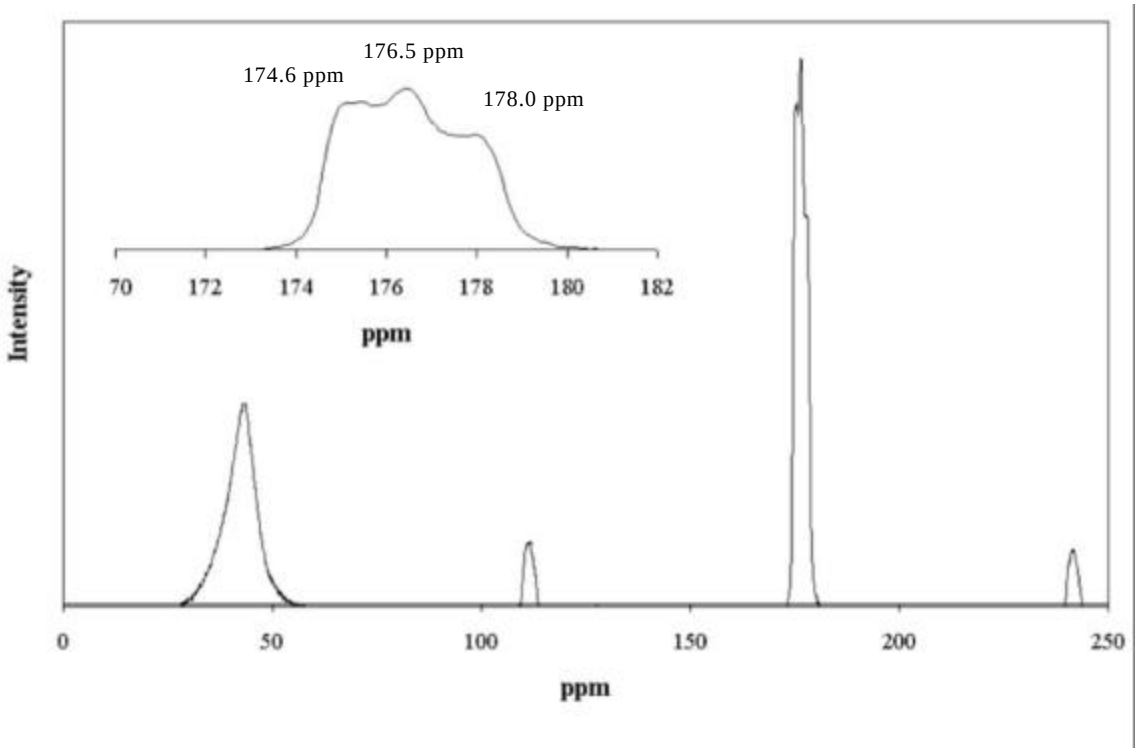

Figure 22. The solid state NMR spectra of glycine taken directly from the bottle purchased from Sigma Aldrich. All three polymorphs are present and can be seen in the region around 174 to180 ppm (α-176.5 ppm, γ- 174.6 ppm, and β- 178.0 ppm).

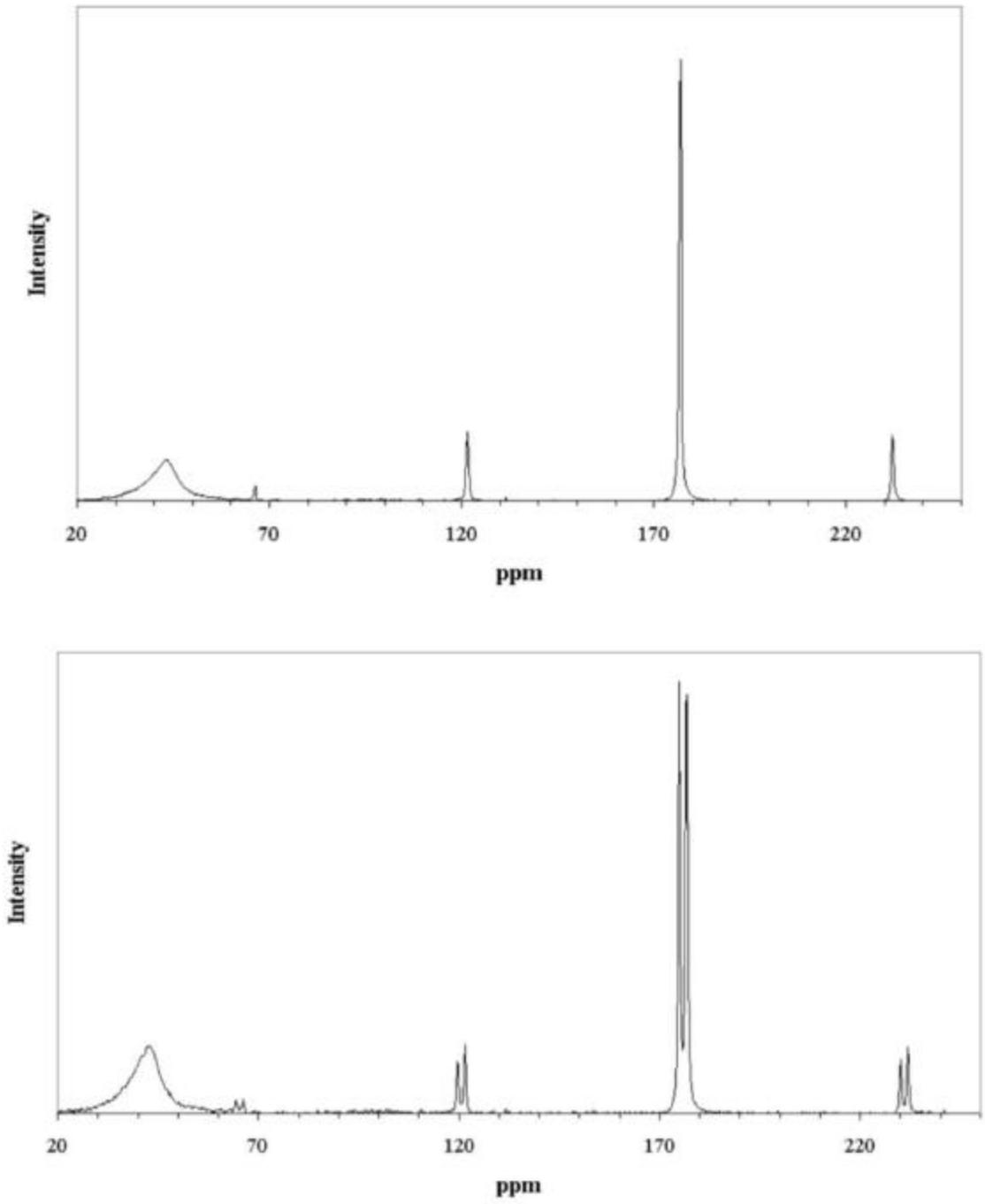

Figure 23. The solid state NMR spectra for α-glycine (top) and γ-glycine (bottom). The α-polymorph is present in γ-glycine.

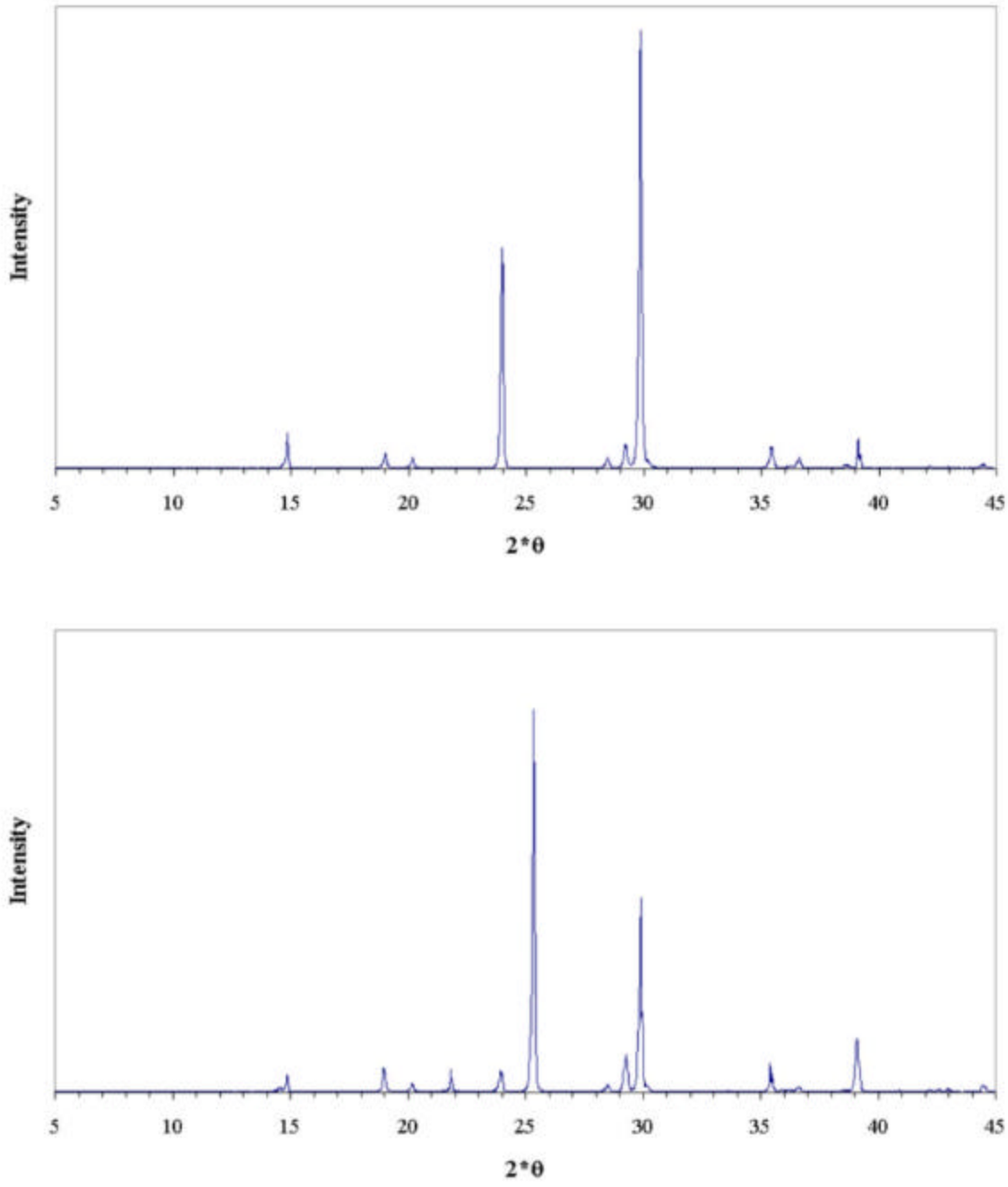

Figure 24. The powder x-ray diffraction spectra for α-glycine (top) and γ-glycine (bottom). The α-polymorphs is clearly seen in the γ-glycine spectrum.

glycine was fairly simple. The α-glycine has an intense peak at an angle of 30° while the γ-glycine has its intense peak at an angle of 25°[55]; so to determine the polymorphic structure, one would look at the entire spectra while paying close attention to the specified angles. The highly unstable β-polymorph did not appear in any glycine spectra.

With the ability to determine the polymorphs, the data could be analyzed efficiently and effectively. Crystal nucleation was not guaranteed even after laser irradiation; thus, many trials were run to get a reasonable amount of nucleated crystals for the analysis process. For the samples irradiated with 1064 nm linearly polarized light at 800 mW, 10 samples nucleated out of 41 irradiated samples, with all 10 being the α-polymorph. When irradiated with 800 mW of right circularly polarized light, 6 samples nucleated out of 17 with 5 being of the α-polymorph and 1 of the γ-polymorph. The pulsed laser's wavelength was changed to the second harmonic light of 532 nm and more samples were irradiated. When the glycine solutions were irradiated with 800 mW of 532 nm linearly polarized light, 3 samples nucleated out of 6 irradiated samples with all 3 being of the α-polymorph. A few more samples were irradiated with 800 mW of 532 nm right circularly polarized light. For the 6 samples irradiated with 532 nm right circularly polarized light, 4 samples nucleated with all 4 samples being the α-polymorph. After 23 nucleations, only one γ- glycine crystal was produced after 70 samples were irradiated with either 1064 nm or 532 nm linearly polarized or right circularly polarized light. As for the controlled samples, all 20 non-irradiated aqueous glycine samples produced the α-polymorph as expected.

When the metal boat was placed into the glycine solution, the laser's polarization did not need to be carefully recorded, but the average laser power was increased to 1.5 W with 1064 nm light. Four samples were subjected to the sound waves for one minute with all 4 nucleating into the α-polymorph, which is the same morphology as the control samples. The average laser power remained at 1.5 W for the next experimental set. Several glycine solutions were irradiated with the highly intense 1064 nm linearly polarized and right or left circularly polarized light. There were 21 samples irradiated with linearly polarized light. All 21 samples nucleated into the α-polymorph. When using 1064 nm right circularly polarized light, 6 total samples were irradiated and all nucleated with 2 being the α-polymorph and 4 being the γ-polymorph. When irradiating with intense left circularly polarized light, all 6 irradiated samples nucleated with 2 being the α-polymorph and 4 being the γ-polymorph. The increased intensity of the laser light may have contributed in the production of more γ- glycine.

A continuous wave argon-ion laser with an average power of 1.8 W at 514.5 nm was employed for an experimental set of data. Two samples were irradiated with linearly polarized light. These two samples nucleated into the α-polymorph. Also, 23 samples of glycine solution were irradiated with right circularly polarized light. Out of 23 samples, only 10 samples nucleated with all 10 being of the α-polymorph. The γ-polymorphs were not produced in this set of experiments, and this result may be due to the fact that continuous wave lasers do not have a peak power as large as a pulsed laser. For the controlled samples, all 10 non-irradiated samples nucleated into α-polymorph (Table 1).

Table 1. Accounts for the laser induced crystallization on glycine.

Glycine Crystallization Parameters				Polymorphs			
Sample Size (mL)	**Wavelength (nm)**	**Light Polarization**	**Average Power (W)**	**Total Number of Trials**	**Number Not Crystallized**	**a**	**g**
Regular Power							
10 - 12	1064	LPL	0.80	41	31	10	0
10 - 12	1064	RCPL	0.80	17	11	9	0
10 -12	532	LPL	0.80	6	3	3	0
10 -12	532	RCPL	0.80	6	2	4	0
10 - 12	N/A	N/A	N/A	20	0	20	0
High Power							
10 - 12	1064	LPL	1.5	21	0	21	0
10 - 12	1064	RCPL	1.5	6	0	2	4
10 - 12	1064	LCPL	1.5	6	0	2	4
Sound							
10 - 12	1064	N/A	1.5	4	0	4	0
Continuous Wave Laser							
10 - 12	514.5	LPL	1.8	2	0	2	0
10 - 12	514.5	RCPL	1.8	23	13	10	0
Blanks							
10 - 12	N/A	N/A	N/A	20	0	20	0
10 - 12	N/A	N/A	N/A	10	0	10	0

Table 1. Continued.

Glycine Crystallization Parameters				Polymorphs			
Sample Size (mL)	**Wavelength (nm)**	**Light Polarization**	**Average Power (W)**	**Total Number of Trials**	**Number Not Crystallized**	**a**	**g**
pH = 4 Irradiated							
10 - 12	1064	LPL	0.700	10	1	0	9
pH = 4 Not Irradiated							
10 - 12	N/A	N/A	N/A	14	0	4	10
Unfocused Laser Light							
2	1064	LPL	0.700	10	1	4	5
2	1064	RCPL	0.700	10	1	5	4

Since the polarization didn't seem to control the formation of γ- glycine, hydrochloric acid was dissolved in several glycine solutions to produce a sample with a pH of 4. There were 14 of these solutions made and left to nucleate on their own. All 14 samples nucleated with 4 being the α-polymorph and 10 being the γ-polymorph. These samples represented the controlled experiments. Next, 10 solutions having a pH of 4 were irradiated with 700 mW of 1064 nm linearly polarized light from the pulsed laser (Quanta Ray DCR). The irradiation had 9 samples to nucleate with all 9 being of the γ-polymorph. The production of more γ- glycine was expected because the pH change similar to the experiments of freeze and spray drying listed in the introduction. Having the results of glycine with a pH of 4 at hand, the glycine was irradiated again, except this time using an average laser power of 700 mW. The 5 cm focal length lens was removed, and the sample size was decreased to 2 mL. The samples were irradiated with 1064 nm linearly polarized and right circularly polarized light through the side of the vial. When 10 samples were irradiated with linearly polarized light, 9 nucleated with 4 of the α-polymorph and 5 of the γ-polymorph. Similar results occurred for the samples irradiated with right circularly polarized light. Ten samples were irradiated; 9 samples nucleated with 5 being the α-polymorph and 4 being the γ-polymorph. With the reduction of sample size and use of an unfocused laser beam, more γ-glycine was produced (see Table 1).

Looking closer at the results, it does not seem to matter what the polarization of laser happened to be because both linearly and circularly polarized light produced the γ-polymorph at times. The γ-polymorph occurred more when the sample sizes were

dropped to 2 mL and when the laser power was increased for the 10 to 12 mL solutions. These results resemble the results for the glycine and hydrochloric acid solutions with pH of 4. Since the results are similar and the laser's polarization does not seem to matter, the major contributing factor to the production of γ- glycine has to be the laser-induced change in pH for an irradiated sample.

From the examples of freeze drying and spray drying in the introduction, γ-glycine forms more readily in an acidic or alkaline solution. When the pH was changed to 4 by the use hydrochloric acid, as expected, more γ- glycine formed because the solution became acidic. As for the 2 mL solutions irradiated with unfocused 1064 nm laser light and the 10 to 12 mL solutions irradiated with intense 1064 nm laser light, the laser power induced a pH change in the localized area of the beam path. The laser's average power and power density had to be higher for the larger solution in order to see the effect while the laser's power could be lower for a smaller solution to see the same effect. The pH of a glycine solution being irradiated with 1064 nm linearly polarized light was monitored using a simple pH meter standardized with a pH 4 buffer. The overall pH of the glycine solution began to decrease upon irradiation. Various sample sizes were used and all displayed a decrease in pH. The greatest decrease in pH over time came from a 5 mL solution of glycine, which decreased from a pH of 4.86 to 4.72 in about 10 minutes (Figure A-8). If the laser is allowed to run for a long period of time, the water temperature begins to increase (Figure A-6), but the rise is negligible during the minute irradiation time.

Since one can see that the pH changes upon irradiation, an idea can be formulated about the effect of the localized pH. The localized pH around the beam should be of a

lower pH than the rest of the solution. In this region the glycine begins to nucleate forming tiny crystals that fall out of solution. If the pH conditions are acidic enough, the nucleation of glycine will result in the crystallization of γ- glycine. This effect of pH can be seen in the freeze drying and spray drying experiments mentioned in the introduction. For the irradiation by 1064 nm laser light, the larger 10 to 12 mL solution's volume was too great to have an effective pH change through the solution; thus, the α-polymorph was formed frequently because most of the solution remained at a pH that promoted the nucleation α- glycine. The laser power had to be increased in order get an overall pH change that could promote the γ- polymorph. When the sample sizes were decreased to 2 mL, the change in pH was greater throughout the solution, resulting in the γ- polymorph being produced more frequently - similar to the glycine solutions with pH 4. An item worth noting is that the smaller the solution increases the chances of the γ- polymorph nucleation.

The laser-induced nucleation and formation of the α- and γ- polymorphs were investigated further. The growth of α-glycine results from an assembly of cyclic dimers[60] that crystallize into sheets of glycine hydrogen bonded molecules arranged perpendicular to the b axis by forming bilayer stacks attracted to one another through van der Waals forces.[60] Helical chains are the building blocks of γ- glycine.[63] Gamma glycine is not bilayered but contains non-centrosymmetric hydrogen bonded helices. The destablization of the cyclic dimer inhibits the formation of α-glycine but promotes the γ-glycine. Since the cyclic dimers form by linking head-to-tail of two zwitterions, charged molecules are expected to inhibit the dimer formation because of respulsion of like charges.[60] Therefore,

the γ- polymorph is promoted more than the α- polymorph in an acidic solution because the solution contains more charged molecules that inhibits the formation of dimeric building blocks of α- glycine. Zwitterions are still present in the solution.

This idea behind the formation of the α- and γ-polymorph differs from the postulation of laser-induced crystallization that says the electric fields of 6×10^7 V/cm induce a partial alignment of molecules in solution similar to the Kerr Effect.[63] Thus the dipole moment, μ, of glycine is 47×10^{-30} C·m, which is eight times that of water[63], and the helical dimers have a polarizability anisotropy of $3.2 \times 10^{-30} m^3$ while the cyclic dimers have a polarizability anisotropy of 2.3×10^{-30} m^3.[63] Therefore, when placed in an applied polarized electric field the helical chains align more effectively.[63] The laser's polarization may have a small effect, but overall, the change in the pH of the solutions is the driving force behind the polymorphic selective nucleation.

This work is not the first observation for laser-induced pH changes. Chen and McCann[62] took note of this effect in 1988. In their experiment, aqueous solutions of CCl_4 were irradiated by a Nd:YAG laser beam for five minutes at a wavelength of 266 nm. Over that time interval the pH of the solution changed from 5.76 to 3.62 due to laser-induced dissociation.[62] They went on to remark that the one photon absorption can be neglected if the laser photon does not possess enough energy to promote a transition from the ground state to the first excited state[62] and that the two photon excitation processes are efficient in the condensed phase because of the density of the material.[62] The typical cross-section for a two-photon process is around ~ 10^{-50} cm^4/molecule.[65, 66] A two-photon induced process is quite high in liquids.[62] A simple rate equation for one and two photon absorptions is

$$\frac{dI}{dl} = -\left(\alpha + \beta I\right) = -N\left(\sigma_1 + \sigma_2 I\right)I_1 \qquad (6.2)$$

where I is the laser power, N is the number density of solute molecules, α and β are absorption coefficients, and σ_1 and σ_2 are the absorption cross-section.[62] Since aqueous glycine was irradiated, the density of water provided a suitable condensed phase that could facilitate a two-photon process.

Conclusion

In conclusion, laser-induced crystallization occurred during the irradiation of supersaturated solutions of glycine. Microscopic size crystals could be seen on the bottom of the vials about 30 minutes after nucleation. After analyzing the crystals by solid state NMR and powder x-ray diffraction, it could be seen that the γ- polymorph formed more readily in smaller solutions irradiated with unfocused laser light and in larger solutions irradiated with intensely focused laser light. The polarization of the laser light did not seem to determine the polymorphs of glycine because both the α- and γ-polymorphs were the results of linearly and circularly polarized light. These results contrast the results of Garetz et al. who noted that linearly polarized light produced γ-glycine and circularly polarized light produced α-glycine. Since the polarization did not seem to play a major role, the pH of the sample solutions was observed closely during irradiation. The solutions became more acidic during the minute irradiation process, which promoted the nucleation of γ-glycine. The results that produced γ-glcyine the most effectively resemble the results for the glycine and hydrochloric acid solutions with pH 4. Now, the formation and nucleation of the glycine polymorphs is said to be pH dependent when it comes to being irradiated with intense laser light rather than being aligned by a

strong electric field; therefore, the laser light is inducing a pH change in the glycine solution. A laser-induced pH change offers a clean method of crystallization because no products have to be added to the solution.

CHAPTER VII

THE SEARCH FOR THE PARITY VIOLATING ENERGY DIFFERENCE IN ALANINE AND VALINE CRYSTALS

This chapter is a moderate revision of a paper by a similar name published in the *Journal of Physical Chemistry A* in 2003 by Rodney Sullivan, Marek Pyda, J. Pak, Bernard Wunderlich, James R. Thompson, Richard Pagni, Hongjun Pan, Craig Barnes, Peter Schwerdtfeger, and Robert Compton:

Sullivan, R.; Pyda M.; Pak J.; Wunderlich, B.; Thompson, J.R.; Pagni, R.; Pan, H.; Barnes, C.; Schwerdtfeger, P.; Compton, R., "Search for Electroweak Interactions in Amino Acid Crystals II. The Salam Hypothesis." *Journal of Physical Chemistry A*, **107**, 34, 6674-6680, 2003.

This paper has contributions from many authors. My primary contributions to this paper include making all the test samples of alanine and valine, participating in the data acquisition for all the experimental techniques except for the magnetic susceptibility and differential scanning calorimetry studies, analyzing the data acquired from the experimental techniques, gathering and organizing the experimental materials, and writing most of the paper. The theoretical calculations were performed by Peter Schwerdtfeger. The paper was modified for this chapter by the omission of a few unnessecary figures in the text, the addition of sections on optical rotatary dispersion and circular dichroism, and the doctoring of sentence structure.

Introduction

The parity-violating (P-odd) weak interaction is the only known chiral force in nondecaying atoms and molecules. The standard model of low energy nuclear physics describes this weak interaction as the virtual exchange of Z^0 bosons between elementary particles. Following the prediction and observation of parity non-conservation in the late 1950's, P-odd effects were observed in the optical activity for atoms[70] and in the occurence of weak transitions between atomic hyperfine states of the same parity[71]. Although expected, similar effects have not been detected in molecules. Interest in P-odd effects in molecules has focused upon the measurement of the so-called parity violating energy difference (PVED) predicted to exist between R and S enantiomers of a chiral

molecule. The PVED calculated for small molecules such as amino acids is exceedingly small [see recent studies][72] and has not yet been detected. A small (~ 10^{-10} eV) energy difference between enantiomorphic crystals of a chiral iron complex was recently reported using Mössbauer spectroscopy; however, the possibility of strain within the crystal precludes an unqualified claim of the measurement of PVED.[73] Early PVED calculations for the amino acids[74-77] predicted that the L- enantiomer lies lower in energy than the D-enantiomer; however, this energy difference is generally believed to be too small to account for the exclusive occurrence of L-amino acids in biomolecules. Clearly, there is no solid evidence that PVED can account for biomolecular homochirality through the Yamagata hypothesis.[72] The Yamagata hypothesis states that enantiomers change from handedness to the other over a long period of time.

In 1991, Salam introduced a startling new hypothesis that was proffered to account for biomolecular chirality, which does not rely upon the long times involved in the Yamagata hypothesis.[78, 79] Salam proposed that the subtle energy difference, PVED, together with a type of Bose condensation phenomenon, may allow for a second order phase transition below a critical temperature T_c allowing the "less" stable D-enantiomer to tunnel into the more stable L-enantiomer. The critical temperature T_c for this transition was identified with that for the BCS theory of superconductivity. Wang *et al*. have recently reported extensive experimental studies of L- and D-alanine and -valine crystals, which were designed to test the Salam hypothesis.[80] These authors report three experimental results which were presented as evidence for the Salam hypothesis: (1) specific heat measurements for both crystals show a second order phase transition at ~ 270 ± 1 K that are different in magnitude for the two enantiomorphs of each amino acid;

(2) differences in the mass susceptibilities for the two enantiomorphs were detected using a SQUID magnetometer in the same temperature region; and (3) Raman spectra of the C^{α}-H deformation modes disappear for the D-alanine at ~ 270 K but reappear again at ~ 100 K; the same vibrational mode for L-alanine does not vanish over this temperature range. In this contribution, we re-examine these measurements and, in addition, study the temperature dependence of x-ray diffraction and C-13 solid state NMR for alanine. We conclude with some critical comments on the Salam hypothesis.

Preparation

Both enantiomers of alanine, $C_3H_7NO_2$, and valine, $C_5H_{11}NO_2$, were purchased from Sigma Aldrich Chemical Company (see Figure A-1). The optical purities of the samples were quoted to be 99 percent and at least 98 percent for the L- and D-forms, respectively. D- and L- alanine and -valine crystals were grown in aqueous solutions using HPLC water in Petri dishes at room temperature, 298 K. The crystallization process took about a week because plastic Saran wrapped lids with 80 0.5 mm holes were placed in the Petri dishes to control the evaporation of the water. These lids also prevented larger biological debris and other particles from falling into the solution during crystal growth. The crystals were recrystallized twice to eliminate further impurities. As discussed later, measurements were performed after each stage of recrystallization. The alanine crystals were shaped like rectangular parallelepipeds. The average alanine crystal had the dimensions of 5 mm x 4 mm x 2 mm. Crystals of both D- and L-alanine were grown using these methods. The D- and L-valine crystals were difficult to grow. The L-valine crystals were more difficult to grow than the D-valine crystals because their aqueous solution was more prone to bacteria growth over long periods of time. The

growing of valine crystals from an aqueous solution was unsuccessful. Thus the data for D- and L-valine crystals were obtained directly from the material purchased from the Sigma Aldrich Chemical Company.

Optical Rotatory Dispersion and Circular Dichroism

A Perkin-Elmer 241 Polarimeter was used to obtain the optical rotatory dispersion of D- and L-valine and -alanine. The polarimeter can be operated at five wavelengths: 589 nm, 578 nm, 546 nm, 436 nm, and 365 nm. The concentration for the alanine enantiomers was 0.088 g/ml and 0.015 g/ml for the valine. The D- and L-forms of both alanine and valine displayed equal and opposite rotations at the five wavelengths controlled by the polarimeter. The optical rotary dispersions were measured at 298 K (Figure 25).

The CDs of D- and L-alanine and –valine in aqueous solutions were taken on an Aviv Model 202 Series Circular Dichroism Spectrometer. The CD of the aqueous solutions of the enantiomers of alanine and valine were obtained in a one-centimeter pathlength cuvette. As expected, both enantiomers of valine and alanine displayed equal magnitude but opposite sign CD spectra (see Figures 26, 27, and 28). Each CD spectrum showed a peak maximum for both the valine and alanine that occurred around 215 nm for alanine and 203 nm for valine. The CD band around 210 nm arose from the $n \rightarrow \pi^*$ transition of the carboxyl group while the amino group contributed to the CD bands especially at 230 nm, which is assigned to the $n \rightarrow \sigma^*$ transition.[81]

D- and L-alanine were dissolved in ethanol and CD spectra were recorded as the temperature was changed by 5 K increments from 298 K to 268 K. The CD spectra of

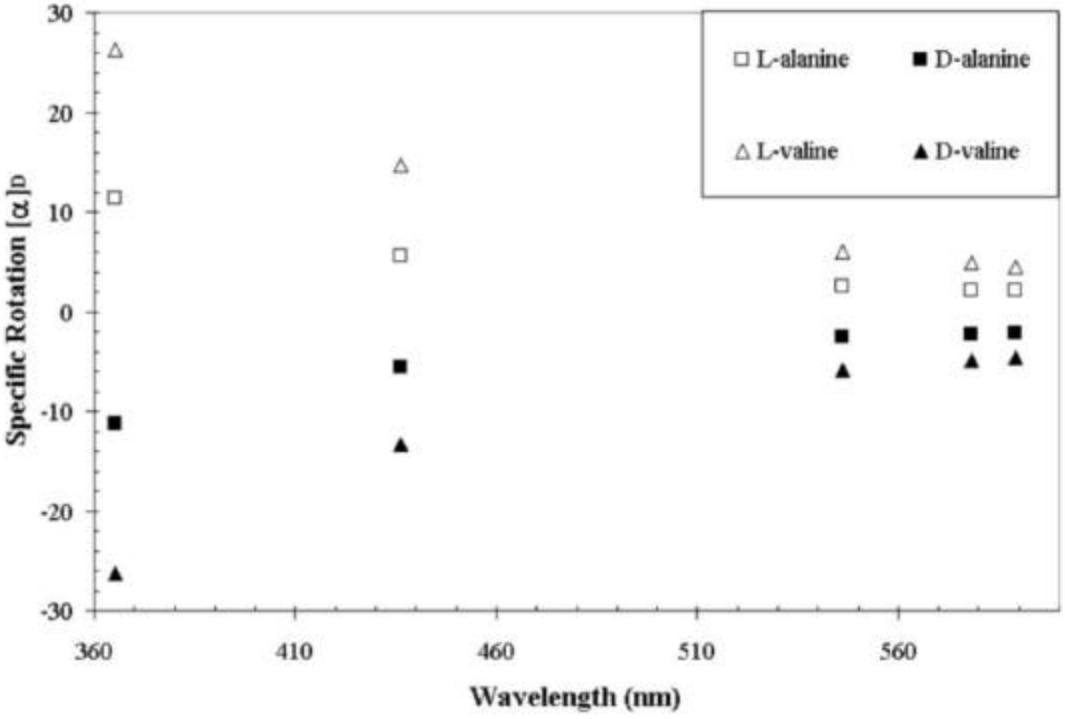

Figure 25. The optical rotary dispersion (ORD) curves for the enantiomers of alanine and valine in aqueous solution.

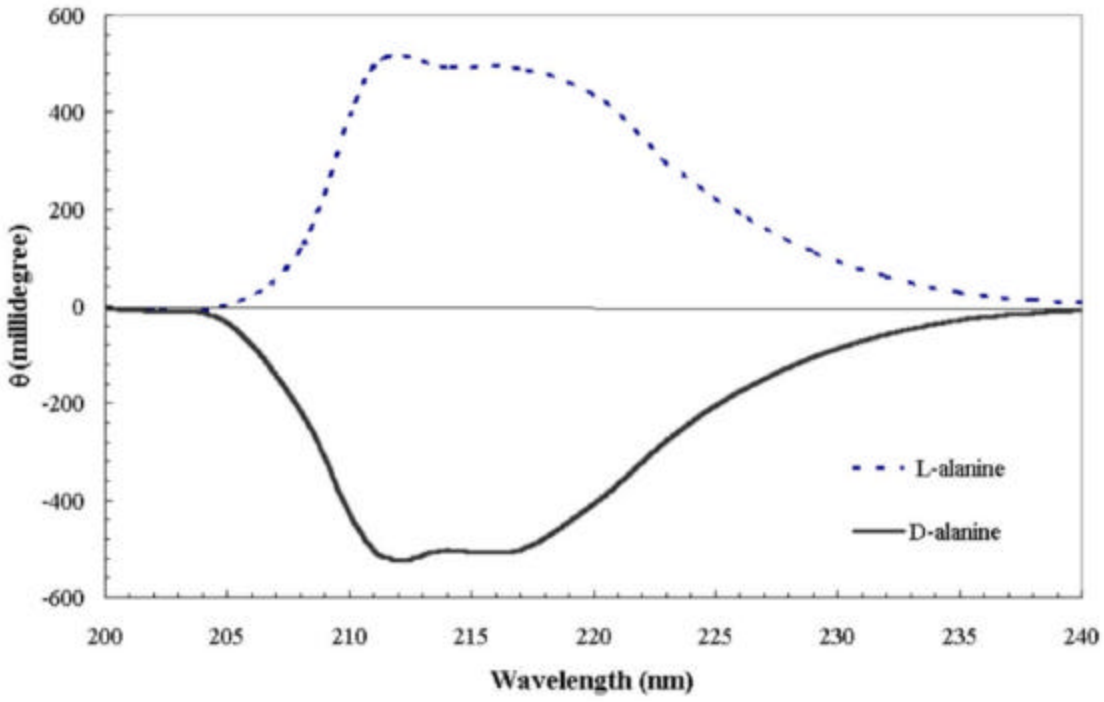

Figure 26. Circular dichroism spectra of aqueous alanine solutions.

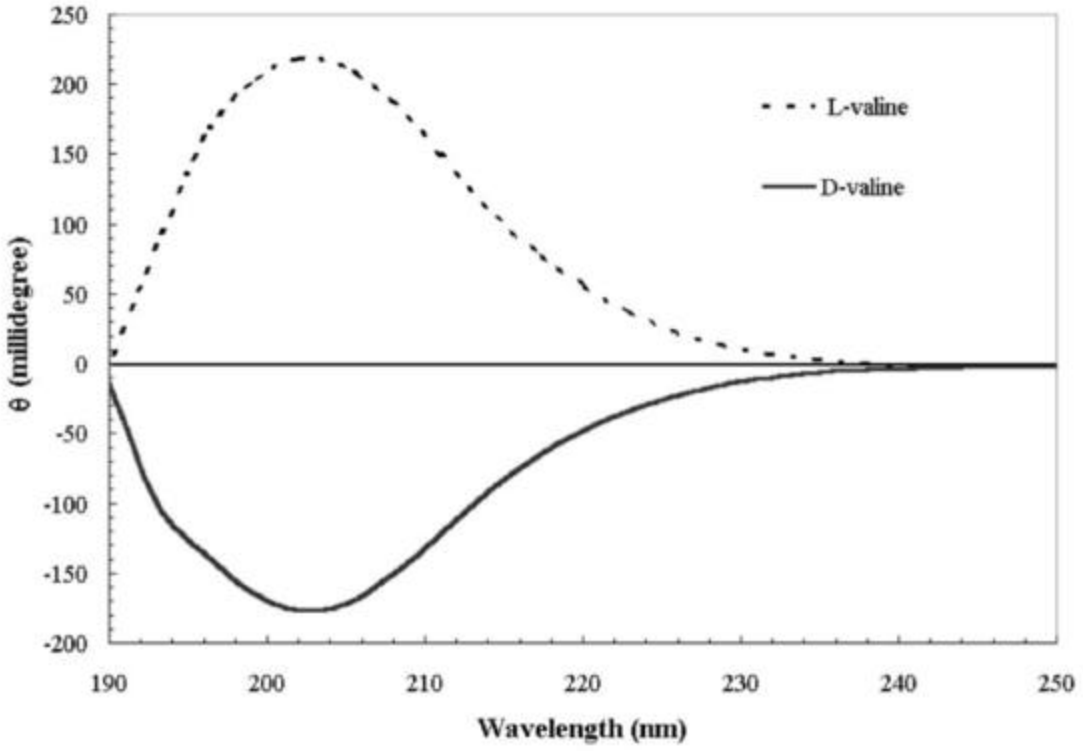

Figure 27. Circular dichroism spectra of aqueous valine solutions.

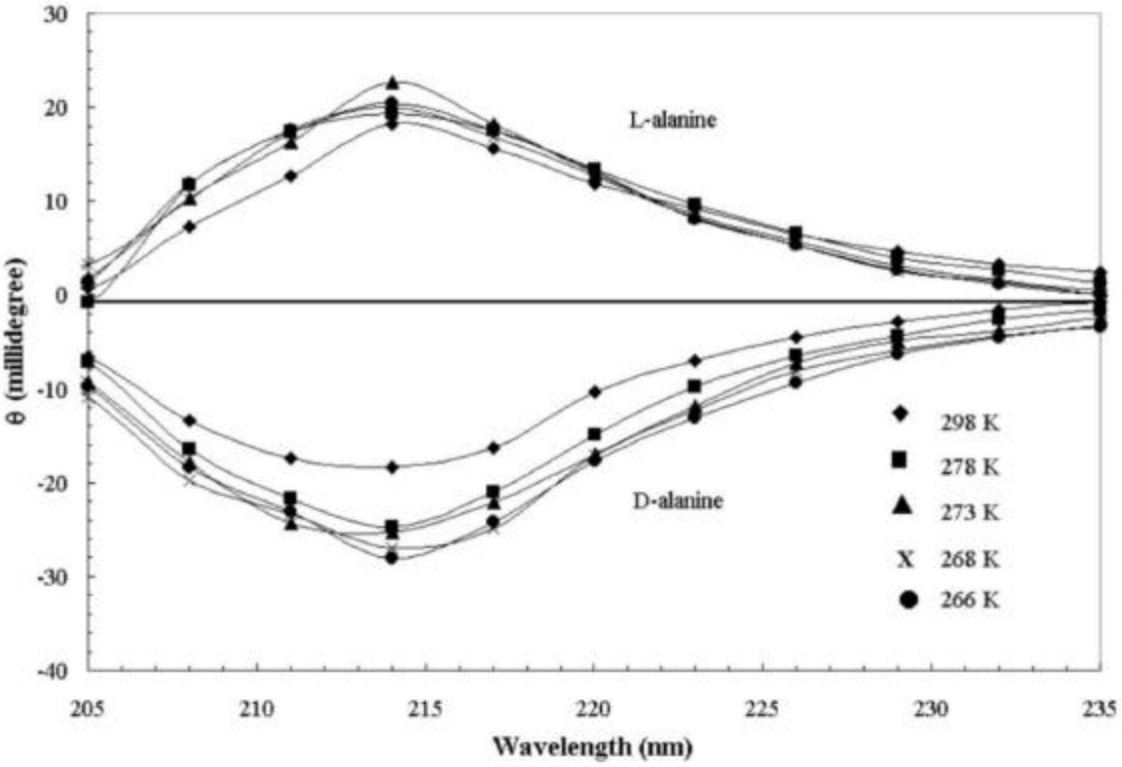

Figure 28. Temperature dependent circular dichroism of D- and L-alanine dissolved in ethanol.

the alanine in ethanol displayed no changes over this temperature range, as presented in Figure 28. The CD for alanine in water was identical to that observed in ethanol.

X-ray Diffraction

X-ray diffraction patterns for single crystals of D- and L-alanine were obtained at 296 K using a Bruker AXS Single Crystal X-Ray Diffractometer with the Smart 1000 System. The space group was found to be $P2_12_12_1$ and orthorhombic with cell dimensions of a =5.7811Å, b = 6.0282Å, and c = 12.3401Å. The temperature of the crystals was varied from 296 K to 258 K and no significant unit cell dimensional changes were noted, as seen in Table 2. The unit cell dimensions stayed virtually the same throughout the temperature range. The x-ray diffraction did not take into account the moving of hydrogen atoms to form zwitterions.

Nuclear Magnetic Resonance

C-13 magic angle spinning NMR spectroscopy of alanine and valine samples was performed on a 400 MHz Solid-State NMR Varian Spectrometer. Alanine crystals were grown from both aqueous solutions and deuterium oxide. D- and L-alanine crystals displayed three peaks at 178, 51, and 21 ppm; representing the COOH, CH, and CH_3 groups, respectively. As the temperature was decreased from 298 K to 248 K in both D- and L-alanine, the peaks became less intense without broadening. The peaks almost completely disappeared at 248 K. Also, no shifts were observed during the temperature dependent experiment (Figure 29 and 30). These temperature effects were observed for D- and L-alanine grown in either water or deuterium oxide.

C-13 NMR spectra for D- and L-valine obtained from Sigma Aldrich revealed five resonances at 178, 61, 32, 23, and 19 ppm. These peaks are due to the C^{13} in the

Table 2. X-ray diffraction data for the D- and L-alanine crystals at 296 K.

Sample	**D-alanine**	**L-alanine**
Empirical formula	$C_3H_7NO_2$	$C_3H_7NO_2$
Formula weight	89.10	89.10
Temperature	296 K	296 K
Wavelength	0.71073Å	0.71073Å
Crystal system	Orthorombic	Orthorombic
Space group	$P2_12_12_1$	$P2_12_12_1$
Unit Cell dimensions	a = 5.7811(3)Å, **a** = 90°	a = 5.7905(3)Å, **a** = 90°
	b = 6.0282(3)Å, **b** = 90°	b = 6.0220(3)Å, **b** = 90°
	c = 12.3401(6)Å, **g** = 90°	c = 12.3435(7)Å, **g** = 90°
Volume	430.05(4)Å^3	430.05(4)Å^3
Z	4	4
Density (calculated)	1.367 Mg/m^3	1.375 Mg/m^3
Absorption coefficient	0.115 mm^{-1}	0.115 mm^{-1}
F(000)	192	192
Crystal size	0.3 x 0.4 x 0.3 mm^3	0.3 x 0.4 x 0.3 mm^3
Theta range for data collection	3.30 to 28.32°	3.30 to 28.32°
Index ranges	-7<=h<7, -8<=k<8, -16<=l<16	-7<=h<7, -8<=k<8, -16<=l<16
Reflections collected	5563	5562
Independent reflections	1044 [R(int) = 0.0249]	1043 [R(int) = 0.0252]
Completeness to theta =28.32°	98.9%	99.1%
Refinement method	Full-matrix least-squares on F^2	Full-matrix least-squares on F^2
Data/ restraints/ parameters	1044 / 0/ 83	1043 / 0/ 83
Goodness-of-fit-on F^2	1.124	1.114
Final R indices [I>2sigma(I)]	R1 = 0.0293, wR2 = 0.0752	R1 = 0.0296, wR2 = 0.0746
R indices (all data)	R1 = 0.0302, wR2 = 0.0758	R1 = 0.0308, wR2 = 0.0760
Absolute structure parameter	0.4(11)	0.3(10)
Largest diff. peak and hole	0.220 and –0.244 e.Å^{-3}	0.151 and –0.258 e.Å^{-3}

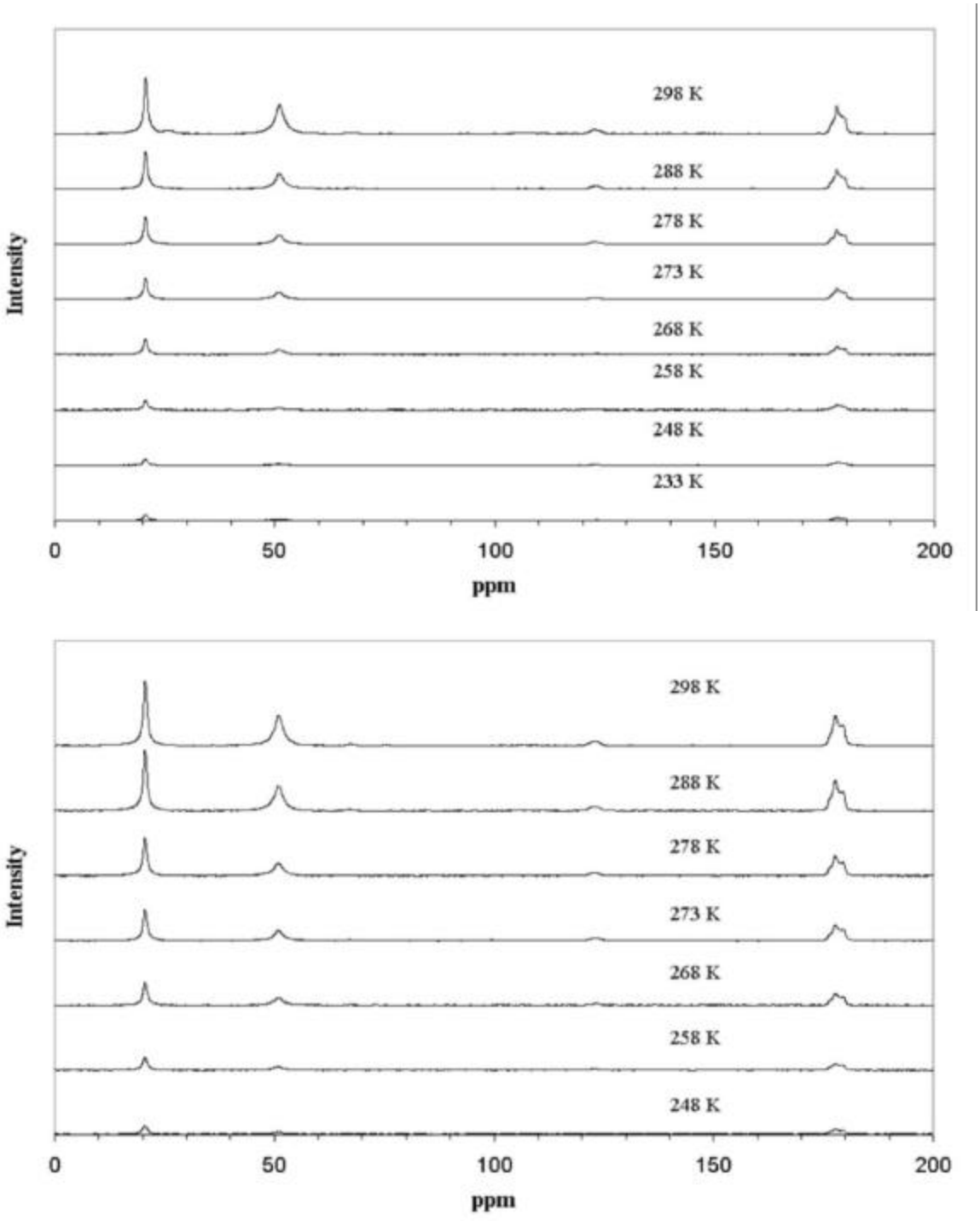

Figure 29. Temperature dependent solid state NMR spectra of D- (top) and L-alanine (bottom) crystals.

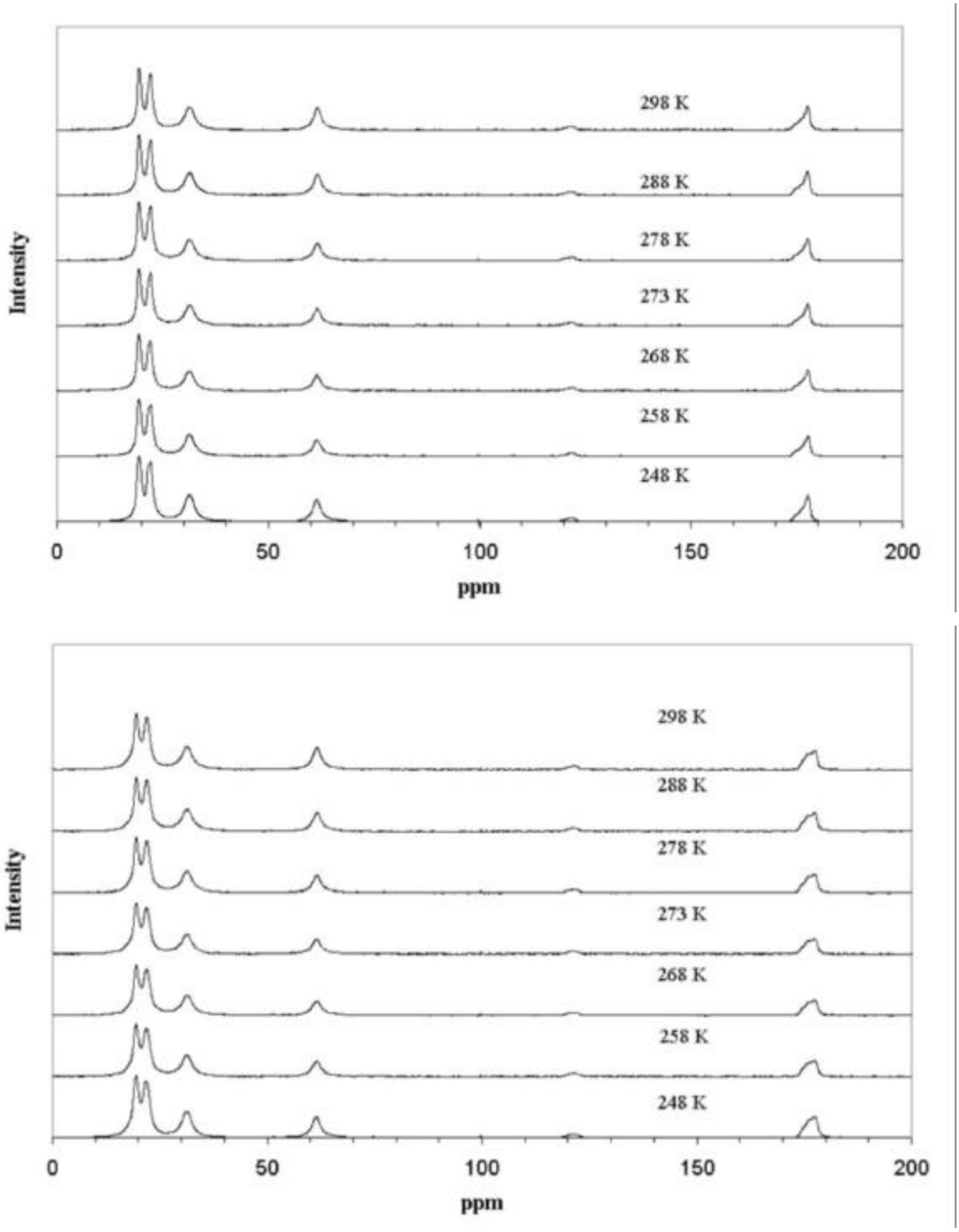

Figure 30. Temperature dependent solid state NMR spectra of D- (top) and L-valine crystals.

COOH, CH, CH_3, and two CH_2 groups, respectively. We could detect no change in the NMR spectra over the temperature range from 298 K to 248 K. The peak widths were also unchanged as presented in Figure 30. The spectra were identical for D- and L-valine grown in water and deuterium oxide. No phase transition is evident in the NMR spectra over this temperature range.

Raman Scattering

The vibrational modes of the C-H bond in D- and L- alanine were recorded using a Dilor XY Modular Laser Raman Spectrometer. Raman spectra were taken with an argon-ion laser with a wavelength of 514.53 nm and power of 100 mW. A variable temperature sample holder device was constructed using a cold plate, a thermo electrical cooler, and a heat sink. An ILX temperature controller was used to vary precisely the temperature settings. Raman spectra of alanine crystals were recorded over a temperature range from 298 K to 270 K. The Raman data show no changes over this temperature range when special attention was focused upon the C–H peaks at 2600 cm^{-1} and 2750 cm^{-1}. An alanine crystal in the shape of a rectangular parallelepiped was placed on the platform with its broad side facing up. When the long crystal axis was rotated 90° with respect to the plane of polarization of the laser beam, an additional peak appeared on the spectra around 3100 cm^{-1} at all the temperatures observed (Figures 31 and 32). This additional peak was not observed in the Raman spectra when the long crystal axis was parallel to the plane of polarization of the laser (Figure 33 and 34). The Raman emissions were collected at 180° (back reflected) with respect to the incident beam. Once again, no changes in the Raman spectra occurred around ~270 K. Wang *et al.*[80] recorded

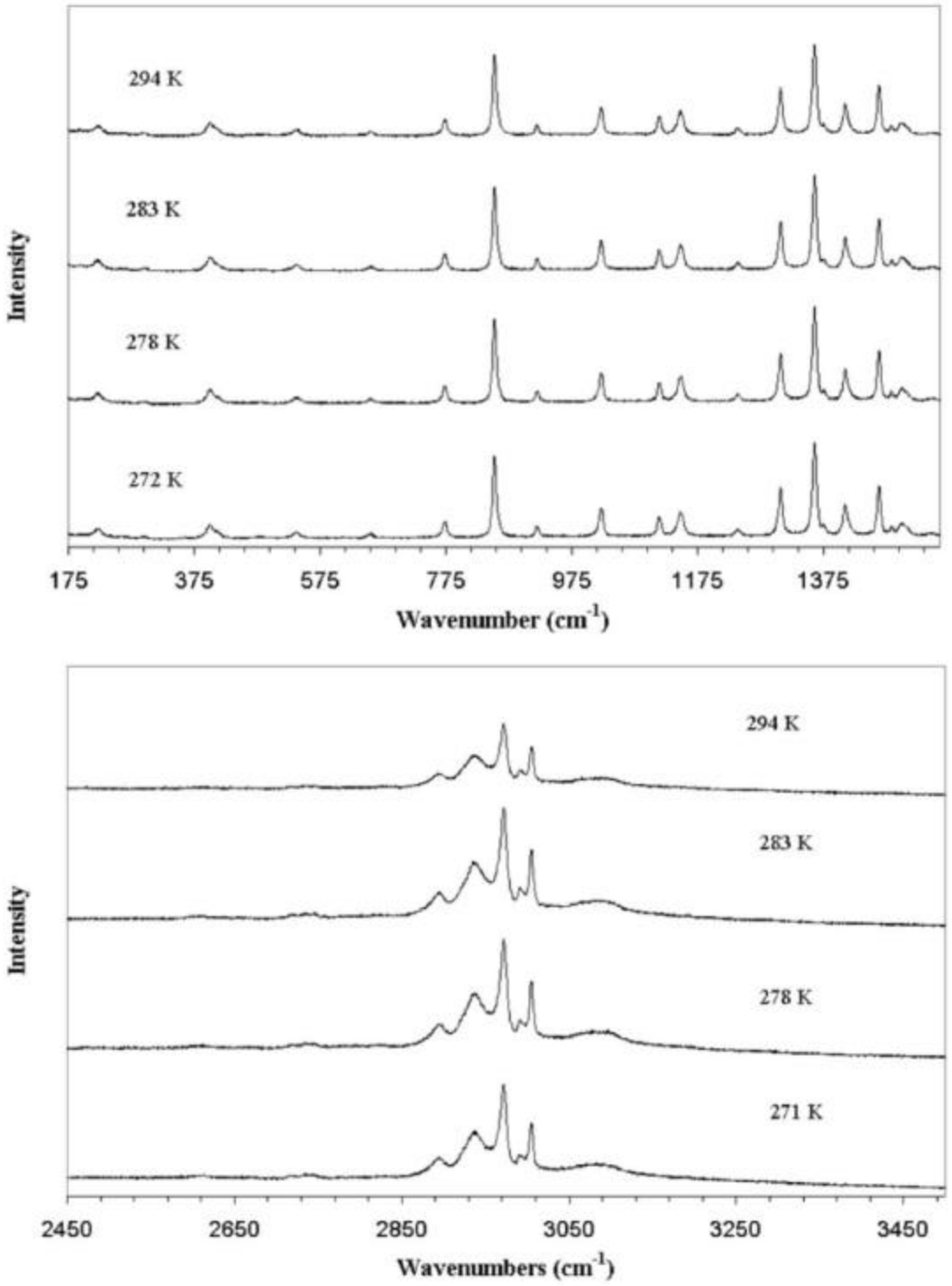

Figure 31. Temperature dependent Raman spectra for the D-alanine crystal with its long crystal axis perpendicular to the laser beam's polarization.

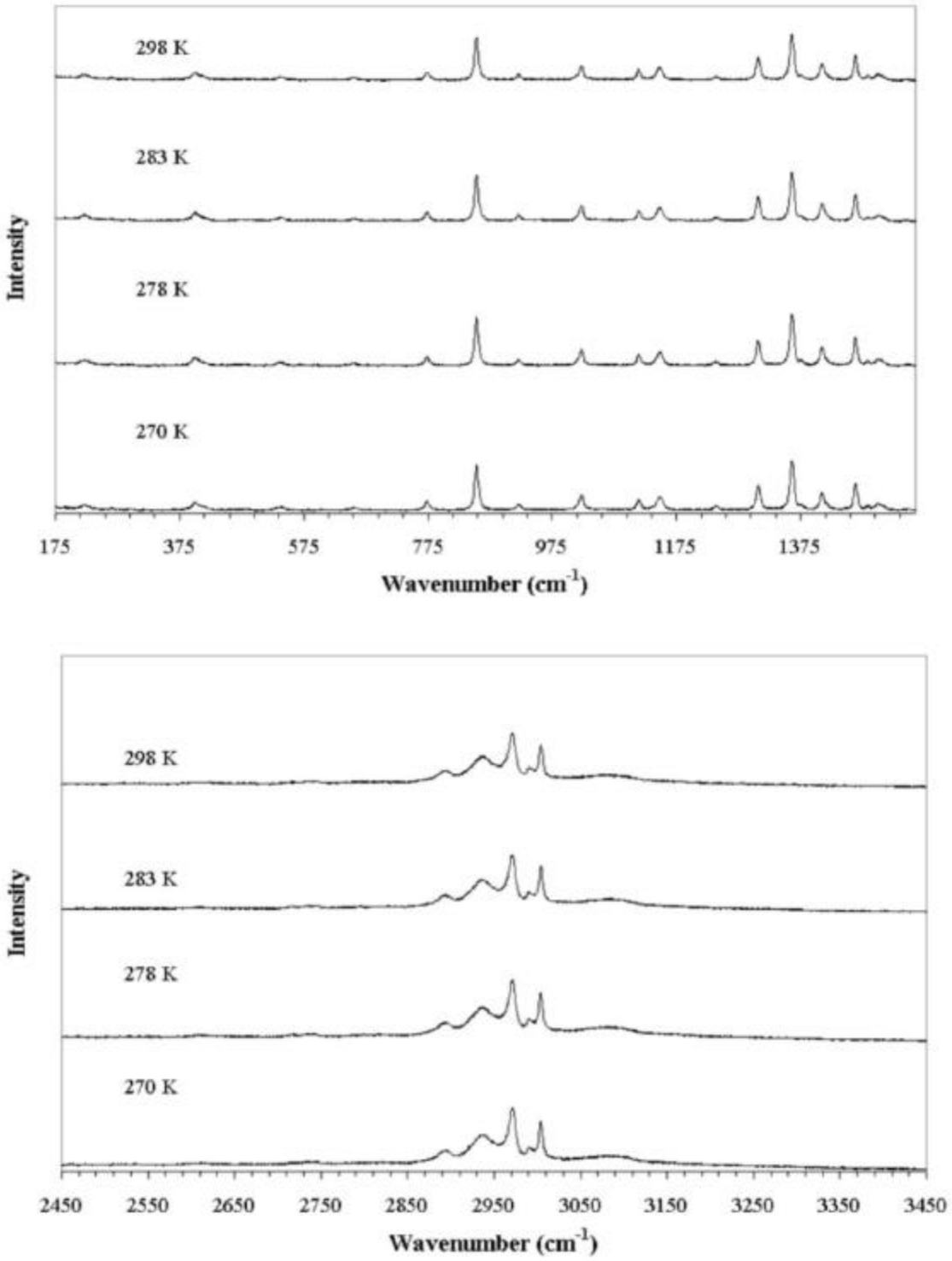

Figure 32. Temperature dependent Raman spectra for the L-alanine crystal with its long crystal axis perpendicular to the laser beam's polarization.

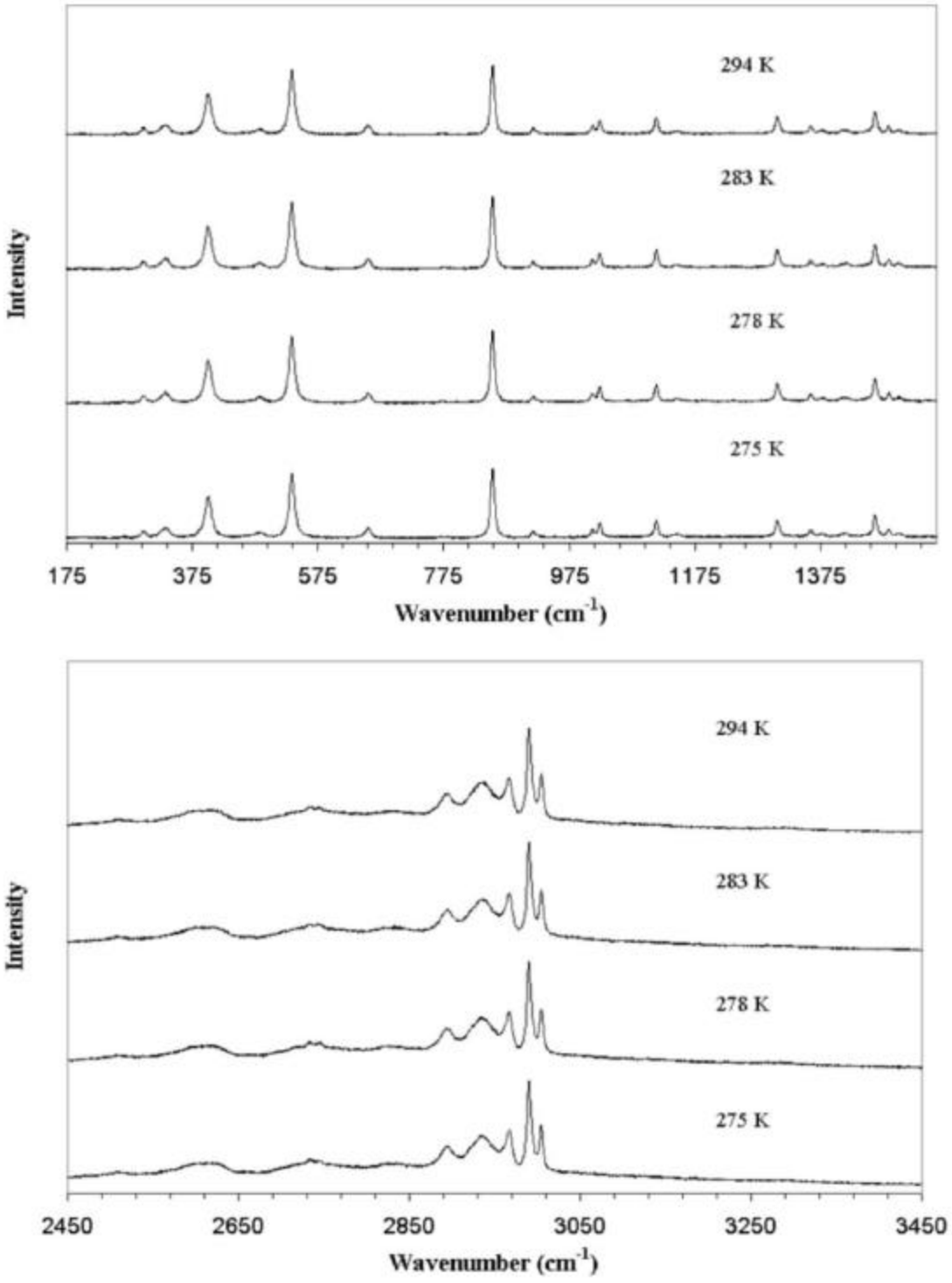

Figure 33. Temperature dependent Raman spectra for the D-alanine crystal with its long crystal axis being parallel to the laser beam's polarization.

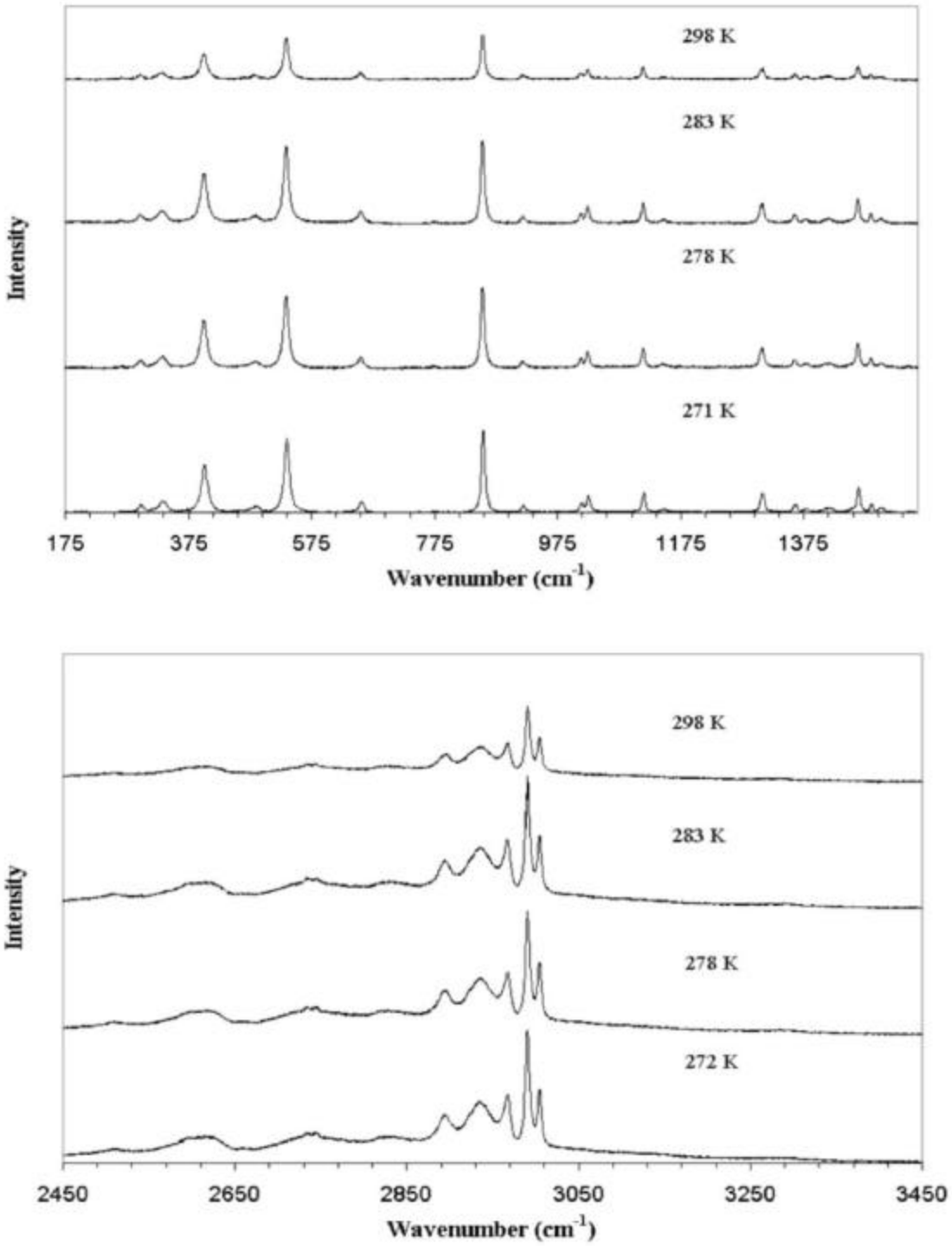

Figure 34. Temperature dependent Raman spectra for L-alanine crystal with its long crystal axis being parallel to the laser beam's polarization.

their Raman spectra using an argon-ion laser with a power of 200 mW at 488 nm while the emissions were collected at 90° to the incident beam. Their Raman lines decreased in intensity to the point that some disappeared around 270 K. This effect was not observed in our studies.

Magnetic Susceptibility

The magnetic susceptibility of single crystals of D- and L-alanine was investigated in the temperature range 5 K to 330 K using a SQUID-based magnetometer (Quantum Design model MPMS-7). The crystals were prepared by repeated recrystallizations. They were stored for an extended period (~6 months) in a small vial with desiccant to insure dryness. Two crystals were selected (mass of 169.0 mg for D-alanine and 129.3 mg for L-alanine) and mounted sequentially in the same long plastic tube for measurement. The two crystals were roughly rectangular and the magnetic field was applied parallel to the longest axis. For the magnetic study, a field H = 10 kOe was applied and the system was allowed to stabilize for one hour before beginning measurements with 4 cm scan lengths. Measurements on the two crystals were conducted consecutively with no change in the magnetic field, by sweeping the temperature T from 300 K to 5 K, then back to 300 K and continuing to 330 K. There was very little hysteresis (Figure 35). The cgs mass magnetic susceptibility, $\chi = m/(H \times \text{mass})$ versus temperature, is presented, and the first order χ is diamagnetic and nearly temperature independent. Curiously, the absolute value of χ is ~ 3 percent greater for the L-alanine crystal than for the D-alanine. This may arise in part from (1) small differences in sample size and geometry that slightly affect the magnetometer sensitivity

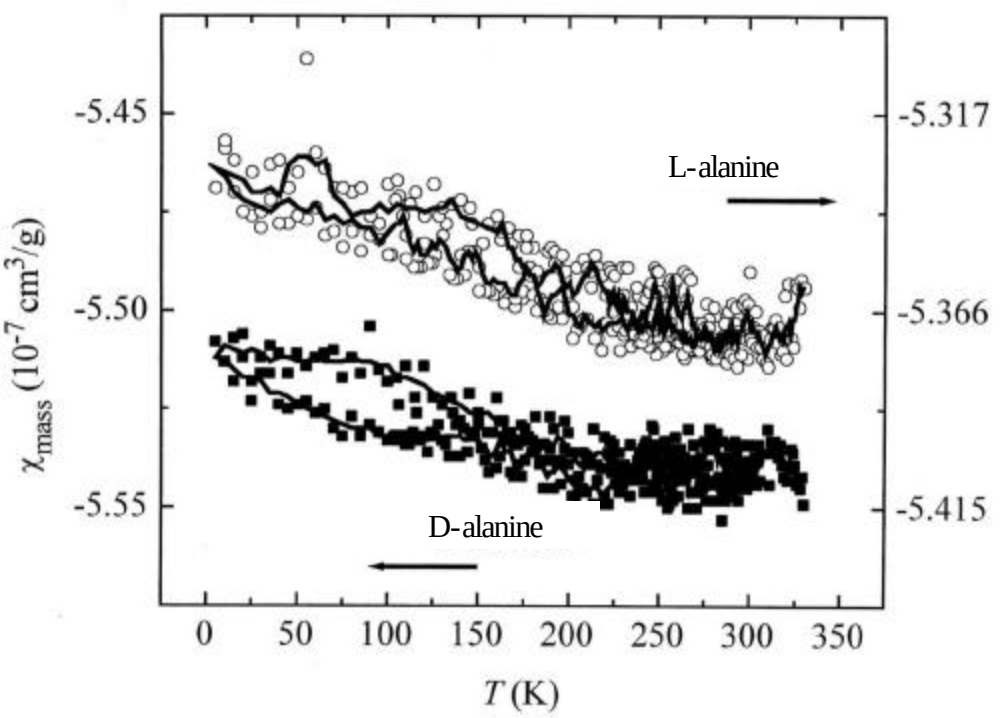

Figure 35. Magnetic susceptibility versus temperature is shown for D- and L-alanine.

and/or (2) from crystalline anisotropy [Jean Bernard Robert, private communication]. Most importantly, the behavior of $\chi(T)$ is nearly identical for the two cases of D- and L-alanine: χ hardly changes near room temperature, then increases by ~0.6 percent upon cooling to 5 K. The similarity in temperature dependencies is evident in Figure 35, in which the data for L-alanine are scaled by a factor of 1.025. These findings on magnetic susceptibility do not concur with those reported by Wang *et al.*[80]

Differential Scanning Calorimetry

The heat capacity and transition phases of crystalline L- and D-alanine and -valine were measured from 220 K to 340 K by standard DSC. Two differential scanning calorimeters were used to measure the transition behavior and heat capacities: a modulated differential scanning calorimeter (MDSC) 2920 of TA Instruments, Inc. and a DSC 820™ from Mettler Toledo Inc. Both the MDSC and DSC are of the heat-flux type. Figure 36 shows a typical example heat capacity measurement from 250 K to 285 K on the crystalline samples of L-alanine and D-alanine grown from aqueous solutions by standard DSC. In both L- and D-alanine, a small endothermic transition occurs around 270 K. However, for valine, only the D-form exhibits an endothermic peak (Figure 37). Typical heat flow measurements for L- and D-valine were performed by standard DSC. A comparison of the experimental data reveals an endothermic peak at -1.54 ^{o}C (271.61 K) for D-valine, but none for L-valine in the same temperature region (Figure 38). The heat of transition for D-valine was estimated to be H_t = 0.15 J/g (17.8 J/mol), which corresponds to a change of entropy of S_t = 0.0655 J/(K mol). All transition parameters are given in Table 3. The absence of a peak in L-valine suggests that an impurity is present in the synthetic D-valine but not in the naturally occurring L-valine, which one

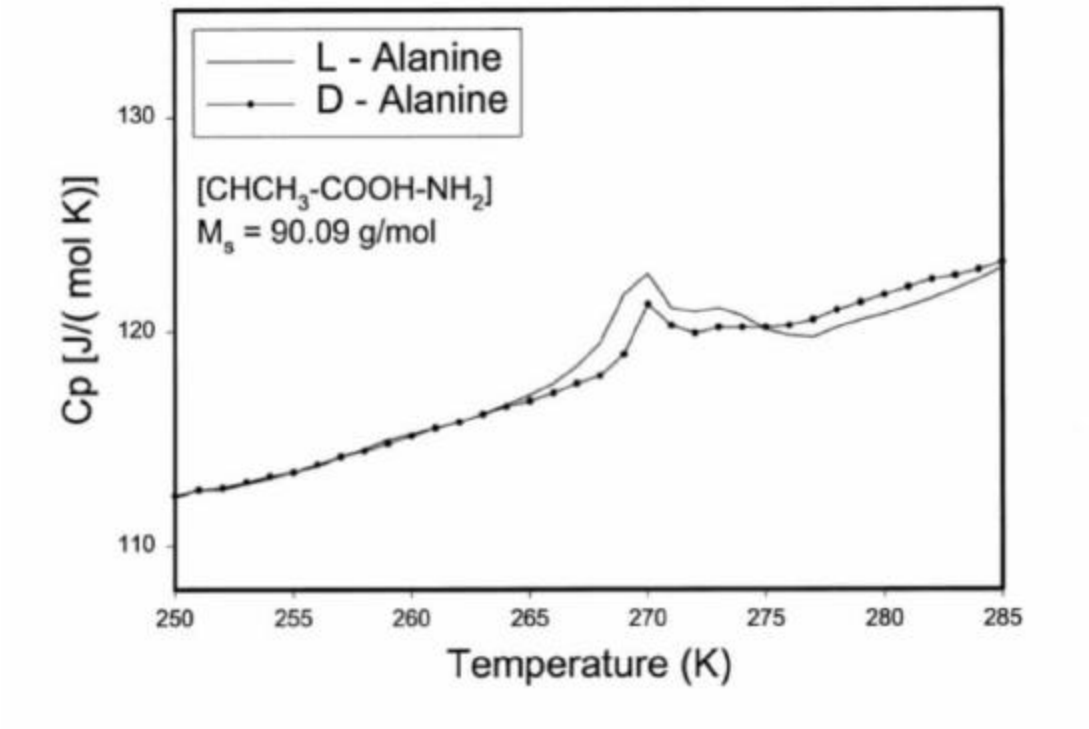

Figure 36. Typical heat capacity measurements of L- and D-alanine by standard DSC.

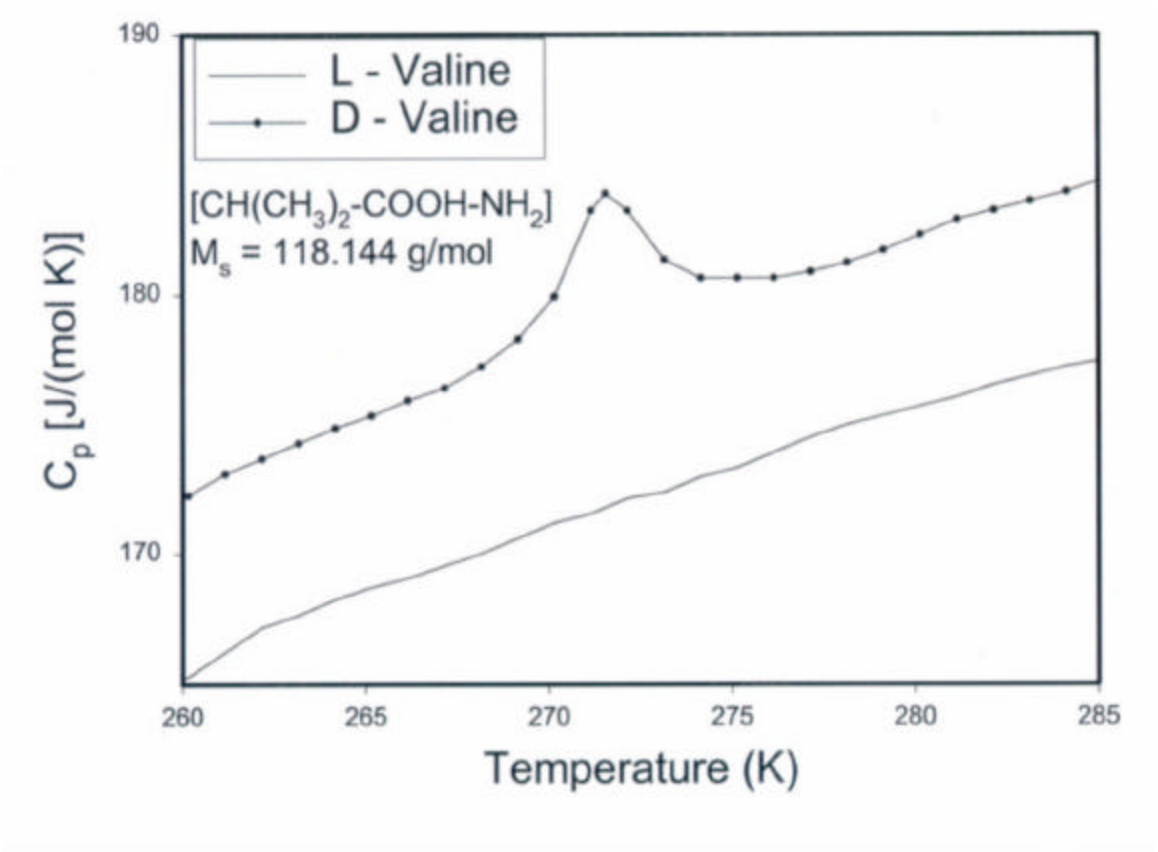

Figure 37. Typical heat capacity measurements of D- and L-valine by standard DSC.

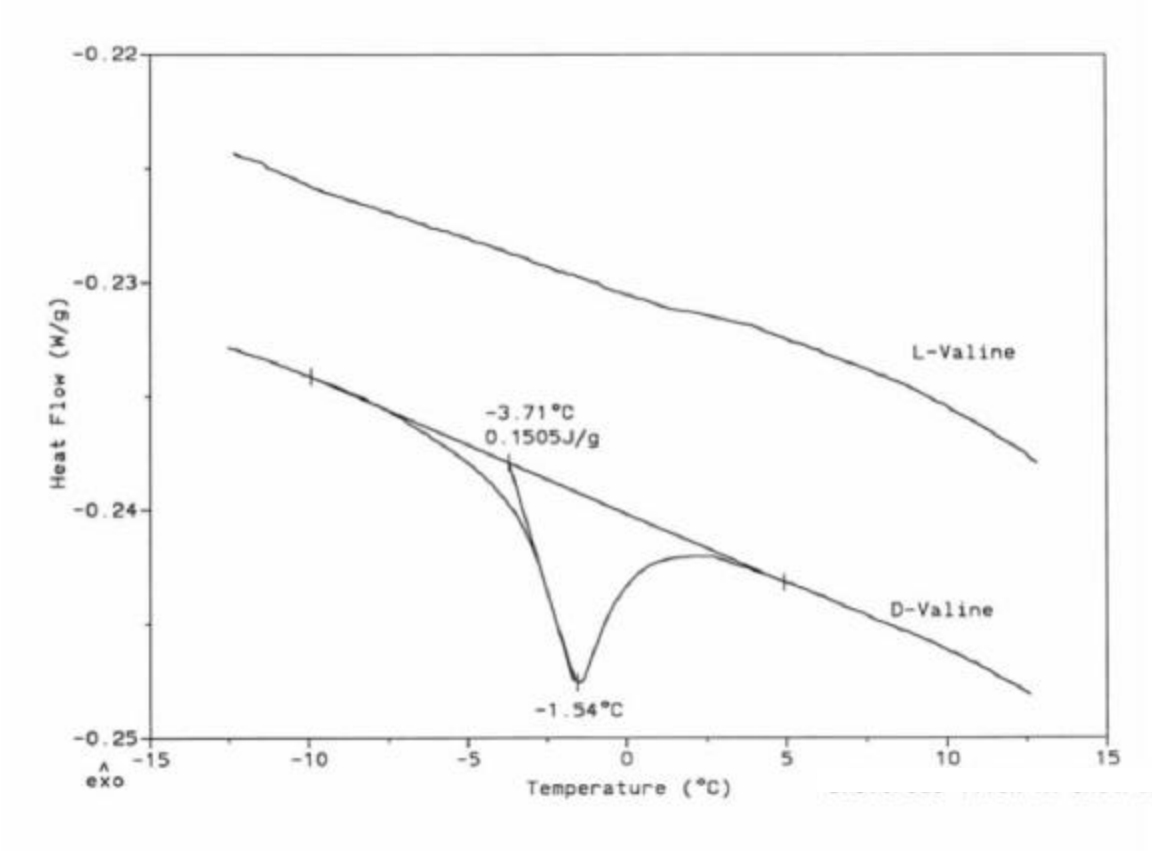

Figure 38. Heat flow of D- and L-valine by standard DSC.

Table 3. Transitional results of L- and D-alanine and –valine crystals.

Sample	Temperature of peak in (K)	Temperature of onset (K)	Heat of transition (J/mol)	Entropy of transition J/(K mol)
L-Alanine	269.59 ± 0.01	267.78 ± 0.01	20.3 ± 0.1	0.076 ± 0.001
D- Alanine	270.02 ± 0.01	268.81 ± 0.01	5.8 ± 0.1	0.021 ± 0.001
L-Valine	-	-	-	-
D-Valine	271.61 ± 0.01	269.44 ± 0.01	17.8 ± 0.1	0.065 ± 0.001

can reasonably assume to be of higher purity. Identical DSC curves were observed for crystals grown in deuterated water. It is interesting to note that all entropy values are hundreds of times smaller than any entropy of transition in liquid crystals, and much smaller than the entropy of fusion [ΔS_t 53 J/(K mol) for alanine]. The heat of transition in all samples was checked after re-crystallization from water. The heat transition at 270 K decreased with the numbers of re-crystallization (Figure 39), again suggesting a reduction in impurity level. The experimental heat capacities over the entire temperature range are linked to vibrational motion in the solid state.

Results and Discussion

This study reports the results for a number of experiments designed to search for phase transitions in two amino acids crystals, alanine and valine. Specifically, we re-examined all of the experiments reported by the group of Wang *et al.*[80] which were presented as evidence for a phase transition at a critical temperature of T_c 270 1 K. These data were taken as support of the Salam hypothesis. The differential scanning calorimetric heat capacity measurements do show an anomaly at 270 1 K for both crystals; however, the effect becomes smaller upon recrystallization. Also, no feature is seen in the naturally occurring L-valine. Careful magnetic susceptibility and Raman spectroscopy measurements show no anomalies over this temperature range. Temperature dependent C-13 solid state NMR and x-ray diffraction also show no anomalies. In light of these measurements, we will examine the Salam hypothesis with regard to the energy barrier existing between enantiomers.

Consider the racemization between enantiomers for an amino acid - such racemization is well known in solution[82] and is catalyzed by a base or an acid.[83] It is well

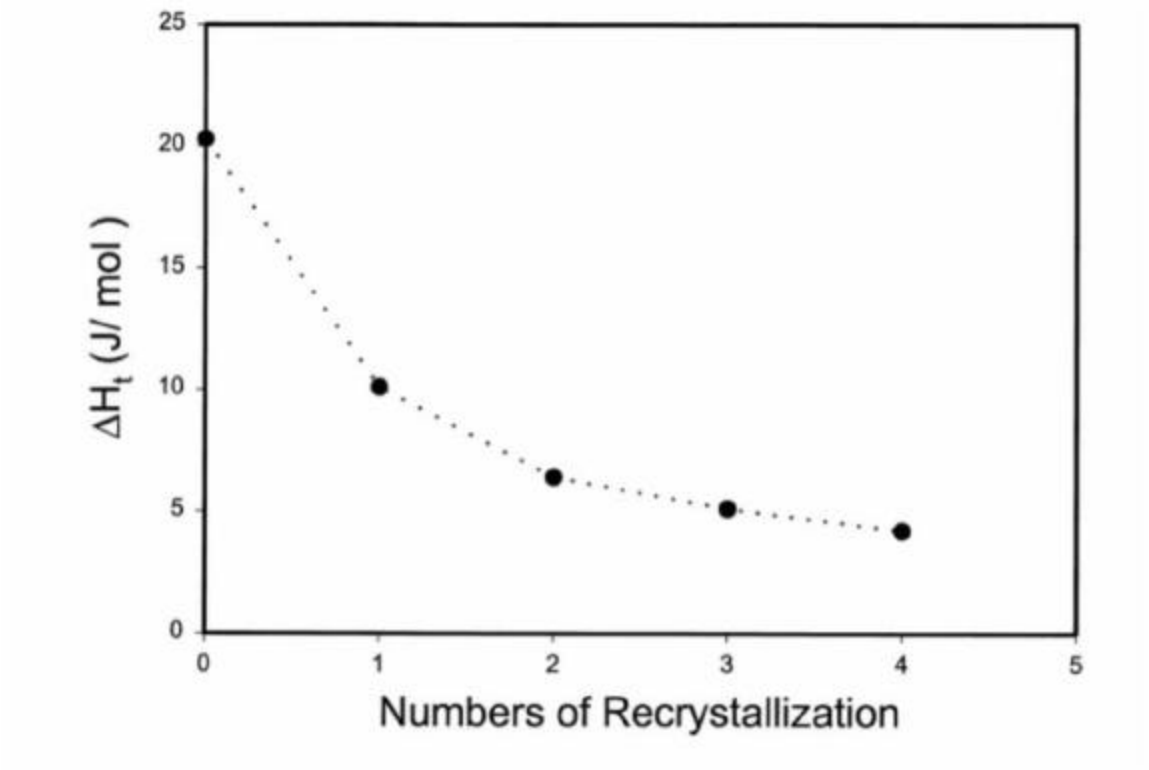

Figure 39. Heat of transition for L-alanine at 270 K as a function of crystallization.

known that aspartic acid racemizes quite rapidly in solution compared to other amino acids and the mechanism is now well understood.[84] The formation of D-amino acids as required in certain bacteria or in the mammalian brain is produced by enzymatic conversion from the L- to the D-form.[85, 86] Racemization reactions of amino acids in the solid state or in the gas phase have not been observed to date. However, aspartic acid racemization in dentine is used as a measure of aging.[87] Although the exact process is not understood; in our opinion this reaction is catalytic in nature and would not occur in a pure sample of aspartic acid.

Salam proposed that at lower temperatures a Bose-Einstein type phase transition would favor the more stable enantiomeric form.[78,79] He regarded racemization as an equilibrium problem and estimated the critical temperature T_c to be lower than 250 K, i.e., for temperatures below the melting point of amino acids. For a single molecule in the solid state (or in the gas phase), the mechanism for hydrogen migration may occur classically by overcoming a rather low barrier for process or by tunneling of the hydrogen atom at the chiral carbon center through the inversion barrier. Bimolecular reactions in the solid state are energetically not preferred.

The stereomutation of methane, CH_4, has been previously investigated and the transition state is estimated to be 439 kJ mol^{-1} above the T_d minimum structure at the MP2 level of theory.[88] This transition state can be best described as a pyramidal complex between methylene in the $^1A_1$ electronic state and H_2.[88] According to the Wentzel-Kramers-Brillouin (WKB) approximation, such a high barrier (with a thickness on the order of Ångstrøms) would prevent any hydrogen tunneling at low temperatures in a reasonable time scale. This barrier can be decreased significantly to about 180 kJ mol^{-1}

for amino acids adsorbed on transition metals.[89] Since the mechanism for the unimolecular racemization of amino acids is not known, the hydrogen migration process for the alanine inversion was investigated by means of quantum chemical procedures (second-order Møller-Plesset, MP2, and density functional B3LYP level of theory using 6-311+G* basis sets).[90]

After an intensive search of possible transition states for the unimolecular gas phase racemization of alanine, the lowest possible energy path was found. The hydrogen atom migrates from the chiral carbon center (denoted as C^*) over a high-energy path bridging the C^* and the nitrogen, N, atoms to the final intermediate state where the hydrogen is bound to the amino group. Racemization then occurs when another hydrogen atom in the amino group migrates back to the chiral carbon center. Other possible paths of lower energy cannot be excluded because the potential energy hypersurface (PES) is quite complicated. However, an intermediate state of lower energy could not be found. This intermediate configuration, $CH_3C(NH_3)COOH$, is a minimum at the PES. This calculation explains the rather high stability of this meta-stable compound, which is only 156 kJ mol^{-1} above the (local) minimum structure at the MP2 level of theory (140 kJ mol^{-1} at the B3LYP level). Here the hydrogen atom is clearly bound to the nitrogen center at a distance of 1.02 Å at the MP2 level (Figure A-9). The transition state is 294 kJ mol^{-1} above the minimum (279 kJ mol^{-1} at the B3LYP level), and below the dissociation limit for the hydrogen abstraction, $CH_3C(NH_2)COOH + H$ (330 kJ mol^{-1} at the MP2 and 328 kJ mol^{-1} at the B3LYP level of theory). Furthermore, the transition state is energetically well below that calculated for CH_4[88]; the barrier is too high and thick to be overcome either classically by hydrogen migration at temperatures below the melting

point of alanine (570 K)[91] or quantum mechanically by hydrogen tunneling. One may assume that the solid state environment would severely restrict any molecular rearrangements; thus increasing the barrier even more for the racemization process. Hence, the Salam phase transition is kinetically hindered and a Bose-Einstein condensation from a racemic mixture to the energetically more stable form due to electroweak interactions is not expected to take place in the solid state at lower temperatures. Bose-Einstein condensations observed in nature usually have no or extremely small barriers to overcome and this is apparently not the case for amino acids.

Conclusion

In conclusion, a wide range of experimental measurements have been presented on the enantiomorphs of L- and D-alanine and -valine in an effort to detect a weak interaction phase transition as described by Salam[79] and to reexamine the results reported by Wang *et al.*[80] supporting such a transition. Although a small difference in the DSC for both L- and D-alanine and –valine is seen at 270 K as reported by Wang *et al.*[80], we present evidence that this effect becomes smaller upon successive recrystallization and is absent in L-valine. Other features reported by Wang *et al.*[80] in support of the Salam hypothesis are not corroborated. On a positive note, a number of new physical measurements were reported on the important amino acid crystals and provided further theoretical insight into the unimolecular racemization of amino acids (alanine).

CHAPTER VIII

CONCLUSIONS

Many different experiments were carried out on various molecules to study their fundamental properties. Though some of the results are not as grand as others, the studies contribute to the overall understanding of chirality because if someone were to find one clean way of manipulating chiral matter, the world as we know it would be changed forever. Thus, investigations probing the wonderful world of chirality were witnessed in these chapters.

In the case of (*R*)-(+)-3-methylcyclopenatone, the resonance enhanced multiphoton ionization method proved to provide new information about the nature of multiphoton ionization circular dichroism. The dissymmetric factor g was larger for the multiphoton circular dichorism effect than the single photon circular dichroism effect. The nature of this multiphoton ionization circular dichroism can be investigated further by observing other chiral molecules and by employing multicolored laser light to the ionization process.

While probing and searching for new methods to study chirality, the area receiving the most attention happens to be in the realm of changing one enantiomer into the other and creating enantiomeric excesses. The parity violating energy difference investigation for the enantiomers of alanine and valine revealed that enantiomeric conversion was not possible for these amino acids at temperatures around 273 K. Future enantiomeric conversions experiments of amino acids may involve studying the chirality at temperatures around that of liquid helium.

For now, slight enantiomeric excesses have been seen in the beta irradiation of 1,1'-binaphthyl. Even with small enantiomeric excess, it's refreshing to know that the presence of left-handed beta particles were able to influence the optical purity of the crystals. This little quark of information about the nature of chirality led to the investigations of laser induced crystallization.

The laser induced crystallization provided excellent results that ranged from the breaking of symmetry in sodium chlorate and asymmetry of sodium bromate through the minute irradiations by right circularly polarized and linearly polarized light, respectively, to the formation of γ-polymorph of glycine induced by a change in pH. Though the results for these experiments turned out well, there is still large room for improvement. Since the crystallization studies are highly statistical, many more experiments could be performed; but the same question will still haunt the experimenter. The question happens to be: How many trials are enough? Also, these crystallization studies depend on a lot of parameters so that if one parameter were changed it may turn out to make a world of difference in the results. As one can obviously see, the quest to gain a better understanding of how to influence chirality has only begun.

LIST OF REFERENCES

1. L. Velluz, M. Legrand, M. Grosjean, Optical Circular Dichroism: Principles, Measurements, and Applications. Verlag Chemic GMBH Weinheim/Bergstr Academic Press Inc., New York 1965.

2. D.A. Lightner and J. E. Gurst Organic Conformational Analysis and Stereochemistry from Circular Dichroism Spectroscopy. Wiley-VCH, A John Wiley and Sons, Inc., New York 2000.

3. P. Crabbe, Optical Rotatory Dispersion and Circular Dichroism in Organic Chemistry. Holden-day, San Francisco 1965.

4. A. Rodger, B. Norden, Circular Dichroism and Linear Dichorism. Oxford Press, Oxford 1997.

5. A.F. Drake, *J. Phys. E: Sci. Intrum.*, **19**, 170-179, 1986.

6. I. Powis, *J. Phys. Chem. A*, **104**, 878-882, 2000.

7. N.A. Cherenkov, *Chem. Phys. Lett.*, **87**, 4, 344-348, 1982.

8. B. Ritchie, *Phys. Rev. A.*, **13**, 1411-1415, 1976.

9. S.F. Mason. Molecular Optical Activity and the Chiral Discriminations. Cambridge University Press, Cambridge 1982.

10. N. Berova, K. Nakanishi, R.W. Woody, Circular Dichroism: Principles and Applications. Wiley-VCH, A John Wiley and Sons, New York, 2000.

11. A.J. Einhorn, Y.H. Pao, and F.W. Phelps, *Spectroscopy Letters* **13**, 4, 227-234, 1980.

12. G. D. Fasman, Circular Dichroism and the Conformational Analysis of Biomolecules. Plenum Press, New York, 1996.

13. J. R Appling, M.G White, R L. Dubs, S.N. Dixit, V. Mckoy, *J. Chem. Phys.*, **87**, 12, 6927-6933, 1987.

14. C. Westphal, J. Bansmann, M. Getztaff, and G Schonhense., *Phys. Rev. Lett.*, **63**, 2, 151-154, 1989.

15. J.D. Byers, H.I.Yee, T. Petralli-Mallow, J.M. Hicks, *Phys. Rev. B*, **49**, 20, 14643-14647, 1994.

16. T.Verbiest, M. Kauranen Y. Van Rompaey, A. Persoons, *Phys. Rev. Lett.*, **77**, 8, 1456-1459, 1996.

17. J. Paul, A. Dorzbach, K. Siegmann, *Phys. Rev. Lett.*, **79**, 16, 2947-2950, 1997.

18. J. Paul, K. Siegmann., *Chem. Phys. Lett.*, **304**, 23-27, 1999.

19. S. Piccirillo, C. Bosman, D. Toja et al., *Angew. Chem. Int. Ed. Engl.*, **36**, 16, 1729-1731, 1997.

20. A. Latini, D. Toja, A. Giardini-Guidoni et al., *Chirality*, **11**, 376-380, 1999.

21. K. Lebarbu, A. Zehnacker, F. Lahmani et al., *Chirality*, **13**, 715-721, 2001.

22. W.C. Johnson Jr., *Rev. Sci. Instrum.*, **42**, 9, 1283-1286, 1971.

23. P.L. Polavaragu, P.K. Bose, L. Hecht, and L.D. Barron, *J. Phys. Chem.*, **97**, 11211-11215, 1993.

24. A. Vrancic, K. Rupnik, and S.P. McGlynn, *Rev. Sci. Instrum.*, **69**, 1, 40-48, 1998.

25. L. O'Toole, P. Brint. *J. Chem Soc. Farady Tran.*, **88**, 9, 1237-1243, 1992.

26. T.J. Cornish, Tomas Baer, *J. Amer. Chem. Soc.*, **110**, 3099-3106, 1988.

27. R.E Pincock, R.R Perkins, A.S. Ma, K.R. Wilson, *Science*, **174**, 1018-1020,1971.

28. R.E Pincock, R.W. Keith, *J. Chem. Educ.*, **50,** 7, 455-457,1973.

29. R.E. Pincock, R.P. Bradshaw, R.R. Perkins, *J. Mol. Evol.*, **4**, 67-75,1979.

30. K. Asakura, Y. Nagasaka, M. Hidaka, M. Hayashi, S. Osanai, D. Kondepudi. *Chirality*, **16**, 131-136, 2004.

31. D.K. Kondepudi, J. Laudalio and K. Asakura. *J. Amer. Chem. Soc*., **121**, 1448-1451,1999.

32. H.T. Junkman, D.A. Wiesma, *Chem. Phys. Lett*., **97**,3, 261-264,1983.

33. W.A. Bonner, *J. Mol. Evol.*, **4,** 23-39,1974.

34. S. Mahurin, M. McGinnis, J.S. Bogard, L.D. Hulett, R.M. Pagni, R.N. Compton, *Chirality*, **13**, 636-640, 2001.

35. A.D. Randolph, M.D. Larson, Theory of Particulate Processes, 2nd edition, Academic Press, San Diego, 1988.

36. K. Asakura, T. Soga, T. Uchida, S. Osanai, D.K. Kondepudi, *Chirality*, **14**, 85, 2002.

37. D.J. Durand, D.K. Kondepudi, P.F. Morelra Jr., F.H. Quina, *Chirality*, **14**, 284, 2002.

38. D. K. Kondepudi, K.Asakura. *Acc. Chem. Res*., **34**, 946, 2001.

39. P.A. Browne, M.M. Harris, R.Z. Mazengo, S. Singh, *J. Chem. Soc. C*, 3990,1971.

40. Keszthely and Vance 1975; Walker, 1976.

41. A.S. Garay, *Biosystems*, **20,** 63-74, 1987.

42. A.G. Griesbock, *Une J. Meierhenrich Angew Chem*., Int. Ed. **41**, 17, 3147-3154, 2002.

43. W. Kuhn, E. Braun, *Naturwissenschaften*, **17**, 227-228, 1929.; W. Kuhn, E. Knopf. *Z. Phys. Chem*., **7**, B, 292, 1930.; W. Kuhn, E. Knopf, *Naturwissenschaften*, **18**, 183, 1930.

44. Y. Shimizu, *J. Chem. Soc. Perkin Trans*., **1**, 1275-1278, 1997.

45. G. Balavoine, A. Moradpour, H.B. Kagan, *J. Amer. Chem. Soc*., **96**, 5152-5158, 1974.

46. H. Sakai, C.P. Safvan, J.J.Larsen, K.M. Hilligsoe, K. Hald, H. Stapelfeldt, *J. Chem. Phys*., **110**, 21, 10235-10238, 1999.

47. W. Kim, P.M. Felker, *J. Chem. Phys*., **104**, 1147, 1996.; **108**, 6763, 1998.

48. S. Guerin, L.P. Yatsenko H.R. Jauslin, O. Faucher, B. Larorel, *Phys. Rev. Lett*., **88**, 23, 233601-1 to 233601-4, 2002.

49. L. Cai, J. Marango, B. Friedvich, *Phys. Rev. Lett*., **86**, 5, 775-778, 2001.

50. B. Friedrich, D.R. Herschbach, *Phys. Rev. Lett*., **74**, 46231995.; *J. Phys. Chem*., **99**, 15686, 1995.

51. H.B. Kagan, G. Balavoine, A. Moradpour, *J. Mol. Evol*., **4**, 41-48, 1974.

52. J. Bartus, O. Vogl, *Monatshefte fur Chemie*, **124**, 217, 1993.

53. F. Legare, A.D. Bandrauk, *Phys. Rev. A*., **64**, 031406, 2001.

54. B. Friedrich, D. Herschbach, *Chem. Phys. Lett*., **262**, 41-46, 1996.

55. S. Chongprasert, S.A. Knopp, S.L. Nail, *J. Pharmaceutical Sciences*, **90**,11,1720-1728, 2001.

56. Y. Iitaka, *Acta Crystallogr*., **14**, 1-10, 1961.

57. L. J. Ksanda, G. Tunell, *Amer. J. Sci*., **35**, A, 173-178, 1938.

58. J. Hengstenberg, F.V. Lenel, *Z. Krist*., **77**, 424-436, 1931.

59. A. Garetz, J. Matic, *Phys. Rev. Lett*., **89**, 17, 175501-1 to 4, 2002.

60. L. Yu, K. NG, *J. Pharmaceutical Sciences*, **91**,11, 2367-2373, 2002.

61. M.J. Akers, N. Milton, S.R. Byrn, S.L. Nail, *Pharmaceutical Research*, **12**, 10, 1457-1461, 1995.

62. C.H. Chen, M.P. McCann, *Chem. Phys. Lett*., **153**, 4, 338-340, 1988.

63. J. Zaccoro, J. Matic, A.S. Myerson, B.A. Garetz, *Crystal Growth and Design*, **1**, 1, 5-8, 2001.

64. M.J. Potrzebowski, P. Tekely, Y. Dusausoy, *Solid State Nuclear Magnetic Resonance*, **11**, 253-257, 1998.

65. R.M. Hochstrasser, G.R. Meredith, H.P. Trommsdorff, *J. Chem. Phys*., **73**, 1009, 1980.

66. P.R. Monsan, W.M. McClain, *J. Chem. Phys*., **53**, 29, 1970.

67. E.R.C. Holcomb, T. Inoue, Kazumi Nishioka, *J. Crystal Growth*, **158**, 336-339, 1996.

68. R.I. Petrova, J.A. Swift *Crystal Growth and Design*, **2**, 6, 573-578, 2002.

69. H. Sakai, H. Hosogai, T. J. Kawaakita, *Cryst. Growth*, **116**, 421-426, 1992.

70. I. Khriplovich, *Parity Nonconservation in Atomic Phenomena*, Gordon and Breach, Amsterdam. 1997.

71. M.A. Bouchait, C. Bouchait, *Rep. Prog. Phys*., **60**, 1351, 1997.; M. A. Bouchiat, C. Bouchait, *Journal De Physiaque*, **35**, 899-927, 1974.

72. R. Wesendrup, J.K. Laerdahl, R.N. Compton, P. Schwerdtfeger, 2003.; J.K. Laerdahl, R. Wesendrup, P. Schwerdtfeger, *Chem. Phys*., **1**, 60-62, 2000.; R. Berger, M. Quack, *Chem. Phys*., **1**, 57-60, 2000.; R. Berger, M.J. Quack, *Chem. Phys*., **112**, 3148-3158, 2000.; M. Quack, *Chem. Phys. Lett*., **132**, 147-153, 1986.; M. Quack, *Angew. Chem.*, **114**, 4812-4825, 2002.; *Angew. Chem.* Int. Ed. English, **41**, 4618-4630, 2002.; A. Basasov, T.K. Ha, M. Quack, " Ab initio calculation of molecular energies including parity violating interactions" in "Chemical Evolution, Physics of the Origin and Evolution of Life, Proc. of the 4th Trieste Conference ",1995. p. 287-296, (Eds.: J. ChelaFlores, F. Raulin), Kluwer Academic Publisher, Dordrecht ,1996.; A. Bakasov, T.K. Ha, M. Quack, *J. Chem. Phys*., **109**, 7263-7285, 1998.

73. A.S. Lahamer, S.M. Mahurin, R.N. Compton, D. House, J.K. Laerdahl, M. Lein, P. Schwerdtfeger, *Phys. Rev. Lett*., **85**, 4470-4473, 2000.

74. R.A. Hegstrom, D.W. Rein, P.G.H. Sandars, *J. Chem. Phys*., **73**, 2329-2341, 1980.

75. D.W. Rein, *J. Mol. Evol*., **4**, 15, 1974.; V. Letokhov, *Phys. Lett*., **19**, 1264, 1967.; S.F. Mason, G. E. Tranter, *Mol. Phys*., 53, 1091-1111, 1984.

76. S. Mason, *Chem. Soc. Rev*., **17**, 347-359, 1988.

77. R. Lazzeretti, R. Zanasi, *Chem. Phys. Lett*., **279**, 349-354, 1997; P. Zanasi, P. Lazzeretti, *Chem. Phys. Lett*., **286**, 240-242, 1988; F. Faglioni, P. Lazzeretti, *Phys. Rev. E*, **65**, 011904-1 – 011904-11, 2002.

78. A. Salam, *J. Mol. Evol*., **33**, 105-113, 1991; A. Salam, *Phys. Lett. B*, , **288**, 153, 1992.

79. A. Salam, "On Biological Macromolecules and the phase transitions they bring about," in "Conceptual Tools for Understanding Nature. Proc. 2nd Intl. Symp. of Science and Epistemology Seminar, Trieste" , 1993, (Eds.: G. Costa, G. Calucci, M. Giorgi), World Scientific Publ., Singapore, 1995.

80. W. Wang, F. Yi, Y. Ni, Z. Zhao, X. Jin, Y. Tang, *J. Biol. Phys*., **26**, 51-65, 2000.

81. H. Nishino, A. Kosaka, G.A. Hembury, F. Aoki, K. Miyauchi, H. Shitomi, H. Onuki, Y. Inoue., *J. Amer. Chem. Soc*., **124**, 11618-11627, 2002.

82. G.G. Smith, G.V. Reddy, *J. Org. Chem*., **54**, 4529, 1989.

83. E.J. Ebbers, G.J.A. Ariaans, J.P.M. Houbiers, A. Bruggink, B. Zwanenburg, *Tetrahedron*, **53**, 9417, 1997.

84. J.L. Radkiewicz, H. Zipse, S. Clarke, K.N. Houk, *J. Am. Chem. Soc*., **118**, 9148, 1996.

85. H. Wolosker, S. Blackshaw, S. H. Snyder, *Proc. Natl. Acad. Sci.*, **96**, 13409, 1999.

86. E. Adams, *Enzymes*, **6**, 479, 1972.

87. P.M. Helfman, J.L. Bada, *Nature*, **262**, 279, 1976.

88. M.J.M. Pepper, I. Shavitt, P. von R. Schleyer, M.N. Glukhovtsev, R. Janoschek, M. Quack, *J. Comput. Chem.*, **16**, 207, 1995.

89. K. Yoshizawa, A. Suzuki, T. Yamabe, *J. Am. Chem. Soc.*, **121**, 5266, 1999.

90. Gaussian 98, Revision A.7, M.J. Frisch, G.W. Trucks, H.B. Schlegel, G.E. Scuseria, M.A. Robb, J.R. Cheeseman, V.G. Zakrzewski, J.A. Montgomery Jr., R.E. Stratmann, J.C. Burant, S. Dapprich, J.M. Millam, A.D. Daniels, K.N. Kudin, M.C. Strain, O. Farkas, J. Tomasi, V. Barone, M. Cossi, R. Cammi, B. Mennucci, C. Pomelli, C. Adamo, S. Clifford, J. Ochterski, G.A. Petersson, P.Y. Ayala, Q. Cui, K. Morokuma, D.K. Malick, A.D. Rabuck, K. Raghavachari, J.B. Foresman, J. Cioslowski, J.V. Ortiz, B.B. Stefanov, G. Liu, A. Liashenko, P. Piskorz, I. Komaromi, R. Gomperts, R.L. Martin, D.J. Fox, T. Keith, M.A. Al-Laham, C.Y. Peng, A. Nanayakkara, C. Gonzalez, M. Challacombe, P.M.W. Gill, B. Johnson, W. Chen, M. W. J. Wong, L. Andres, C. Gonzalez, M. Head-Gordon, E.S. Replogle, J.A. Pople, *Gaussian Inc.*, Pittsburgh PA, © , 1998.

91. D.R. Lide, (Ed.) Handbook of Chemistry and Physics, 82nd ed.; CRC Press: New York, 2001.

APPENDIX

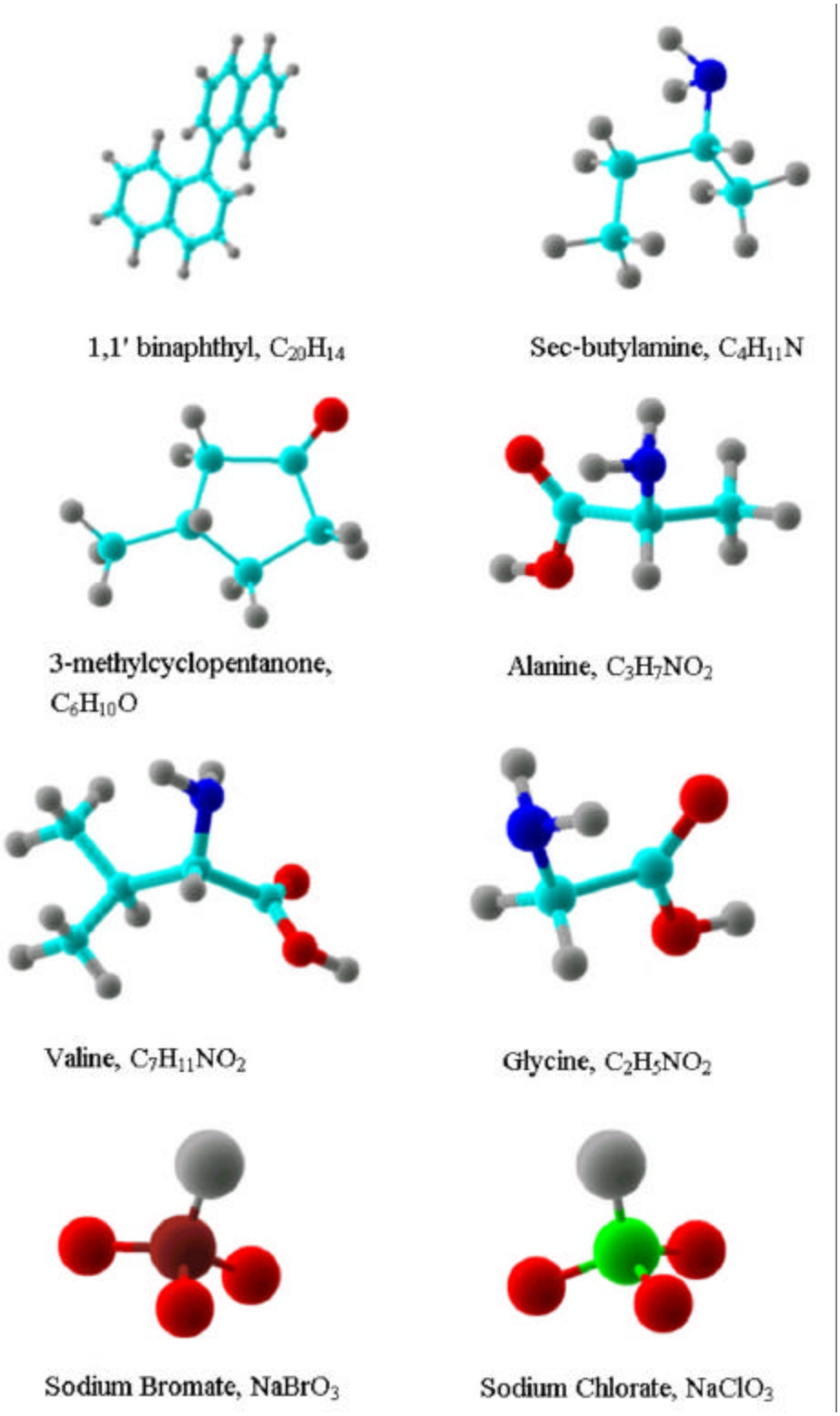

Figure A-1. A list of molecules and their structures used in the dissertation.

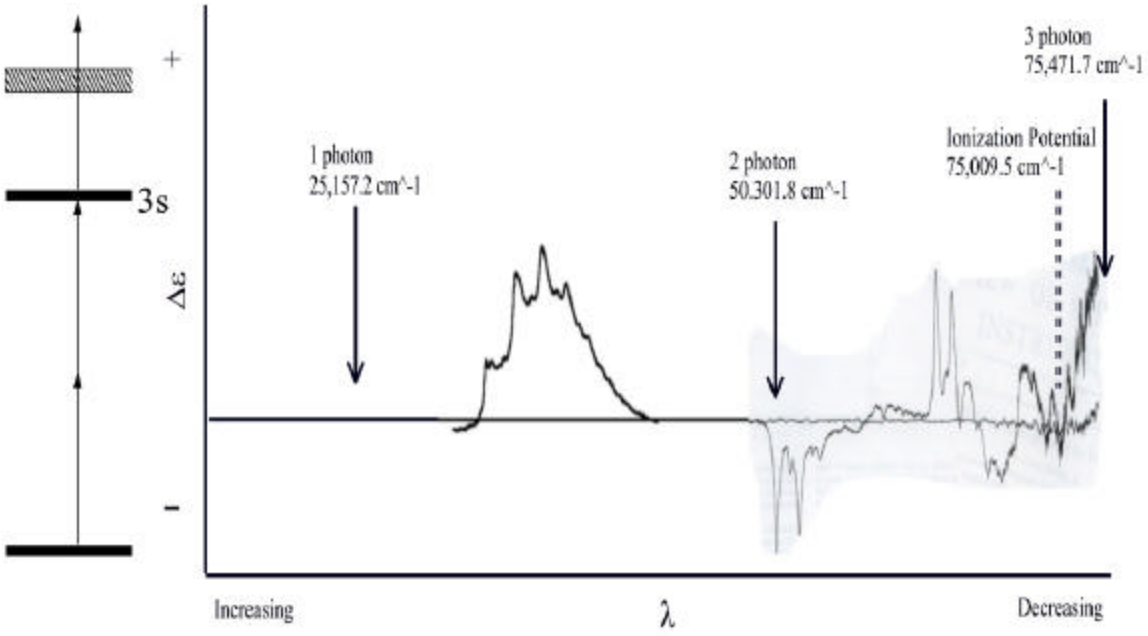

Figure A-2. Simplistic representation of the (2+1) REMPI that occurred in racemic and (*R*)-(+)-3-methylcyclopentanone. The first two photon correspond to the n → 3s transition while a third photon ionizes the molecule. The positions for three photon are shown on the CD.[22]

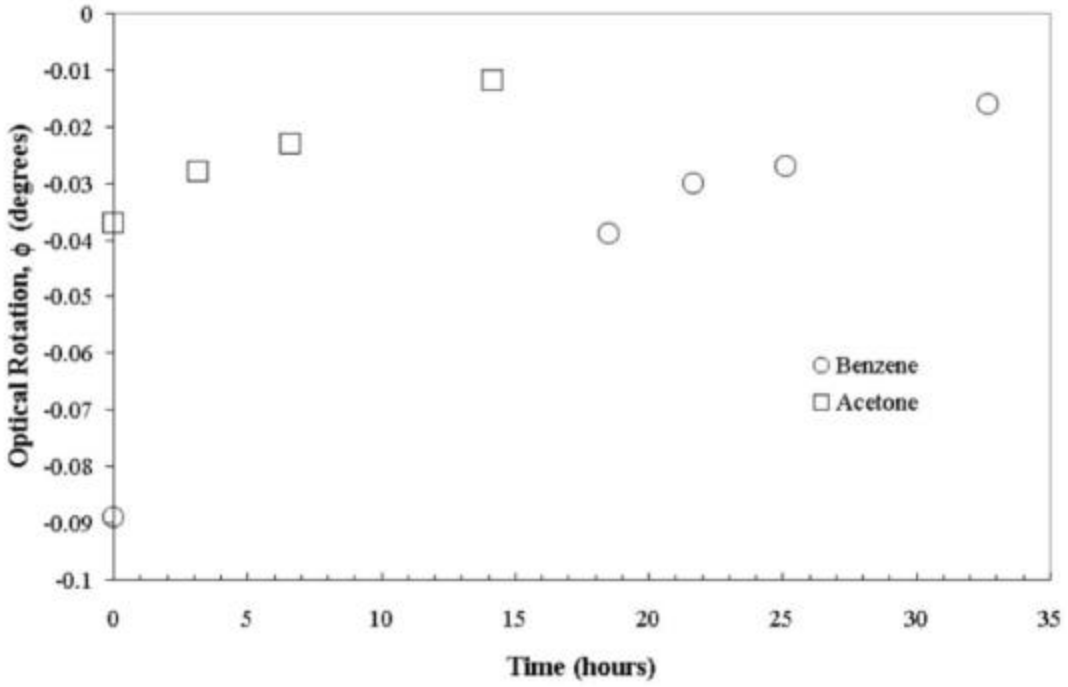

Figure A-3. Decrease of optical activity for 1,1'-binaphthyl dissolved in acetone and benzene.

Table A-1. Data for the frequency of specific rotations for the 1,1'-binaphthyl samples irradiated and not irradiated by the Sr^{90} beta source.

Frequency of Specific Rotation			**Frequency of Specific Rotation**		
Specific Rotation, $[a]_D$	**Under the Sr-90 Source**	**Not Under Sr-90 Source**	**Specific Rotation, $[a]_D$**	**Under the Sr-90 Source**	**Not Under Sr-90 Source**
-175	0	0	5	0	1
-170	0	0	10	1	0
-165	0	0	15	0	1
-160	0	0	20	0	0
-155	0	0	25	1	0
-150	0	0	30	0	1
-145	1	0	35	0	0
-140	0	1	40	1	0
-135	0	0	45	0	0
-130	0	0	50	0	0
-125	1	0	55	0	0
-120	0	0	60	0	1
-115	0	0	65	0	0
-110	0	0	70	0	0
-105	0	0	75	0	0
-100	1	0	80	0	0
-95	0	0	85	0	0
-90	0	0	90	0	0
-85	0	0	95	0	0
-80	0	0	100	2	0
-75	0	0	105	0	0
-70	0	0	110	0	0
-65	0	0	115	0	0
-60	0	0	120	0	0
-55	0	0	125	1	0
-50	0	1	130	0	0
-45	0	0	135	0	0
-40	0	0	140	0	0
-35	0	1	145	0	0
-30	0	0	150	0	0
-25	0	0	155	0	0
-20	1	0	160	0	0
-15	0	1	165	0	0
-10	0	0	170	0	0
-5	1	3	175	0	0
0	1	2			

Table A-2. Data for the specific rotations scatter plot of 1,1'-binaphthyl irradiated and not irradiated under the Sr^{90} beat source.

	Specific Rotation, [a]$_D$	
Number of Trials	**Samples under the Sr-90 Source**	**Samples not under the Sr-90 Source**
1	97.5	0.38
2	39.84	7.036
3	-145.94	-5.24
4	-124.98	-47.2
5	-1.554	-14.76
6	94	-1.04
7	9.86	28.4
8	0.24	0.47
9	-20.7	-16.3
10	122.5	62.14
11	23.14	-138
12	-101.02	-2.44
13		-34.94

Table A-3. Data for the laser-induced crystallizations of sodium chlorate crystals grown in Petri dishes.

LPL	**Number of Crystals**		**Percentage (%)**	
Trial Number	**Left (l)**	**Right (d)**	**Left (l)**	**Right (d)**
1	44	16	73.3	26.7
2	18	13	58.1	41.9
3	28	17	62.2	37.8
4	41	39	51.25	48.75
5	25	15	62.5	37.5
6	18	24	42.86	57.14
7	15	23	39.47	60.53
8	9	6	60	40
9	3	25	12	88
10	4	29	13.8	86.2
11	45	59	43.3	56.7
12	54	111	32.7	67.3
13	164	186	46.9	53.1
14	735	995	42.5	57.5
Total	1203	1558		
Average			45.77714	54.22286
LCPL	**Number of Crystals**		**Percentage (%)**	
Trial Number	**Left (l)**	**Right (d)**	**Left (l)**	**Right (d)**
1	43	35	55.1	44.9
2	24	16	60	40
3	38	20	65.5	34.5
4	22	20	52.4	47.6
5	18	20	47.4	52.6
6	10	19	34.5	65.5
7	6	6	50	50
8	22	15	59.5	40.5
9	3	27	11.1	88.9
10	0	30	0	100
11	184	101	64.6	35.4
12	53	90	37.1	62.9
13	683	577	54.2	45.8
14	841	785	51.7	48.3
15	475	501	48.7	51.3
16	498	506	49.6	50.4
17	644	627	50.7	49.3
18	407	398	50.6	49.4

Table A-3. Continued.

Total	3971	3793		
Average			46.81667	53.18333

RCPL	**Number of Crystals**		**Percentage (%)**	
Trial Number	**Left (l)**	**Right (d)**	**Left (l)**	**Right (d)**
1	16	15	51.6	48.4
2	10	7	58.8	41.2
3	26	31	45.6	54.4
4	24	31	43.6	56.4
5	15	25	37.5	62.5
6	19	16	54.3	45.7
7	12	12	50	50
8	14	10	58.3	41.7
9	3	19	15.8	84.2
10	3	18	16.7	83.3
11	57	50	53.3	46.7
12	20	31	39.2	60.8
13	173	113	60.5	39.5
14	45	69	39.5	60.5
15	1117	1254	47.1	52.9
16	451	206	68.6	31.4
Total	2005	1907		
Average			46.275	53.725
Blank	**Number of Crystals**		**Percentage (%)**	
Trial Number	**Left (l)**	**Right (d)**	**Left (l)**	**Right (d)**
1	27	30	47.5	52.6
2	43	36	54.4	45.6
3	39	22	63.9	36.1
4	43	39	52.4	47.6
5	15	17	46.9	53.1
6	15	14	51.7	48.3
7	8	19	29.6	70.4
8	101	153	39.8	60.2
9	155	181	46.1	53.9
10	69	94	42.3	57.7
11	58	58	50	50
12	377	366	50.7	49.3
13	63	64	49.6	50.4
14	432	479	47.4	52.6
15	671	543	55.3	44.7
16	688	700	49.6	50.4
Total	2804	2815		
Average			48.575	51.43125

Table A-4. Data for the laser-induced crystallizations of sodium chlorate crystals suspended and analyzed in a mixture of carbon disulfide and carbon tetrachloride.

RCPL			**LPL**		
Sample	**Weight (g)**	**Rotation (degree)**	**Sample**	**Weight (g)**	**Rotation (degree)**
1	0.55	0.2	1	0.737	0.018
2	0.43	1.136	2	0.908	-0.188
3	0.866	0.78	3	0.597	-5.102
4	0.438	1.69	4	0.632	-0.036
5	0.487	0.1	5	0.758	0.048
6	1.067	0.354	6	0.812	-0.356
7	0.444	0.44	7	0.096	0.11
8	0.389	-0.679	8	0.473	0.308
9	0.502	0.978	9	0.203	0.192
10	0.66	0.151	10	0.294	-0.032
11	0.41	-0.656	11	0.084	0.064
12	0.779	1.149	12	0.665	-0.718
13	0.246	-4.79	13	0.696	2.903
14	0.451	-2.789	14	0.503	-0.794
15	0.293	4.297	15	0.754	-8.126
16	0.41	-0.689	16	0.668	2.828
17	0.666	0.447	17	0.407	4.117
18	0.363	6.552	18	0.677	-4.718
19	0.666	0.248	19	0.502	2.59
20	0.433	2.754	20	0.35	5.84
Average	0.528	0.584	**Average**	0.541	-0.0526
Blank					
Sample	**Weight (g)**	**Rotation (degree)**			
1	0.421	-0.967			
2	0.421	3.298			
3	0.345	-5.391			
4	0.427	-3.531			
5	0.337	0.97			
6	0.45	-2.754			
7	0.528	1.95			
8	0.412	-1.913			
9	0.343	0.393			
10	0.422	0.929			

Table A-4. Continued.

11	0.385	1.913			
12	0.231	1.871			
13	0.444	-0.83			
14	0.356	0.295			
Average	0.394	-0.269			
Trends					
	Total Number	**l (-)**	**Percentage (%)**	**d (+)**	**Percentage (%)**
Blanks	14	6	42.9	8	57.1
RCPL	20	5	25	15	75
LPL	20	9	45	11	55

Table A-5. Data for the laser-induced crystallizations of sodium bromate crystals suspended and analyzed in a mixture of carbon disulfide and carbon tetrachloride.

RCPL			LPL		
Sample	**Weight (g)**	**Rotation (degree)**	**Sample**	**Weight (g)**	**Rotation (degree)**
1	0.728	-0.12	1	0.5	-0.002
2	0.607	-0.025	2	0.5	0.006
3	0.741	-1.672	3	0.5	-0.012
4	0.761	-0.09	4	0.5	-0.007
5	0.643	-0.726	5	0.5	0.025
6	0.63	0.177	6	0.5	-0.054
7	0.561	1.167	7	0.5	0.032
8	0.553	1.583	8	0.5	-0.027
9	0.662	0.008	9	0.5	-0.039
10	0.702	0.986	10	0.5	0.007
11	0.539	3.344	11	0.5	0.409
12	0.517	-0.76	12	0.657	-0.042
13	0.412	-0.091	13	0.542	-0.221
14	0.661	-0.071	14	0.597	0.34
15	0.505	-0.307	15	0.561	1.031
16	0.581	0.952	16	0.523	-0.279
17	0.631	-0.751	17	0.633	0.155
18	0.649	1.375	18	0.586	-1.19
19	0.531	1.432	19	0.624	0.645
20	0.504	-0.048	20	0.664	-0.012
21	0.431	0.14	21	0.395	-2.69
22	0.432	-0.297	22	0.274	2.758
23	0.485	-0.124	23	0.281	0.679
24	0.237	0.345	24	0.155	-1.105
25	0.511	0.166	25	0.406	1.263
26	0.338	0.441	26	0.551	1.748
27	0.203	0.257	27	0.619	-0.124
28	0.509	-0.541	28	0.459	-0.124
29	0.502	-0.209	29	0.324	0.33
30	0.421	-0.72	30	0.499	-1.121
31	0.357	-0.344	31	0.489	-0.109
32	0.479	-1.063	32	0.378	0.125
33	0.442	-2.315	33	0.263	0.409
34	0.444	0.776	34	0.453	1.302
35	0.385	-0.566	35	0.378	1.039
36	0.427	-0.579	36	0.442	0.079
37	0.449	-0.192	37	0.522	-2.57

Table A-5. Continued.

38	0.379	-0.129	38	0.392	-0.259
39	0.459	-0.853	39	0.415	0.11
40	0.422	-0.505	40	0.472	-0.242
Average	0.511	0.00128	41	0.193	-0.235
			Average	0.469	0.0495
Blank					
Sample	**Weight (g)**	**Rotation (degree)**			
1	0.904	-0.2242			
2	0.506	-0.272			
3	1.016	1.2			
4	0.577	-0.08			
5	0.5	-0.34			
6	0.5	-0.015			
7	0.698	-1.493			
8	0.609	-0.365			
9	0.698	-1.002			
10	0.697	-0.827			
11	0.675	-4.136			
12	0.768	-1.553			
13	0.598	1.444			
14	0.611	-3.175			
15	0.894	-1.947			
16	0.672	-1.282			
17	0.947	0.972			
18	0.902	-0.599			
19	0.925	0.261			
20	1.027	-0.437			
21	0.894	-0.124			
22	0.822	-0.704			
23	0.727	-0.311			
24	0.921	-1.37			
25	0.902	-0.366			
26	0.778	-0.872			
27	0.827	-0.328			
28	0.977	-0.91			
29	0.804	0.106			
30	0.943	0.18			
31	0.977	0.083			
32	0.825	-1.956			
33	0.79	0.175			

Table A-5. Continued.

34	0.784	0.878			
35	0.832	-0.31			
36	0.895	0.189			
37	0.828	-0.038			
Average	0.791	-0.528			
Trends					
	Total Number	**I (-)**	**Percentage (%)**	**d (+)**	**Percentage (%)**
Blanks	37	27	72.97297	10	27.02703
RCPL	40	25	62.5	15	37.5
LPL	41	21	51.21951	20	48.78049

Table A-6. Data for the sound, the single shot, and the high power laser light experiments for the crystallization of sodium bromate.

RCPL	**Single Shot (SS)**		**LPL**	**Single Shot (SS)**	
Sample	**Weight (g)**	**Rotation (degree)**	**Sample**	**Weight (g)**	**Rotation (degree)**
1	0.175	-0.299	1	0.371	-0.973
2	0.736	-1.012	2	0.623	0.246
3	0.601	-0.674	3	0.484	-0.41
4	0.947	-0.504	4	0.549	-1.667
5	0.91	-2.746	5	0.481	-2.108
6	0.625	-0.163	6	0.482	-1.764
7	0.933	0.135	7	0.663	-2.517
8	0.744	0.29	8	0.58	-1.299
9	0.625	-0.129	9	0.553	-1.193
10	0.614	0.101	10	0.538	-1.904
11	0.342	-0.323	11	0.577	-1.152
12	0.304	-1.031	12	0.672	-1.753
13	0.511	-1.137	13	0.297	-2.208
14	0.247	2.505	14	0.589	-3.254
Average	0.594	-0.356	15	0.626	-2.561
			16	0.342	-0.395
			17	0.524	-0.491
			18	0.609	-3.54
			Average	0.531	-1.608
Sound					
Sample	**Weight (g)**	**Rotation (degree)**			
1	0.345	-1.734			
2	0.401	-0.377			
3	0.357	-0.232			
4	0.47	-0.665			
5	0.423	-0.663			
6	0.334	-1.079			
7	0.474	-0.306			
8	0.35	-0.564			
9	0.371	-0.234			
10	0.307	-0.765			
11	0.158	-0.126			
12	0.139	-0.556			
13	0.41	-0.154			
14	0.101	-0.039			
15	0.336	-0.142			

Table A-6. Continued.

16	0.354	-0.223			
17	0.464	-0.173			
18	0.309	-0.713			
19	0.351	-0.939			
20	0.27	-0.311			
Average	0.336	-0.500			
LPL	**High Power (HP)**				
Sample	**Weight (g)**	**Rotation (degree)**			
1	0.578	-0.084			
2	0.622	-0.513			
3	0.593	-0.786			
4	0.596	-0.127			
5	0.522	-1.246			
6	0.278	-0.381			
7	0.575	-0.687			
8	0.552	-1.145			
9	0.701	-0.065			
10	0.684	-0.763			
11	0.512	-0.526			
12	0.715	1.121			
13	0.572	-0.563			
14	0.606	-0.312			
15	0.578	0.285			
16	0.508	-1.161			
17	0.582	-0.568			
18	0.615	-0.128			
19	0.573	-0.146			
20	0.64	-0.226			
Average	0.580	-0.401			
Trends					
	Total Number	**l (-)**	**Percentage (%)**	**d (+)**	**Percentage (%)**
Sound	20	20	100	0	0
RCPL (SS)	14	10	71.42857	4	28.57143
LPL (SS)	18	17	94.44444	1	5.555556
LPL(HP)	20	18	90	2	10

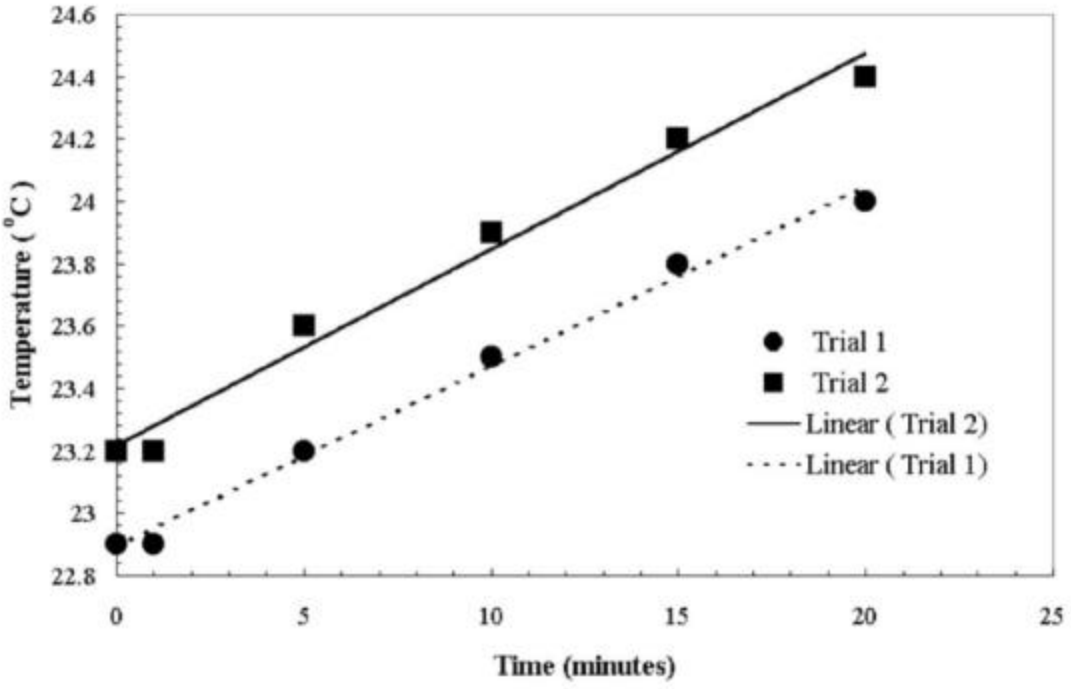

Figure A-4. Rise in the temperature over time of water for the sodium chlorate and the sodium bromate laser-induced crystallizations.

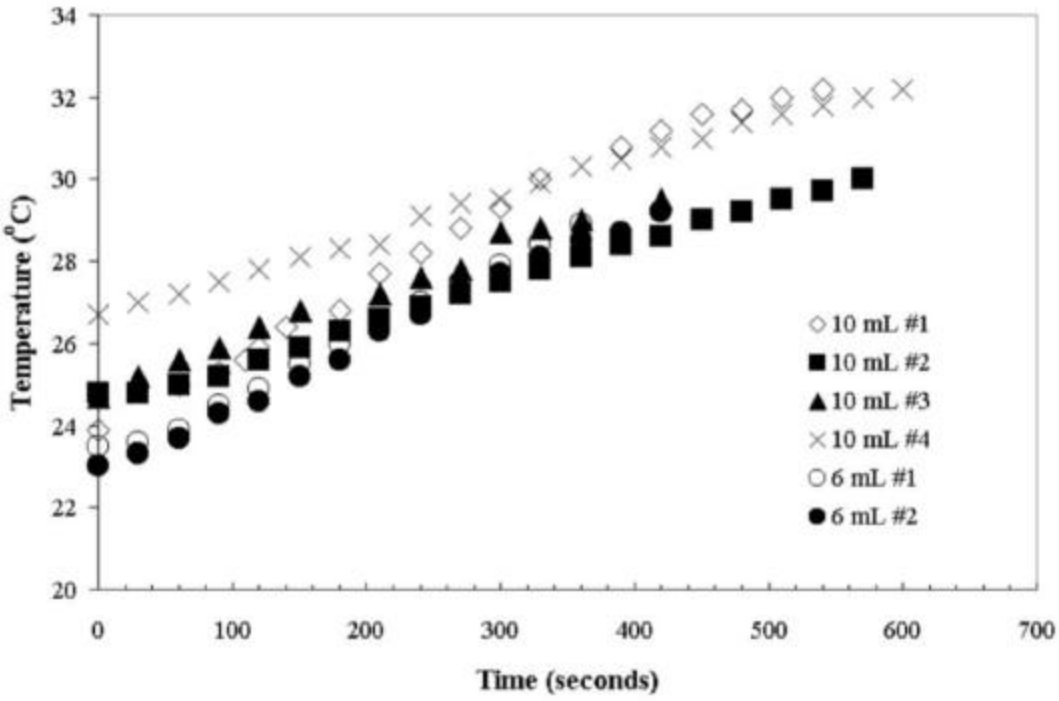

Figure A-5. Rise in water temperature over time for the laser-induced crystallization of glycine.

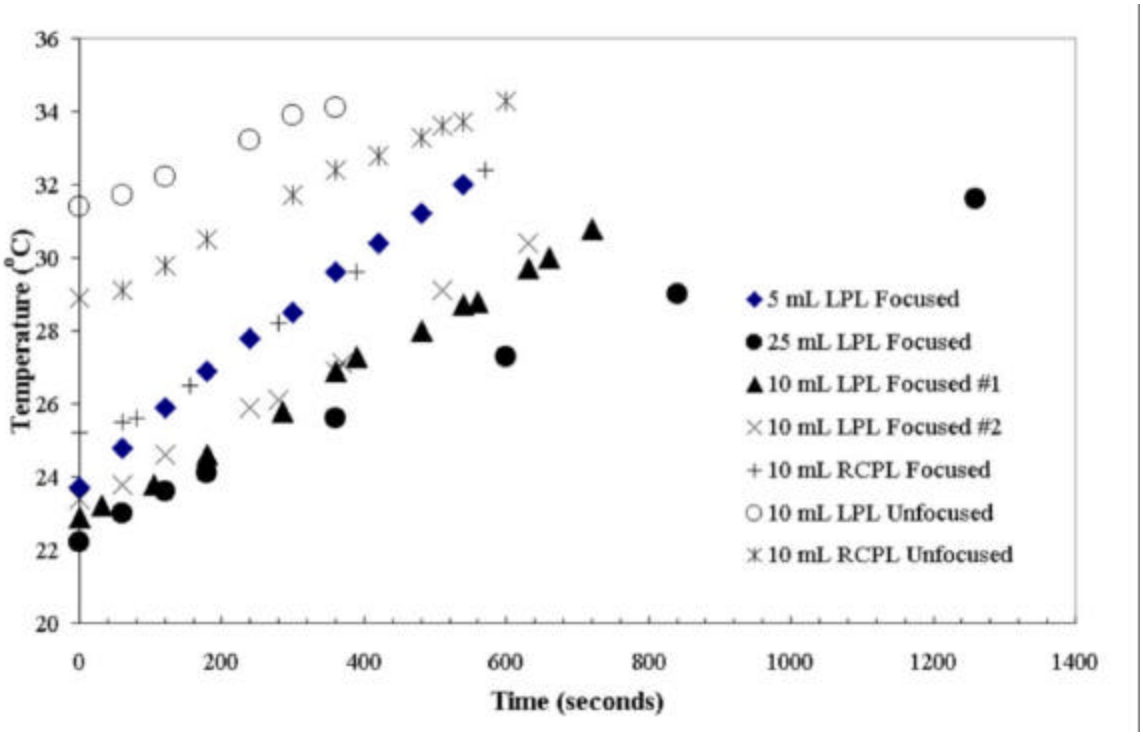

Figure A-6. Rise in temperature for a glycine solution used in the laser-induced cystallization experiments. Various sample sizes were used.

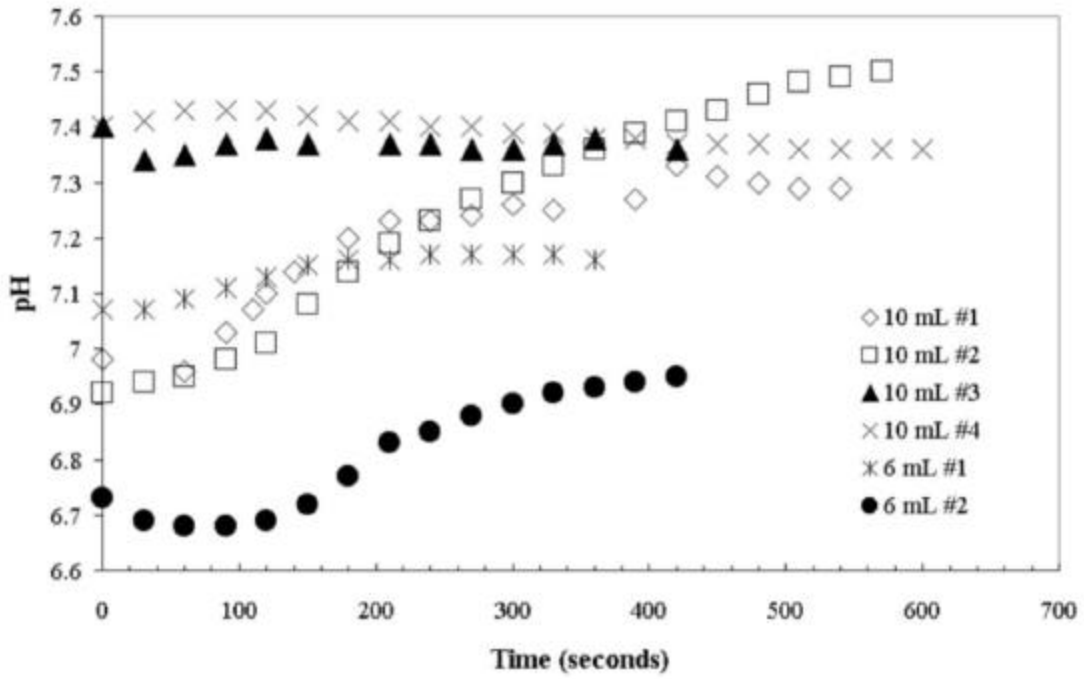

Figure A-7. Change in the pH of water over time when irradiated by 1064 nm intense laser light.

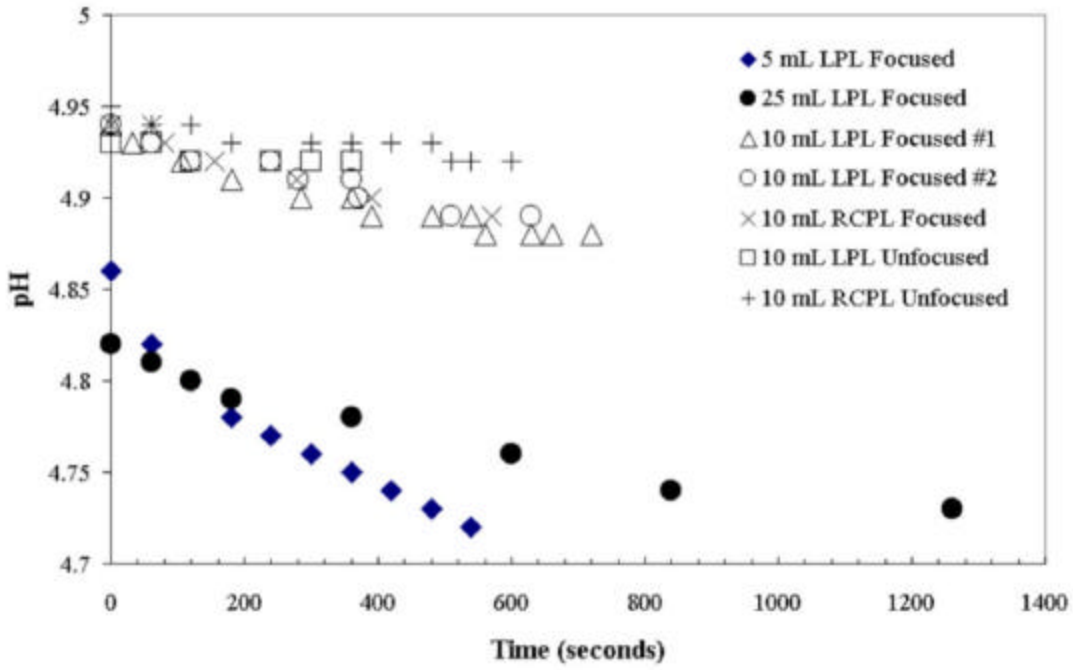

Figure A-8. Change in the pH of glycine when irradiated by intense 1064 nm laser light. Various sample sizes were used.

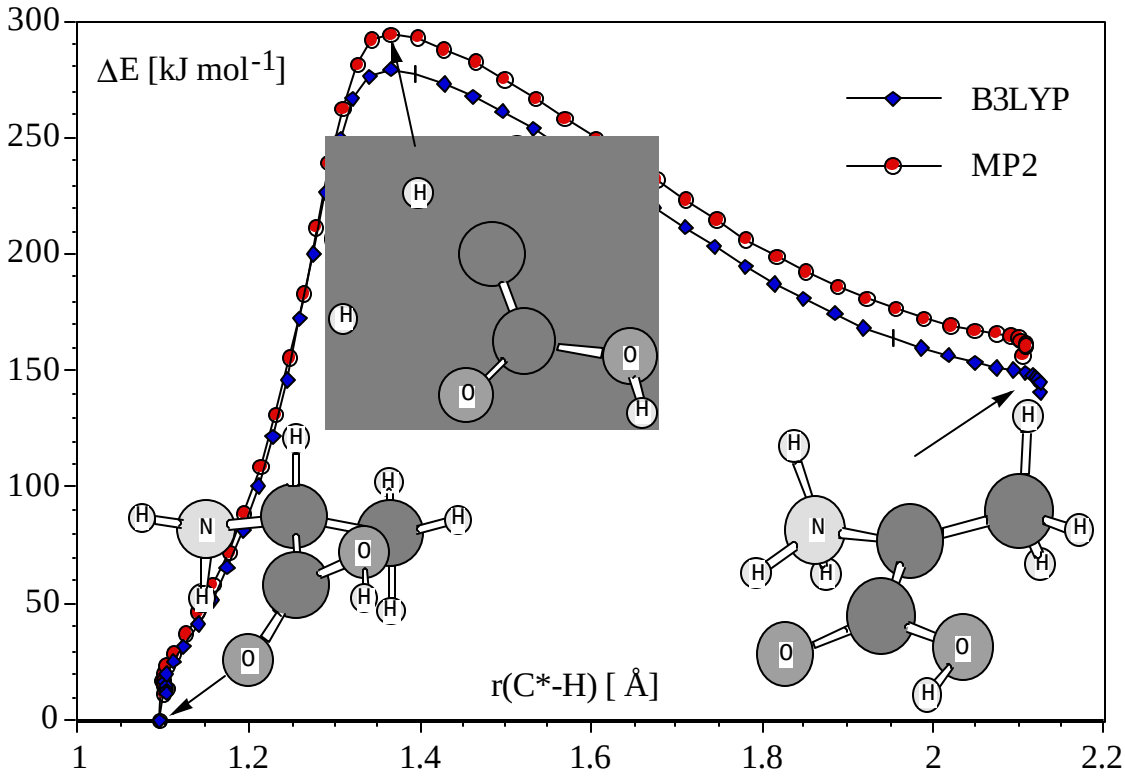

Figure A-9. Minimum energy path for the hydrogen migration from the chiral carbon center (C^*) to the amino group. For the reaction coordinate the C^*-H bond distance is chosen.

VITA

Rodney Jamel Sullivan was born in Greenville, South Carolina, on June 10, 1977. He attended public schools in Greenville County where he graduated from Travelers Rest High School in May 1995. He enrolled at Presbyterian College in Clinton, South Carolina, in August 1995 and received a Bachelor of Science degree in physics in May 1999. After a six-month vacation, he entered the graduate physics program at the University of Tennessee, Knoxville, where he worked under the provision of Dr. Robert N. Compton in the area of chemical physics. The doctoral degree was received in December 2004.